UNIVERSIDAD DE EXTREMADURA

TESIS DOCTORAL

DESARROLLO DE HERRAMIENTAS ORIENTADAS AL ESTUDIO DE ELECTROLIZADORES PEM PARA IMPLEMENTACIÓN DE RÉPLICA DIGITAL

Francisco Javier Folgado Gaspar

PROGRAMA DE DOCTORADO EN INGENIERÍAS INDUSTRIALES

Directores de la Tesis:

Fdo: Dr. D. Isaías González Pérez **Fdo: Dr. D. Antonio José Calderón Godoy**

Esta tesis cuenta con la autorización de los directores de la misma y de la Comisión Académica del programa. Dichas autorizaciones constan en el Servicio de la Escuela Internacional de Doctorado de la Universidad de Extremadura

2024

Agradecimientos

En primer lugar, me gustaría dar las gracias a mis directores de Tesis: Dr. Isaías González Pérez y Dr. Antonio José Calderón Godoy, por brindarme la oportunidad de realizar esta Tesis Doctoral. Les agradezco su encomiable labor de tutela y guía durante estos años, así como su paciencia y sus consejos. A su vez, no solo han actuado como directores, sino que he tenido la suerte de poder trabajar "codo con codo" como compañeros de trabajo e investigación, haciéndome "uno más del grupo" desde el primer día e integrándome en sus ideas y proyectos. Tras esta etapa que se cierra, espero poder continuar este camino disfrutando de su compañía y de lo que considero unos magníficos mentores y amigos.

A Espe, por su alegría y constante apoyo, impulsándome siempre a crecer y perseguir mis metas.

A mi amigo Rayen, que me ha acompañado desde los inicios de mi etapa universitaria, compartiendo experiencias durante nuestros estudios de Grado. Por su compañía, apoyo y consejos.

Finalmente, a mi familia: a mis padres y hermana por su apoyo y paciencia. Han sido partícipes desde el inicio de mi etapa estudiantil, animándome a superarme día a día y a lograr mis metas.

Resumen

La escasez de los combustibles fósiles y la transición energética hacia el consumo de fuentes de energías renovables han propiciado un auge en el desarrollo de tecnologías para el aprovechamiento del hidrógeno. Para la generación de este gas, se emplean electrolizadores, dispositivos basados en el proceso electroquímico de la electrólisis por el cual se separa un compuesto en sus componentes fundamentales. A través de este proceso, se obtiene hidrógeno a partir de carburos o de elementos no contaminantes como el agua.

La operación de estos dispositivos es compleja y su implementación en un sistema físico no es inmediata. Por ello, es necesario comprender con antelación el proceso de funcionamiento de estos equipos, así como las variables clave que lo condicionan. Derivado de esta necesidad, surge la motivación y temática que da lugar a la presente Tesis Doctoral.

El objetivo de la Tesis Doctoral es el desarrollo de herramientas orientadas al estudio de electrolizadores tipo PEM (*Proton Exchange Membrane*) para la implementación de una réplica digital.

En este sentido, una réplica digital, también conocida como gemelo digital, es una contraparte virtual del dispositivo físico que reproduce de forma precisa el comportamiento de dicho equipo. La réplica digital pone a disposición el equipo de forma virtual, permitiendo el estudio de su comportamiento de forma aislada del resto de la instalación asociada. A su vez, es posible someter a la réplica digital a condiciones de operación y puntos de trabajo fuera de los rangos nominales. Esta representación digital puede ser empleada para múltiples tareas como las relativa a la optimización de la operación, mantenimiento preventivo y predictivo, análisis de desviaciones y estados operativos anómalos, etc.

La principal contribución de la Tesis Doctoral consiste en el desarrollo de tres herramientas orientadas al estudio de electrolizadores tipo PEM. En primer lugar, un simulador multi-modelo que permite el estudio y comparación de hasta un total de 4 modelos escogidos de la bibliografía científica revisada. En segundo lugar, un sistema de monitorización para un electrolizador PEM enmarcado en una smart microgrid (microrred inteligente) basada en energías renovables e hibridada con hidrógeno. Por último, la información obtenida a partir de estas dos herramientas es aplicada en el diseño de una réplica digital de un electrolizador PEM.

El desarrollo y aplicación de estas herramientas ha facilitado el estudio en profundidad sobre el funcionamiento del electrolizador PEM, así como sus variables clave y la relación entre estas. A su vez, las herramientas diseñadas han permitido el análisis y comparación de la operación del electrolizador PEM en diversos puntos de trabajo, permitiendo observar los efectos derivados de las variaciones en sus variables clave. Por último, los resultados obtenidos del estudio del electrolizador PEM enfatizan las necesidades de monitorización, control y optimización sobre dichas variables para asegurar un funcionamiento correcto y evitar mecanismos de degradación a largo plazo.

La investigación desarrollada en la Tesis Doctoral proporciona una serie de herramientas y conocimientos de utilidad dentro del ámbito industrial, más concretamente en el campo energético, ya que permiten comprender en profundidad el funcionamiento de los electrolizadores PEM, así como las variables clave que lo condicionan. De igual forma, se ponen de manifiesto las necesidades y requisitos del estudio previo de estos equipos y uso de estas herramientas para lograr una correcta implementación y optimización de los electrolizadores PEM en un sistema real.

Contenido

Figuras

Capítulo 1. Introducción

1.1. Preámbulo

Según el Real Decreto 99/2011, de 206 de enero, por el cual se regulan las enseñanzas oficiales de doctorado, modificado por los Real Decreto 534/2013, de 12 de julio, Real Decreto 43/2015, de 2 de febrero, y Real Decreto 195/2015, de 13 de mayo; esta Tesis Doctoral se enmarca en el "Programa de Doctorado en Ingenierías Industriales", ya que la investigación incluida en esta se encuentra aplicada al campo de la Ingeniería Industrial.

La elaboración de esta Tesis Doctoral se ha desarrollado bajo los criterios marcados por el artículo 33 "Tesis doctorales presentadas como compendio de publicaciones", de la Resolución de 14 de diciembre de 2021 (DOE de 28 de diciembre de 2021), por el cual se aprueba la Normativa de Doctorado de la Universidad de Extremadura. En dicha resolución se establecen los requisitos mínimos necesarios para la publicación de la Tesis Doctoral siguiendo la estructura de compendio de publicaciones.

1.2. Contexto científico

Los trabajos expuestos en la Tesis Doctoral se encuentran enmarcados dentro del proyecto de investigación con referencia IB1841 y título "Transformación digital en las energías renovables: Desarrollo de réplica digital de Smart Microgrid basada en energías renovables e hidrógeno".

El objetivo principal de este proyecto consiste en el diseño e implementación de un sistema ciberfísico que incorpore una representación o réplica digital de una smart microgrid basada en energías renovables e hidrógeno. Para ello, se plantea confeccionar el gemelo digital de los elementos clave que conforman la microgrid.

La smart microgrid está compuesta por dos subsistemas. En primer lugar, un sistema primario de generación y almacenamiento eléctrico por medio de paneles fotovoltaicos y baterías Ion-Litio. Por otro lado, un sistema de apoyo de generación, almacenamiento y consumo de hidrógeno mediante un electrolizador PEM, un sistema de tanques de hidruros metálicos y una pila de combustible PEM, respectivamente. En la Figura 1 se presentan los componentes que forman la smart microgrid.

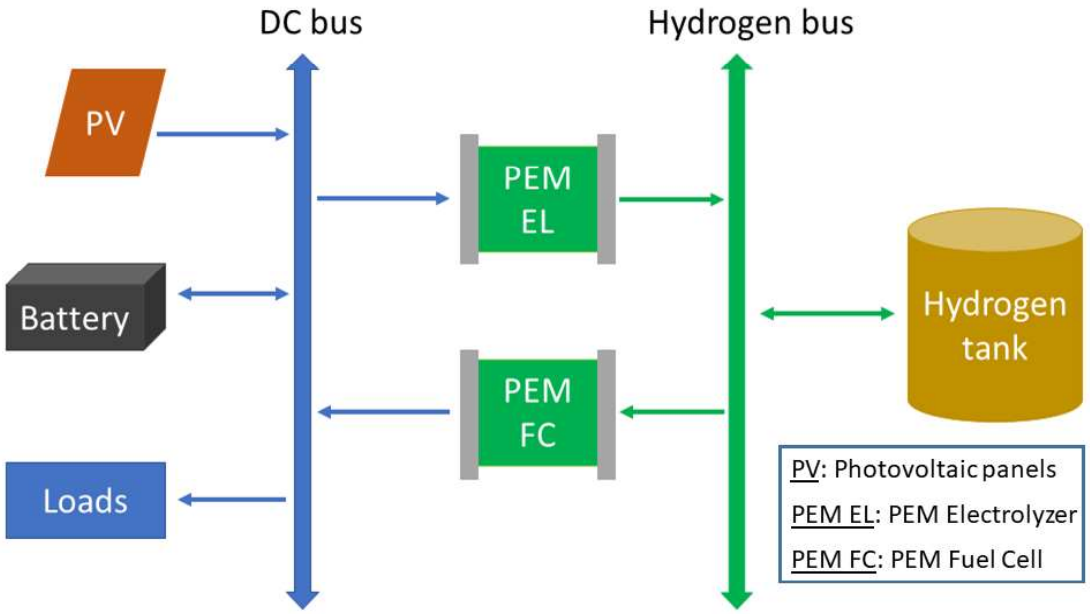

Figura 1. Componentes de la smart microgrid.

El hidrógeno empleado en el subsistema de apoyo es comúnmente denominado como hidrógeno verde. La connotación "verde" se atribuye al hidrógeno que es generado a partir de energías renovables y cuyo proceso de obtención no produce subproductos contaminantes. En este caso, el electrolizador PEM se encuentra alimentado por un suministro de corriente proveniente de los paneles fotovoltaicos, y realiza el proceso de electrolisis sobre un caudal de agua destilada cuyo resultado genera únicamente hidrógeno y oxígeno.

Las herramientas descritas en la Tesis Doctoral se contextualizan dentro de los trabajos realizados para desarrollar la réplica digital del electrolizador PEM del subsistema de apoyo de la smart microgrid.

1.3. Coherencia e importancia unitaria de la Tesis Doctoral

La presente Tesis Doctoral se compone de un total de tres artículos científicos que tienen un objetivo general común: desarrollar herramientas orientadas al estudio de electrolizadores PEM. A partir de estos artículos científicos se cumplen con todos los objetivos definidos en el Capítulo 2. El contenido de estos artículos se enmarca en el contexto Industrial, concretamente en el ámbito de las energías renovables y del aprovechamiento del hidrógeno en aplicaciones energéticas como las microgrids o smart microgrids.

Las herramientas descritas en la Tesis Doctoral y en los artículos científicos presentan una estrecha relación y coherencia desde un enfoque tanto de diseño y desarrollo, como en un enfoque práctico de aplicación.

Desde el punto de vista del diseño y desarrollo, cada una de las herramientas se apoya de la información y resultados obtenidos de la herramienta previamente diseñada. Tomando como punto final el desarrollo de la réplica digital, es necesario comenzar con un estudio teórico del funcionamiento del electrolizador PEM. Con este fin, se diseña el simulador multi-modelo, por el cual se obtiene información del comportamiento del electrolizador, contrastada mediante simulaciones individuales de cada modelo y análisis comparativo de los resultados obtenidos. Esta información resulta crucial para determinar las variables clave que afectan sobre el electrolizador PEM, lo que determina las necesidades requeridas para el siguiente paso: el estudio experimental del funcionamiento del electrolizador PEM.

Para el desarrollo de la réplica digital, es necesario disponer de datos experimentales que definan el funcionamiento del equipo físico. Por ello, en el estudio experimental se aplican los conocimientos

adquiridos mediante el simulador multi-modelo para diseñar el sistema de monitorización. Mediante este sistema, se adquieren los datos experimentales de las variables clave del electrolizador. Estos datos son aplicados para definir el modelo de la réplica digital.

Por último, para el diseño de la réplica digital se realiza un análisis experimental sobre el electrolizador. Dicho análisis combina los conocimientos obtenidos en las etapas de estudio teórico y experimental mediante el uso de las herramientas correspondientes.

Desde una perspectiva de aplicación práctica, cada herramienta dispone de una serie de funcionalidades particulares que lo caracterizan para su uso de forma individual en cada etapa del estudio del electrolizador PEM (estudio teórico, estudio experimental, análisis experimental). Sin embargo, existen determinadas sinergias derivadas del uso combinado de estas herramientas.

- **Simulador multi-modelo + Sistema de monitorización**: los datos experimentales obtenidos pueden ser utilizados como entrada en el simulador para obtener datos teóricos del electrolizador en los cuatro modelos. De esta forma, se puede realizar un análisis comparativo teórico-experimental, donde se observen las diferencias entre los modelos estudiados y el comportamiento del equipo real.
- **Sistema de monitorización + réplica digital:** los datos obtenidos de la réplica digital pueden ser comparados con los datos experimentales del sistema de monitorización para detectar/analizar desviaciones y errores en las variables clave del electrolizador.

El diagrama de la Figura 2 representa las distintas etapas descritas, así como las herramientas desarrolladas y su interconexión.

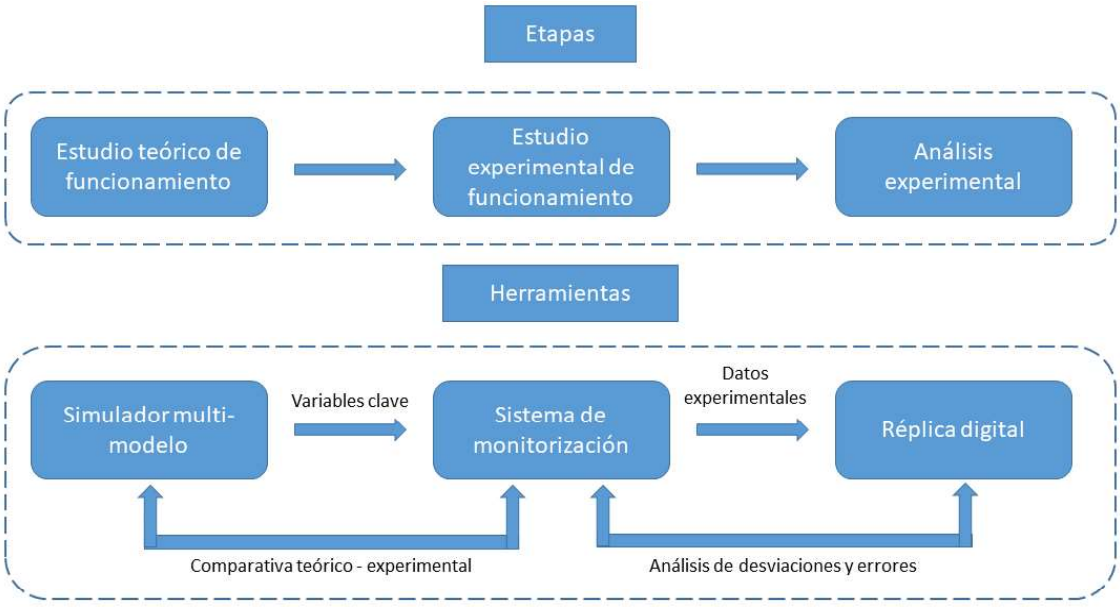

Figura 2. Etapas y herramientas desarrolladas.

1.4. Rendimiento científico

En este apartado se expone el rendimiento científico generado durante el desarrollo de la presente Tesis Doctoral. Para ello, se muestra el conjunto de publicaciones relacionadas directa e indirectamente con la investigación llevada a cabo, diferenciando las publicaciones de artículos indexados en *Journal Citation Reports* y las comunicaciones presentadas a congresos.

1.4.1. Compendio de publicaciones

Todas las revistas en las que se han publicado los artículos se encuentran indexadas en la *Web of Science* (WOS) del *Institute for Science Information* (ISI) y dentro de los recursos de investigación del *Journal Citation Reports* (JCR). El compendio de publicaciones de la presente Tesis Doctoral se conforma por un total de 3 artículos. El título y orden de presentación de dichos artículos se muestra en la Tabla 1.

Tabla 1. Relación de artículos científicos del compendio de publicaciones

Numeración	Título
Artículo 1	Simulation platform for the assessment of PEM electrolyzer models oriented to implement digital Replicas
Artículo 2	Data acquisition and monitoring system framed in Industrial Internet of Things for PEM hydrogen generators
Artículo 3	PEM Electrolyzer Digital Replica based on internal resistance determination applied to hydrogen energy storage

1.4.2. Artículos indexados en *Journal Citation Reports*

A continuación, se listan la totalidad de artículos científicos publicados durante el desarrollo de la Tesis Doctoral. Entre las publicaciones, se diferencian los artículos incluidos en el compendio de publicaciones (documentos anexos).

González I., Calderón A.J., Folgado F.J., IoT real time system for monitoring lithium-ion battery long-term operation in microgrids, Journal of Energy Storage, 2022; 51: 104596. DOI: 10.1016/j.est.2022.104596

Anexo-I Folgado F.J., González I., Calderón A.J., Simulation platform for the assessment of PEM electrolyzer models oriented to implement digital Replicas, Energy Conversion and Management, 2022; 267: 115917. DOI: 10.1016/j.enconman.2022.115917

Anexo-II Folgado F.J., González I., Calderón A.J., Data acquisition and monitoring system framed in Industrial Internet of Things for PEM hydrogen generators, Internet of Things, 2023; 22: 100795. DOI: 10.1016/j.iot.2023.100795

Anexo-III Folgado F.J., González I., Calderón A.J., PEM Electrolyzer Digital Replica based on internal resistance determination applied to hydrogen energy storage, Journal of Energy Storage, 2024; 75: 109694

1.4.3. Contribuciones a congresos

A lo largo del desarrollo de la presente Tesis Doctoral, se ha participado en congresos de índole nacional e internacional, como se indica a continuación.

- Folgado F.J., Calderón A.J., González I. Calderón M., Portalo J.M., Orellana D., Design of a Simulation Platform to Test the Suitability of Different PEM Electrolyzer Models to Implement Digital Replicas, presented at: The 11th International Conference on Simulation and Modeling Methodologies, Technologies and Applications (SIMULTECH 2021), Proceedings of the 11th International Conference on Simulation and Modeling Methodologies, Technologies and

Applications (SIMULTECH 2021), 07-09 July, 2021. Online. SCITEPRESS, p. 430-437 ISBN: 978-989-758-528-9. DOI: 10.5220/0010582104300437

- González I., Folgado F.J., Calderón D., Calderón A.J., Lithium-ion battery integration in microgrid: Communication network for energy management through SOC-based intelligent control algorithms, presented at: XVI Simposio CEA de Control Inteligente, Actas del XVI Simposio de Control Inteligente, 01-03 December, 2021. Las Palmas de Gran Canaria, Canarias, España. p. 21-23. ISBN: 978-84-09-36817-4

- Folgado F.J., González I., Calderón M., Calderón A.J., Graphical user interface based on Matlab for simulation of electrolyzers, presented at: XVI Simposio CEA de Control Inteligente, Actas del XVI Simposio de Control Inteligente, 01-03 December, 2021. Las Palmas de Gran Canaria, Canarias, España. p. 15-19. ISBN: 978-84-09-36817-4

- Folgado, F.J., González I., Calderón A.J., Studying Matlab Appdesigner as alternative tool for teaching industrial monitoring/supervision, presented at: The 16th annual International Technology, Education and Development Conference (INTED 2022), INTED2022 Proceedings, 07-08 March, 2022. Online. IATED Academy, p. 2892-2898. ISSN: 2340-1079. ISBN: 978-84-09-37758-9. DOI: 10.21125/inted.2022

- Calderón A.J., González I., Folgado F.J., Introducing digital twins in automation and robotics laboratory sessions, presented at: The 16th annual International Technology, Education and Development Conference (INTED 2022), INTED2022 Proceedings, 07-08 March, 2022. Online. IATED Academy, p. 2709-2715. ISSN: 2340-1079. ISBN: 978-84-09-37758-9. DOI: 10.21125/inted.2022

- Folgado F.J., Orellana D., González I., Calderón A.J., Processes supervision system for green hydrogen production: Experimental characterization and data acquisition of PEM electrolyzer, presented at: The 1st International Electronic Conference on Processes: Processes System Innovation, Engineering Proceedings, 17-31 May, 2022. Online. MDPI/Processes, 19(1)-36. DOI: 10.3390/ECP2022-12651

- Folgado F.J., González I., Calderón A.J., PEM electrolyzer digital twin embedded within MATLAB-based graphical user interface, presented at: The 1st International Electronic Conference on Processes: Processes System Innovation, Engineering Proceedings, 17-31 May, 2022. Online. MDPI/Processes, 19(1)-21. DOI: 10.3390/ECP2022-12676

- Folgado F.J., González I., Fernández J.F., Orellana D., Calderón A.J., Data aggregator implemented through industrial gateway IOT 2050 for smart microgrid, presented at: XVII Simposio CEA de Control Inteligente, Actas del XVII Simposio de Control Inteligente, 27-29 June, 2022. León, Castilla y León, España. p.24-27. ISBN: 978-84-18490-65-1. DOI: 10.18002/simceaci

- González I., Folgado F.J, Orellana, D. Calderón D., Calderón A.J., PV panel monitoring system for cell temperature analysis and comparison by embedded models, presented at: XVII Simposio CEA de Control Inteligente, Actas del XVII Simposio de Control Inteligente, 27-29 June, 2022. León, Castilla y León, España. p.42-46. ISBN: 978-84-18490-65-1. DOI: 10.18002/simceaci

- Folgado F.J., González I., Orellana D., Calderón D., Calderón A.J., Web-based HMI for renewable energies microgrid through Grafana environment, presented at: XVII Simposio CEA de Control Inteligente, Actas del XVII Simposio de Control Inteligente, 27-29 June, 2022. León, Castilla y León, España. p.116-119. ISBN: 978-84-18490-65-1. DOI: 10.18002/simceaci

- Folgado F.J., Orellana D., González I., Calderón A.J., Integration framework for sensor through IoT embedded microcontroller in automation system for hydrogen generator management, presented at: XLIII Jornadas de Automática, Libro de Actas XLIII Jornadas de Automática, 07-09 September, 2022. Logroño, La Rioja, España. p.1063-1069. ISBN: 978-84-9749-841-8. DOI: 10.17979/spudc.9788497498418

- González I., Folgado F.J., Calderón A.J., Visualisation and analysis of digital and analog temperature sensors in PV generator through IoT software, presented at: The 9th International Electronic Conference on Sensors and Applications, Engineering Proceedings, 01-15 November, 2022. Online. MDPI/Sensors, 27(1)-59. DOI: 10.3390/ecsa-9-13283

- Folgado F.J., González I., Calderón A.J., Safety measures for hydrogen generation based on sensor signal algorithms, presented at: The 9th International Electronic Conference on Sensors and Applications, Engineering Proceedings, 01-15 November, 2022. Online. MDPI/Sensors, 27(1)-24. DOI: 10.3390/ecsa-9-13284

- González I., Calderón A.J., Folgado F.J., IoT software for industrial monitoring in supervisory systems course: initial experience with Grafana, presented at: 17th annual International Technology, Education and Development Conference (INTED 2023), INTED2023 Proceedings, 06-08 March, 2023. Online. IATED Academy, p. 4925-4931. ISSN: 2340-1079. ISBN: 978-84-09-49026-4. DOI: 10.21125/inted.2023

- Folgado F.J., González I., Calderón A.J., First steps on the educational use of node-red as industrial 4.0 middleware for automation and supervision disciplines, presented at: 17th annual International Technology, Education and Development Conference (INTED 2023), INTED2023 Proceedings, 06-08 March, 2023. Online. IATED Academy, p. 4884-4890. ISSN: 2340-1079. ISBN: 978-84-09-49026-4. DOI: 10.21125/inted.2023

- Calderón D., Folgado F.J., González I., Calderón A.J., Characterization of PEM Fuel Cell in the Context of Smart Microgrids Involving Renewable Energies, presented at: The 2nd International Electronic Conference on Processes: Process Engineering—Current State and Future Trends (ECP 2023), Engineering Proceedings, 17-31 May, 2023. Online. MDPI/Processes, 37(1)-55. DOI: 10.3390/ECP2023-14634

- Folgado F.J., González I., Calderón M., Calderón D., Calderón A.J., IoT Monitoring Solution for a Middle-Scale Grid Powered by PV Solar Tracker, presented at: The 2nd International Electronic Conference on Processes: Process Engineering—Current State and Future Trends (ECP 2023), Engineering Proceedings, 17-31 May, 2023. Online. MDPI/Processes, 37(1)-40. DOI: 10.3390/ECP2023-14635

- Calderón A.J., Folgado F.J., Calderón D., González I., Application of a Simulation Platform for the Study and Experimental Comparison of PEM Electrolyzer Models, presented at: The 20th International Conference on Informatics in Control, Automation and Robotics (ICINCO 2023), Proceedings of the 20th International Conference on Informatics in Control, Automation and Robotics (ICINCO 2023), 13-15 November, 2023. Rome, Italy. Volume 2, pages 289-296. ISBN: 978-989-758-670-5. ISSN: 2184-2809. DOI: 10.5220/0012202800003543

1.5. Contenido y estructura de la tesis

La Tesis Doctoral se ha estructurado en 5 capítulos cuyo contenido se resume a continuación.

Capítulo 1, *Introducción*. Se describe el contexto científico en el cual se enmarca la Tesis Doctoral, así como la coherencia e importancia unitaria de los trabajos realizados y presentados a partir de artículos científicos.

Capítulo 2, *Objetivos*. Se expone el objetivo general de la Tesis Doctoral, así como los objetivos parciales planteados para lograr dicho objetivo general.

Capítulo 3, *Descripción de publicaciones*. Se presentan las tres publicaciones que conforman el compendio de artículos de la Tesis Doctoral, mostrando los indicios de calidad de las publicaciones y un resumen de cada uno.

Capítulo 4, *Resultados y discusión*. Se describen y discuten los resultados presentados en los artículos científicos del compendio de publicaciones de la Tesis Doctoral.

Capítulo 5, *Conclusiones*. Se describen las conclusiones de la Tesis Doctoral y se exponen las posibles líneas de trabajo futuras derivadas de la investigación.

Los Anexos I, II y III cierran la memoria de esta Tesis, incluyendo una copia completa de los artículos que conforman el compendio de publicaciones.

Capítulo 2. Objetivos

2.1. Objetivo general

La presente Tesis Doctoral tiene como objetivo general el desarrollo de herramientas orientadas al estudio de electrolizadores PEM, con el fin de implementar una réplica digital de un electrolizador enmarcado en una smart microgrid basada en energías renovables e hibridada con hidrógeno. En relación con las herramientas mencionadas, la Tesis Doctoral versa sobre el diseño, desarrollo e implementación de una plataforma de simulación multi-modelo, un sistema de monitorización y una réplica digital dedicada a electrolizadores PEM. Por un lado, la plataforma de simulación facilita el estudio teórico de la operación del electrolizador PEM por medio de un entorno gráfico intuitivo y de fácil manejo, permitiendo realizar múltiples simulaciones y comparar los resultados obtenidos entre los diversos modelos disponibles. Por otro lado, el sistema de monitorización permite visualizar el comportamiento del electrolizador PEM instalado en la smart microgrid y registrar datos experimentales de su funcionamiento. Por último, los resultados obtenidos a partir de la aplicación de estas herramientas permiten el diseño y desarrollo de la réplica digital del electrolizador PEM.

2.2. Objetivos parciales

El objetivo general de la Tesis Doctoral se encuentra divido en 6 Objetivos Parciales (OP), a partir de los cuales se genera una estructura secuencial de hitos que reflejan en mayor detalle el alcance de la investigación:

Objetivo Parcial 1 (OP 1): Identificación y estudio de modelos de electrolizadores PEM para comprender su funcionamiento teórico, y selección de modelos para su implementación en el simulador multi-modelo.

Objetivo Parcial 2 (OP 2): Diseño de la interfaz gráfica de usuario, programación y validación del simulador multi-modelo.

Objetivo Parcial 3 (OP 3): Desarrollo de la infraestructura de adquisición y almacenamiento de datos para el sistema de monitorización.

Objetivo Parcial 4 (OP 4): Diseño de la interfaz gráfica e implementación del sistema de monitorización del electrolizador PEM físico. Validación del sistema y adquisición de datos experimentales.

Objetivo Parcial 5 (OP 5): Filtrado, comparación y análisis de datos simulados y experimentales del electrolizador PEM para diseño de réplica digital

Objetivo Parcial 6 (OP 6): Ejecución de ensayos experimentales y análisis de resultados obtenidos para desarrollo de modelo de electrolizador PEM. Validación de la réplica digital del electrolizador PEM instalado en la smart microgrid.

El diagrama de la Figura 3 representa la estructura secuencial de estos objetivos parciales y su desarrollo para completar el objetivo general de la Tesis Doctoral.

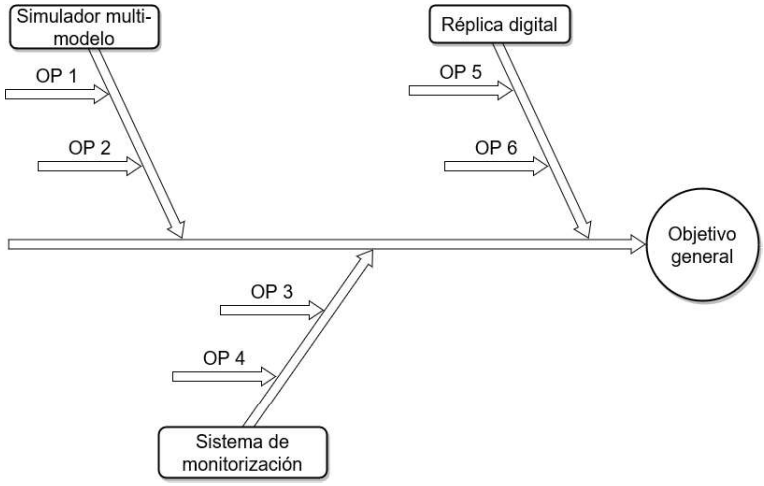

Figura 3. Objetivos de la Tesis Doctoral. Estructura secuencial y objetivos parciales.

Capítulo 3. Descripción de las publicaciones

A continuación, se exponen los tres artículos científicos que conforman el compendio de publicaciones de la presente Tesis Doctoral, indicando los datos editoriales, los indicios de calidad y un resumen de su contenido.

3.1. Simulation platform for the assessment of PEM electrolyzer models oriented to implement digital Replicas

3.1.1. Datos editoriales

Título	Simulation platform for the assessment of PEM electrolyzer models oriented to implement digital Replicas				
Autores	Francisco Javier Folgado Gaspar, Isaías González Pérez y Antonio José Calderón Godoy				
Revista	Energy Conversion and Management			**Año**	2022
Volumen	267	**Página**	115917	**Editorial**	Elsevier
DOI	10.1016/j.enconman.2022.115917			**ISSN**	1879-2227

3.1.2. Indicios de calidad

Fuente de impacto	Web of Science (WOS) / Journal Citation Reports	**Índice de Impacto**	10.4
Categoría	Energy & Fuels	**Cuartil**	Q1
Posición de la revista en la categoría	17	**Número de revistas en la categoría**	119
Citas en Web of Science	13	**Citas en Scopus**	14
Citas en Google Scholar	19	**Citas en ResearchGate**	15

3.1.3 Resumen

Este artículo presenta el desarrollo e implementación de una plataforma de simulación basada en MATLAB/Simulink dedicada al análisis de modelos de electrolizadores PEM. A su vez, dicha plataforma incluye una interfaz gráfica de usuario diseñada a partir de la toolbox *App Designer* de MATLAB, mediante la cual el usuario puede controlar la plataforma de simulación y visualizar los resultados obtenidos.

El principio de funcionamiento de la plataforma de simulación reside en la interacción entre tres entornos: Simulink, el espacio de trabajo de MATLAB (*Workspace*), y la interfaz gráfica. En el entorno Simulink se recrean los cuatro modelos seleccionados de la bibliografía revisada y que forman parte de los modelos disponibles en la plataforma de simulación. La interfaz gráfica permite al usuario ejecutar simulaciones de los modelos, visualizar y comparar los resultados obtenidos e incluso modificar los parámetros característicos del modelo seleccionado. Por último, el *Workspace* de MATLAB sirve como una base de datos temporal que permite intercambiar información entre el resto de los entornos.

Los modelos empleados en el entorno Simulink están basados en modelos de circuito equivalente. Dichos modelos describen el comportamiento del electrolizador mediante componentes eléctricos sencillos tales como resistencias, condensadores, fuentes de alimentación, etc. En el artículo, se aborda la descripción de las expresiones que relacionan estos componentes eléctricos con las variables clave del electrolizador PEM, tales como el voltaje, la corriente de entrada, el caudal de hidrógeno generado, el rendimiento o la potencia consumida.

A nivel de diseño, la interfaz gráfica se encuentra estructurada en diversas pestañas y su manejo reside en la navegación entre estas. La pestaña Principal muestra una serie de botones que permiten acceder a las pestañas específicas de cada Modelo o a la pestaña de Comparación de resultados. La pestaña del Modelo permite ejecutar simulaciones, modificar los parámetros del modelo y visualizar los resultados de forma gráfica mediante la representación de las curvas características del electrolizador. La pestaña de Comparación ofrece un espacio gráfico donde representar curvas características de diversos modelos.

Por último, se muestra y describe el funcionamiento completo de la plataforma de mediante un caso de simulación utilizando uno de los modelos disponibles. En este caso, se presentan cada una de las pestañas donde se muestran los resultados obtenidos de la simulación, realizando un análisis de los mismos.

En la Figura 4 se ilustra el resumen gráfico o *graphical abstract* publicado junto al artículo. En esta figura se realiza una composición gráfica a partir de las figuras empleadas en el artículo con el fin de describir el funcionamiento de la plataforma de simulación multi-modelo.

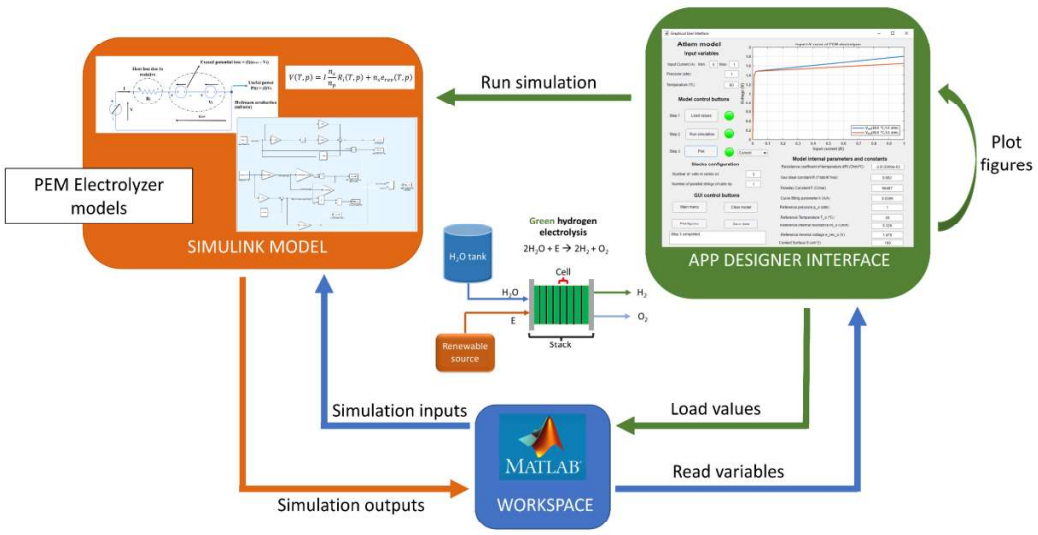

Figura 4. Resumen gráfico del artículo 1.

3.2. Data acquisition and monitoring system framed in Industrial Internet of Things for PEM hydrogen generators

3.2.1. Datos editoriales

Título	Data acquisition and monitoring system framed in Industrial Internet of Things for PEM hydrogen generators				
Autores	Francisco Javier Folgado Gaspar, Isaías González Pérez y Antonio José Calderón Godoy				
Revista	Internet of Things Engineering Cyber Physical Human Systems			**Año**	2023
Volumen	22	**Página**	100795	**Editorial**	Elsevier
DOI	10.1016/j.iot.2023.100795			**ISSN**	2543-1536

3.2.2 Indicios de calidad

Fuente de impacto	Web of Science (WOS) / Journal Citation Reports	**Índice de Impacto**	5.9
Categoría	Engineering, Electrical & Electronic	**Cuartil**	Q1
Posición de la revista en la categoría	53	**Número de revistas en la categoría**	275
Citas en Web of Science	8	**Citas en Scopus**	7
Citas en Google Scholar	11	**Citas en ResearchGate**	14

3.2.2. Resumen

Este artículo presenta el diseño, desarrollo e implementación de un sistema de adquisición de datos y monitorización para electrolizadores PEM. Para este fin, se ha dispuesto de un sistema de generación de hidrógeno verde por medio de un electrolizador PEM y un conjunto de dispositivos auxiliares para su funcionamiento.

El sistema desarrollado se ha estructurado siguiendo una arquitectura funcional de cuatro capas enmarcada en el Internet de las Cosas Industrial (*Industrial IoT, IIoT*), aplicando software propio del IoT en el entorno industrial, integradas con hardware y comunicaciones habituales en dicho entorno.

Como paso inicial, se describen los componentes que forman parte del sistema de generación de hidrógeno, así como el conjunto de sensores que permiten la medición de las variables clave del electrolizador. Esta información es recopilada y centralizada en tiempo real por medio de un autómata programable (*Programmable Logic Controller*, *PLC*).

A continuación, se utiliza Node-RED para realizar la lectura de los datos medidos y recogidos en el PLC. Node-RED es un middleware IoT caracterizado por su versatilidad de funciones y programación gráfica basada en bloques o nodos. Este software realiza la lectura de datos desde el PLC por medio del protocolo de comunicación *Modbus Transmisión Control Protocol/Internet Protocol* (TCP/IP) para almacenarlo en una base de datos a través del lenguaje de programación *Structured Query Language* (SQL).

La información del electrolizador es almacenada en MariaDB, una base de datos relacional de código abierto basada en MySQL. En esta base de datos, la información es guardada de manera estructurada mediante tablas y columnas.

Por último, se encuentra Grafana, un software IoT dedicado a la monitorización y representación por medio de datos almacenados en bases de datos. Dicho software presenta una interfaz gráfica customizable basada en elementos gráficos tales como diversos tipos de gráficas, indicadores numéricos, así como herramientas o *gadgets* instalables para ampliar sus funcionalidades. Estos elementos son distribuidos en un panel o *dashboard* para crear una interfaz gráfica de monitorización de las variables clave del electrolizador. Las gráficas presentadas en el *dashboard* agrupan variables relacionadas entre sí, como el voltaje y la corriente de entrada. Para determinar esta agrupación se ha empleado de un modelo, previamente estudiado, de tipo circuito equivalente del electrolizador.

Finalmente, se muestra el funcionamiento del sistema implementado y se describen los resultados observados en las distintas gráficas del *dashboard* para unas condiciones de operación nominal del electrolizador PEM.

En la Figura 5 se ilustra el resumen gráfico o *graphical abstract* publicado junto al artículo. En esta figura se realiza una composición gráfica a partir de las figuras empleadas en el artículo con el fin de describir la estructura de cuatro capas, así como el funcionamiento de cada una de las partes que componen el sistema de adquisición de datos y monitorización para el electrolizador PEM.

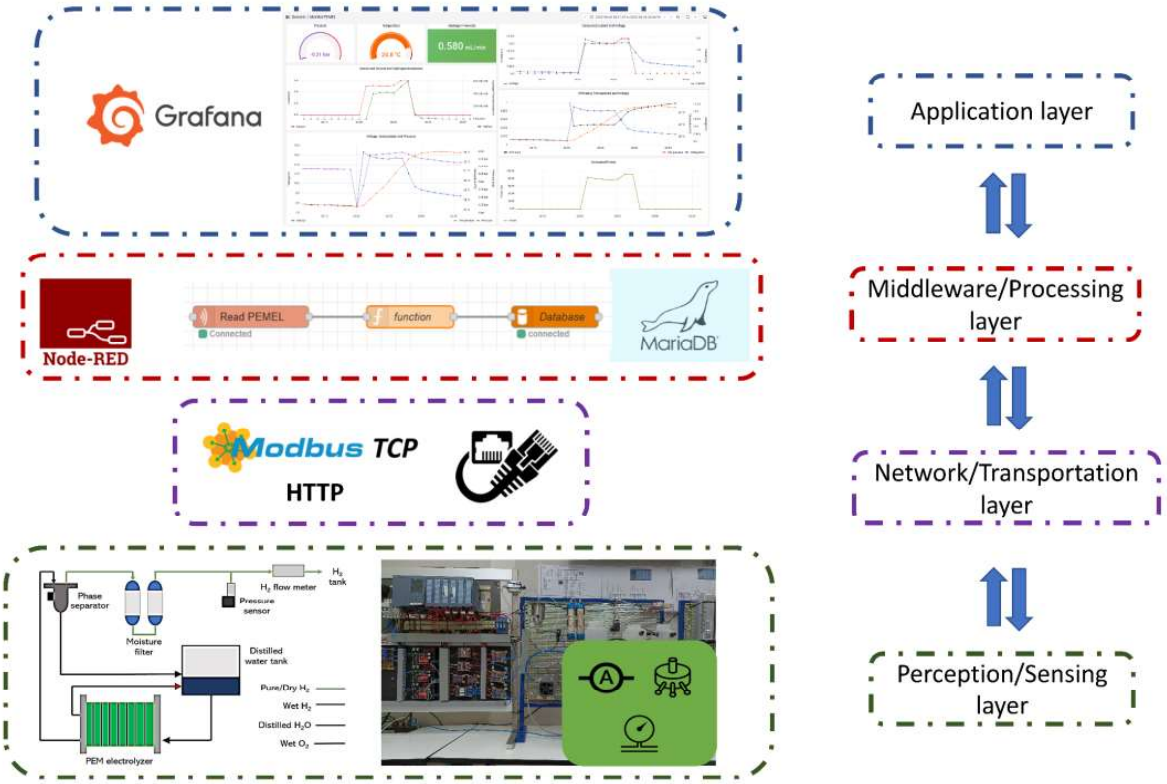

Figura 5. Resumen gráfico del artículo 2.

3.3. PEM Electrolyzer Digital Replica based on internal resistance determination applied to hydrogen energy storage

3.3.1. Datos editoriales

Título	PEM Electrolyzer Digital Replica based on internal resistance determination applied to hydrogen energy storage				
Autores	Francisco Javier Folgado Gaspar, Isaías González Pérez y Antonio José Calderón Godoy				
Revista	Journal of Energy Storage			**Año**	2024
Volumen	75	**Página**	109694	**Editorial**	Elsevier
DOI	10.1016/j.est.2023.109694			**ISSN**	2352-152X

3.3.2. Indicios de calidad

Fuente de impacto	Web of Science (WOS) / Journal Citation Reports	**Índice de Impacto**	9.4
Categoría	Energy & Fuels	**Cuartil**	Q1
Posición de la revista en la categoría	19	**Número de revistas en la categoría**	119
Citas en Web of Science	0	**Citas en Scopus**	0
Citas en Google Scholar	0	**Citas en ResearchGate**	0

3.3.3 Resumen

En este artículo se presenta el diseño y desarrollo de la réplica digital del electrolizador PEM utilizado en el sistema de apoyo basado en hidrógeno de la smart microgrid. Para ello, se dispone de una instalación de generación de hidrógeno verde por medio de un electrolizador compuesto por un conjunto o "stack" de 6 celdas conectadas en serie. Dicho stack se encuentra acompañado por sensores y actuadores que monitorizan y controlan el correcto funcionamiento de la instalación a partir de un PLC.

Para el desarrollo de la réplica digital, se plantea un modelo basado en un circuito equivalente que defina el comportamiento de cada una de las celdas que componen el stack. En este modelo, cada una de las celdas se encuentra caracterizada por el valor de su resistencia interna.

Para determinar la resistencia interna, se realizan ensayos de funcionamiento en diversos puntos de operación de temperatura y corriente de entrada, monitorizando el voltaje individual de cada celda. A continuación, se realiza un proceso de filtrado de datos y se utiliza la toolbox Curve Fitting de MATLAB para obtener la expresión que define el valor de la resistencia interna de cada celda para todo el rango de temperatura y corriente de entrada.

Una vez determinado el modelo de la celda PEM, se definen las expresiones relativas al funcionamiento del electrolizador, entendiendo este como el conjunto de las celdas que lo componen.

Por último, se realiza una validación del modelo de la celda PEM y de la réplica del electrolizador. Por un lado, se realiza una comparativa gráfica mediante las curvas obtenidas a partir de los datos experimentales y los obtenidos teóricamente por medio del modelo de la celda y la réplica del electrolizador. A su vez, esta comparativa es complementada con métricas estadísticas como el Error Cuadrático Medio

(*Root Mean Square Error*, RMSE), el Error Medio Absoluto (*Mean Absolute Error*, MAE) y el Coeficiente de Determinación (*Coefficient of Determination*, R^2).

En la Figura 6 se ilustra el resumen gráfico o *graphical abstract* publicado junto al artículo. En esta figura se realiza una composición gráfica a partir de las figuras, expresiones matemáticas y resultados mostrados en el artículo. Dicha composición tiene como objetivo plasmar cada una de las etapas ejecutadas para el desarrollo y validación de la réplica digital del electrolizador PEM.

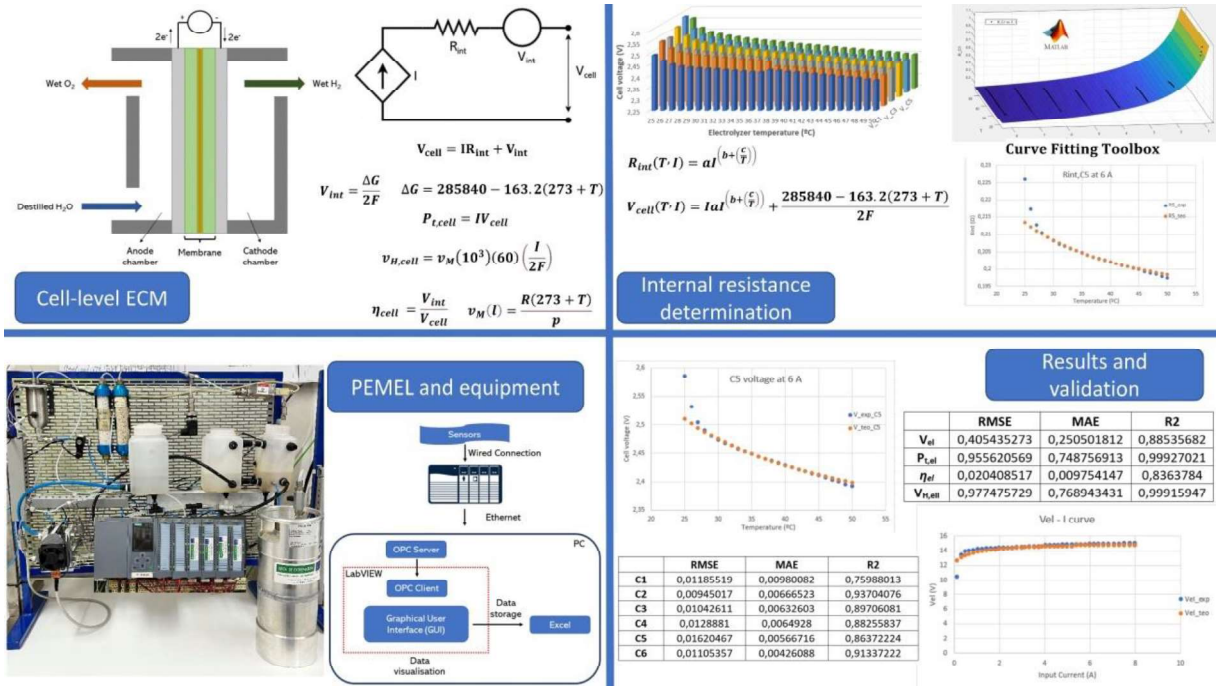

Figura 6. Resumen gráfico del artículo 3

.

Capítulo 4. Resultados y discusión

En este capítulo se describen y discuten los resultados presentados en los artículos científicos del compendio de publicaciones de la Tesis Doctoral.

4.1. Simulador multi-modelo

En el artículo 1 se aborda el diseño y desarrollo de la plataforma de simulación multi-modelo. Los resultados mostrados en dicho artículo se agrupan en torno a 3 pilares: el principio de funcionamiento del simulador, el manejo de la interfaz gráfica, y la implementación de la plataforma para el estudio de los modelos.

El principio de funcionamiento del simulador se basa en la interacción entre 3 entornos: Simulink, el *Workspace* de MATLAB, y la interfaz gráfica de usuario diseñada a partir de la toolbox *App Designer* de MATLAB. Estos entornos interactúan entre sí compartiendo información; Simulink aloja los modelos del electrolizador PEM y realiza la simulación, la interfaz gráfica facilita el control de dicha simulación y la visualización de los resultados, y el *Workspace* sirve como enlace entre ambos entornos para intercambiar información durante el proceso. El diagrama de la Figura 7 ilustra los entornos que forman parte del simulador, así como las diversas interacciones entre estos.

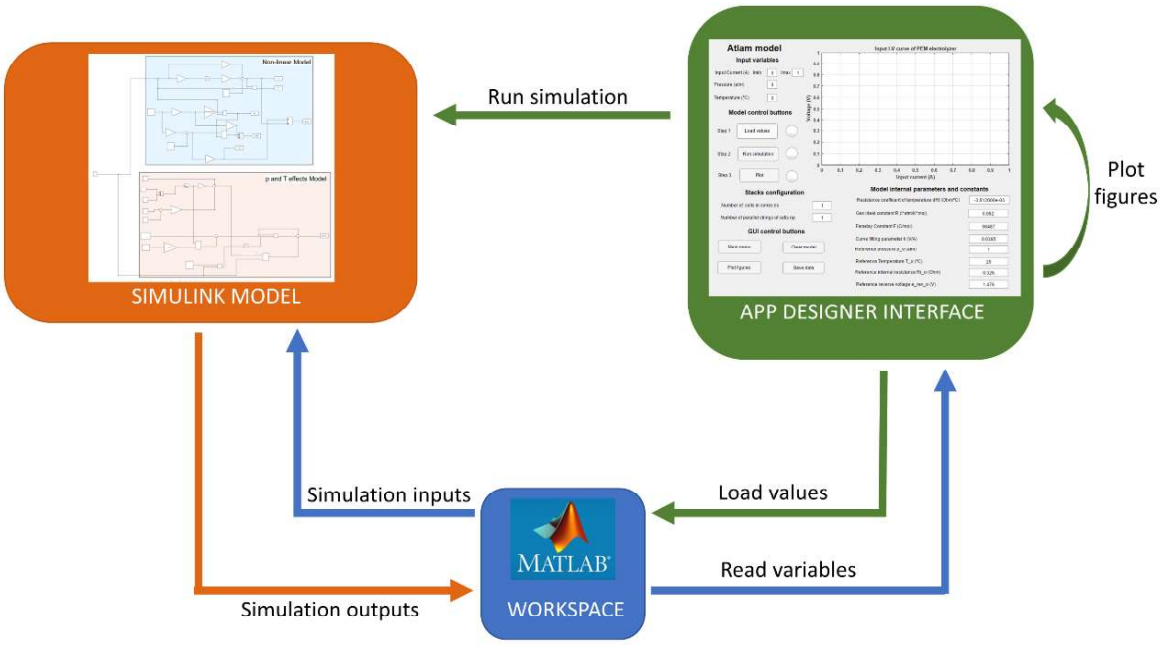

Figura 7. Interacciones entre entornos de la plataforma de simulación multi-modelo. (Fuente: Fig.5 artículo 1)

Este funcionamiento basado en entornos interconectados supone una dependencia entre estos durante la operación nominal del simulador, debido a la necesidad de intercambio de datos entre los entornos. No obstante, al sectorizar las funciones del simulador en entornos independientes, la configuración y programación de cada uno de estos puede ser abordada de manera individual.

Esta estructura basada en entornos permite realizar modificaciones y/o mejoras en un entorno específico sin afectar a la programación del resto de entornos. Por ejemplo, permite trabajar en el diseño de un nuevo modelo del electrolizador en Simulink, sin afectar al funcionamiento actual de la plataforma.

Como valor añadido, los 3 entornos se encuentran embebidos dentro del software MATLAB, lo que facilita la implementación de la herramienta al depender únicamente de un programa.

La operación del simulador multi-modelo es efectuada por el usuario mediante una interfaz gráfica. Dicha interfaz centraliza en un único entorno gráfico los elementos de control del simulador, los campos de entrada para la configuración de los modelos simulados, así como los elementos gráficos destinados a visualizar los resultados obtenidos tras las simulaciones.

En relación con la interacción usuario-interfaz, se ha optado por una estructura de navegación basada en pestañas debido a que presenta una serie de ventajas desde el punto de vista gráfico y funcional. A nivel gráfico, el uso de pestañas permite separar y agrupar los elementos gráficos comunes a cada uno de los modelos. De esta forma, la información es mostrada al usuario de una manera ordenada y clara. En la Figura 8 se muestra el aspecto de la pestaña principal de la interfaz del simulador. Los botones de dicha pestaña permiten realizar la navegación desde el menú principal hacia la pestaña deseada.

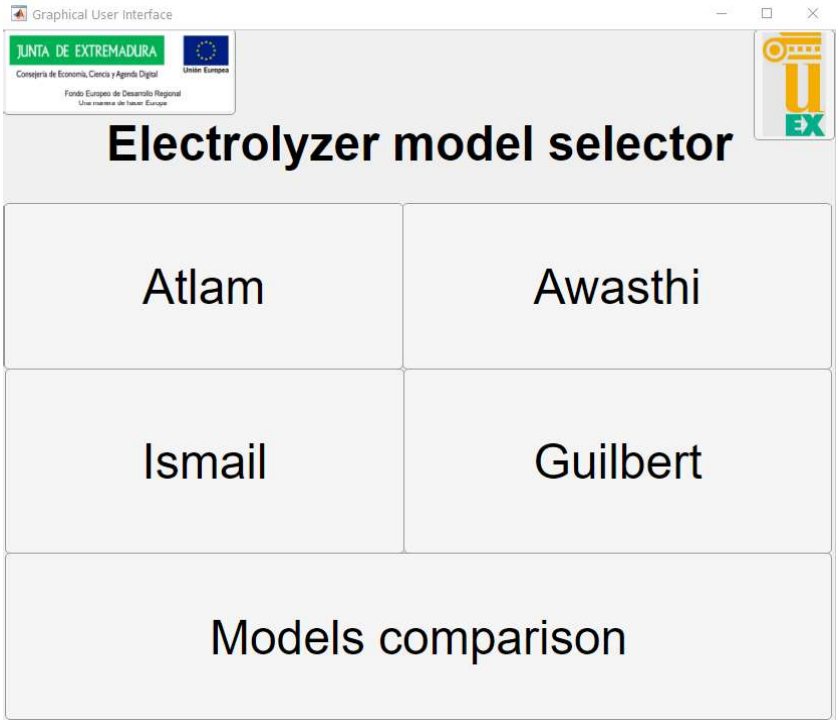

Figura 8. Pestaña principal de la interfaz del simulador multi-modelo (Fuente: Fig.11 artículo 1)

Desde un punto de vista funcional, la navegación por pestañas evita la interacción simultánea con elementos de diferentes pestañas. Esta restricción en la interactividad permite la creación de una disposición uniforme de elementos para todas las pestañas de los modelos. Dicha disposición uniforme ha sido implementada en las pestañas de los modelos, con el fin de facilitar el manejo de la interfaz por parte del usuario y minimizar las posibles confusiones o modificaciones no deseadas en un modelo particular. Como ejemplo de esta disposición, en la Figura 9 se visualiza la pestaña dedicada al modelo denominado *Atlam*.

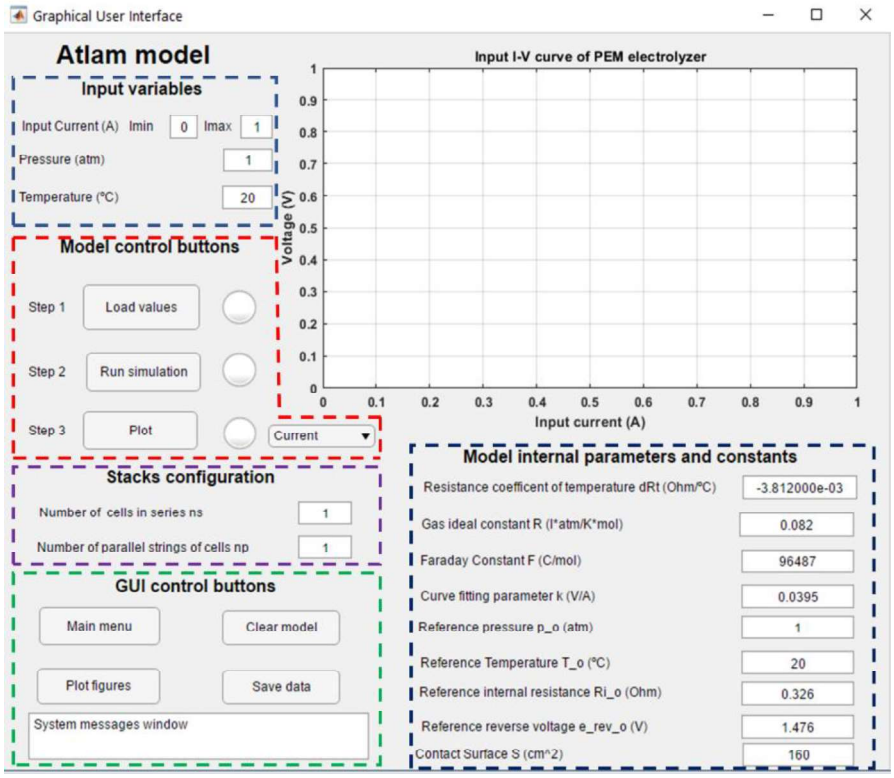

Figura 9. Disposición uniforme de controles y elementos gráficos en la pestaña de modelo. Ejemplo pestaña modelo *Atlam* (Fuente: Fig.12 artículo 1)

El objetivo principal del simulador reside en facilitar al usuario el estudio del funcionamiento de los electrolizadores PEM por medio simulaciones. Para ello, la plataforma dispone de un total de 4 modelos. La interfaz gráfica permite realizar simulaciones individuales de cada modelo, pudiendo incluso realizar múltiples simulaciones sobre el mismo modelo y comparar los resultados. Para simular diversos puntos de trabajo y configuraciones del electrolizador PEM, el usuario tiene a disposición para modificar las siguientes variables: Rango de corriente de entrada, presión y temperatura de trabajo, número de celdas en serie y número de celdas en paralelo.

Los resultados de estas simulaciones son mostrados en la interfaz únicamente de manera gráfica por medio de las curvas características que definen el comportamiento del electrolizador PEM. Estas curvas son plasmadas en diversos espacios gráficos repartidos entre la pestaña del modelo y una pestaña adicional propia del modelo llamada *Plot figures*. En la Figura 10a y 10b se visualiza el aspecto de las pestañas asociadas al modelo *Atlam* tras realizar dos simulaciones distintas.

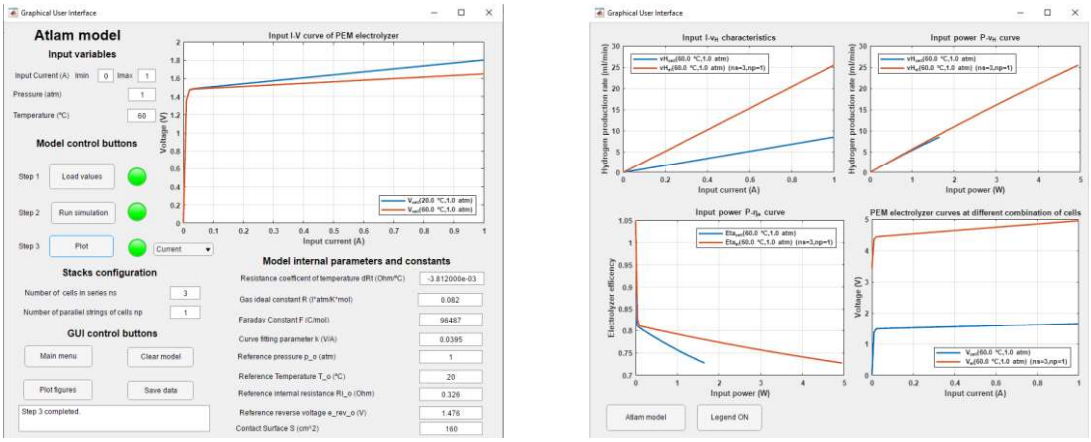

(a) **(b)**

Figura 10. Aspecto de las pestañas asociadas al modelo *Atlam* tras dos simulaciones. (a) Pestaña del modelo. (b) Pestaña *Plot figures* del modelo. (Fuente: Fig.17 y Fig.18 artículo 1)

De forma adicional, la plataforma de simulación cuenta con una función para exportar los datos de las simulaciones realizadas a un formato compatible con Excel. Para ello, cada pestaña del modelo cuenta con un botón *Save data* para almacenar los datos en el *Workspace* de MATLAB y realizar el proceso de exportación.

Como última funcionalidad, la interfaz gráfica presenta una pestaña dedicada a la comparación entre modelos (*Models comparison*). Dicha pestaña permite representar en un espacio gráfico común, las últimas simulaciones realizadas en cada modelo. Para ello, el usuario puede seleccionar la curva característica y los modelos que se desean comparar. En la Figura 11 se ilustra un caso de comparación para una curva característica donde se observan los 4 modelos del simulador.

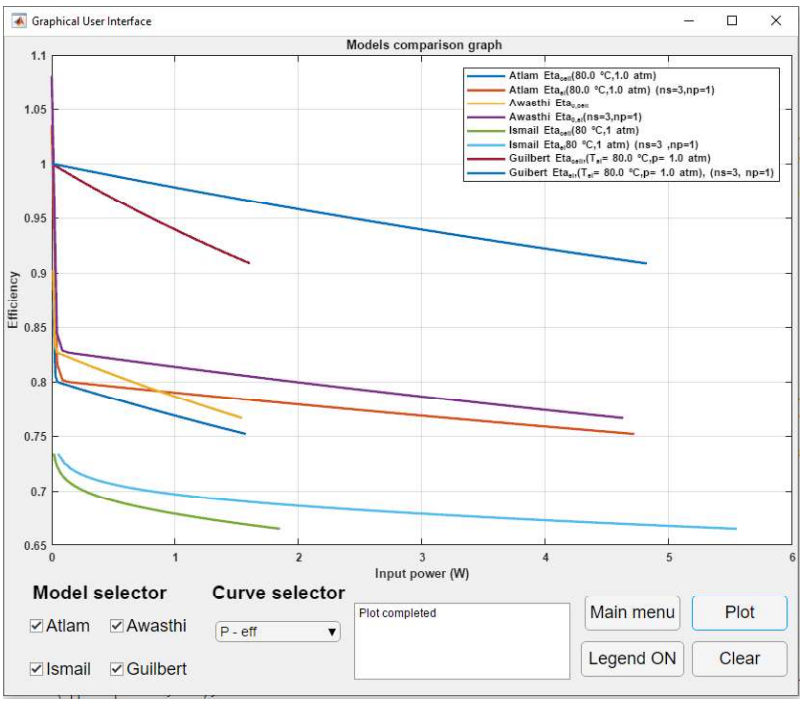

Figura 11. Comparación de modelos mediante representación de curvas características en pestaña *Models comparison*. (Fuente: Fig.23 artículo 1)

4.2. Sistema de monitorización

En el artículo 2 se aborda el diseño, desarrollo e implementación del sistema de adquisición de datos y monitorización dedicado a electrolizadores PEM. El funcionamiento de la herramienta es mostrado en dicho artículo en torno a la arquitectura IIoT de 4 capas utilizada para el desarrollo del sistema implementado. El diagrama de Figura 12 ilustra cada una de las capas de la arquitectura acompañadas de los elementos o entornos/programas incluidos en cada uno de ellos.

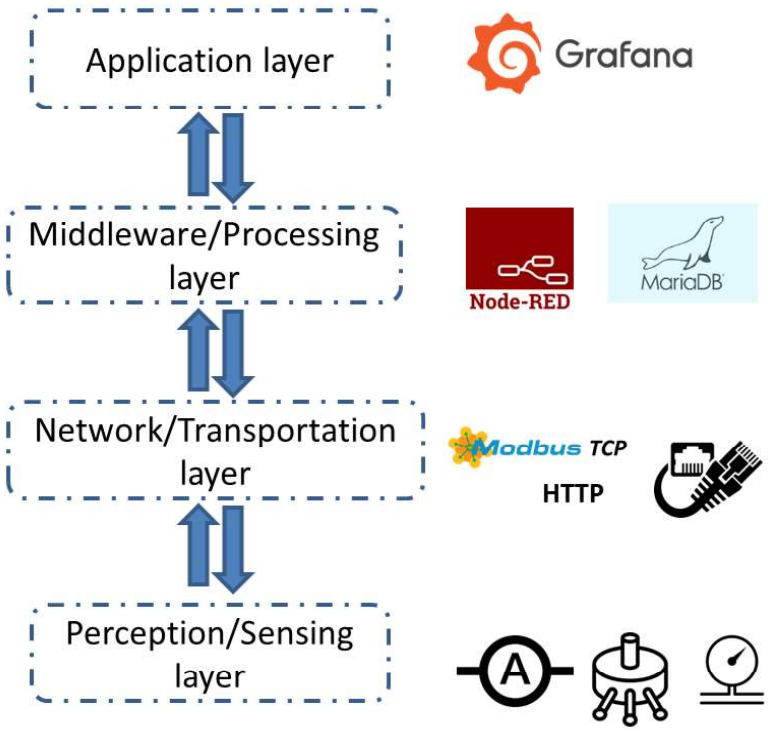

Figura 12. Arquitectura IIoT de 4 capas empleada para el sistema de adquisición de datos y monitorización. (Fuente: Fig.1 artículo 2)

En la capa de percepción/sensores se han agrupado todos los dispositivos, sensores y actuadores que acompañan al electrolizador PEM en la instalación experimental. Estos dispositivos controlan el funcionamiento del electrolizador y permiten recopilar información relacionada con sus variables clave. Con el objetivo de centralizar esta información, se decide instalar un PLC como sistema de adquisición de datos (*Data Acquisition, DAQ*). El uso de dispositivos comerciales de categoría industrial., como el autómata S7-1500 de Siemens, o diversos sensores y actuadores, asemejan la operación de la instalación experimental a la de una planta dentro de un entorno industrial.

Esta filosofía de trabajo en el entorno industrial se ve expandida en la capa de red/transporte. La información recopilada por el PLC es transmitida hacia entorno intermediario (middleware) donde se realiza el procesamiento de los datos. Dicho intercambio de datos es ejecutado por medio del protocolo *Modbus Transmision Control Protocol/Internet Protoco*l (Modbus TCP/IP). Este protocolo está ampliamente extendido, siendo considerado como uno de los protocolos estándar del ámbito industrial y del IoT. Por ende, el uso de Modbus TCP/IP en esta aplicación facilita la integración y comunicación con nuevos y dispositivos y entornos.

En la capa de middleware/procesamiento se encuentran los entornos de Node-RED y MariaDB. Por un lado, Node-RED es empleado como un middleware que realiza las funciones de: lectura de datos procedentes del PLC, procesamiento de los datos, y comunicación con MariaDB. Por otro lado, MariaDB es una base de datos cuya función principal consisten en el almacenamiento de los datos enviados por Node-RED. Este conjunto de programas son la base donde se sustenta el sistema de monitorización.

La capa de aplicación está protagonizada por el software Grafana, un entorno IoT dedicado a la monitorización de información almacenada en bases de datos por medio de elementos gráficos o paneles. En esta aplicación, Grafana es empleado como sistema de monitorización, donde se comunica con MariaDB para representar el conjunto de datos almacenados en la base de datos.

Node-RED, MariaDB y Grafana son programas dentro de la filosofía IoT y comparten diversas cualidades en común, como: software de código abierto (*Open-Source*), acceso gratuito, bajos requisitos computacionales, compatibilidad con diversos sistemas operativos, gran capacidad de intercomunicación con dispositivos y/o entornos, configuración y edición mediante un editor web, capacidad para ampliar funcionalidades mediante instalación de librerías gratuitas. El uso de este conjunto de software y las cualidades que presentan, ofrecen una serie de ventajas en el desarrollo de la herramienta:

- **Integración del software en un único dispositivo:** Los bajos requisitos computacionales de los entornos IoT descritos permiten su instalación conjunta en un dispositivo común, sin necesidad de un equipo de elevadas prestaciones.
- **Distribución del software en diversos dispositivos**: La elevada capacidad de intercomunicación del software empleado habilita la posibilidad de crear un sistema distribuido. En este sistema, se dispondría cada programa en un dispositivo individual, así como de una red de comunicación por medio de Ethernet y el protocolo Modbus TCP/IP. Esta tipología alternativa permite sectorizar las funciones en diversos dispositivos, manteniendo las mismas características y ventajas en el funcionamiento de la herramienta.
- **Versatilidad y mejora**: La instalación de nuevas funciones mediante el uso de librerías permite ampliar y/o mejorar las funciones existentes, dotando de versatilidad a la herramienta diseñada.
- **Configuración y edición en remoto:** Al disponer cada software de editor web, cada uno de los entornos es configurable desde un navegador web. Esta característica facilita el acceso y configuración de la herramienta desde cualquier dispositivo que tenga acceso a la red local y dirección IP del equipo donde se encuentra instalado el programa.

En los resultados del artículo se muestra el funcionamiento de la herramienta implementada a través del sistema de monitorización. La información recopilada de la instalación experimental es representada en

Grafana por medio de una única pantalla o *dashboard*. De esta manera, se facilita al usuario la visualización del estado de la instalación por medio de una interfaz clara y accesible. En la Figura 13 se observa el dashboard diseñado funcionando en tiempo real.

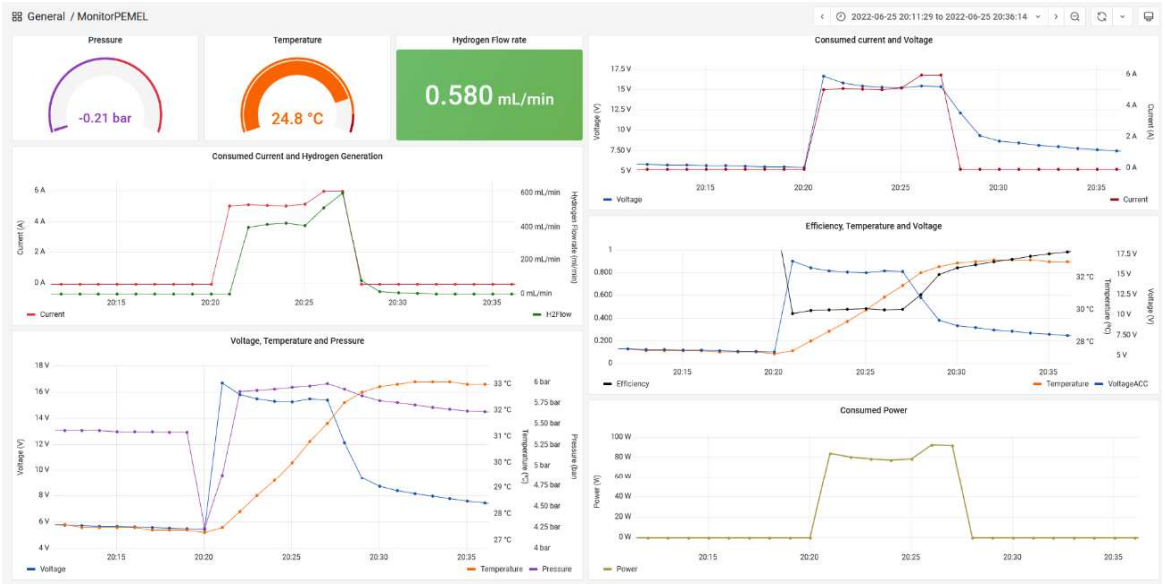

Figura 13. Sistema de monitorización implementado. *Dashboard* de Grafana en funcionamiento. (Fuente: Fig.6 artículo 2)

Con objeto de mejorar la inspección y estudio de la operación del electrolizador, se ha realizado una agrupación de variables clave en los diversos paneles tipo gráfica del dashboard. Dicha agrupación es resultado directo del análisis del funcionamiento del electrolizador por medio de las simulaciones realizadas en la plataforma de simulación. Concretamente, se ha utilizado el modelo denominado en el simulador como *Atlam* para identificar los parámetros clave del electrolizador, así como la relación entre estos. Algunos de estos parámetros, como la potencia consumida o la eficiencia del electrolizador, no pueden ser medidos directamente a través de sensores. Sin embargo, Grafana posee la capacidad de realizar operaciones y funciones matemáticas sobre los datos leídos de la base de datos. Esta funcionalidad permite calcular estos parámetros no medibles de forma indirecta a partir de otras variables.

Por último, en la Figura 14 se muestra la instalación experimental junto al sistema monitorización implementado funcionando durante la operación nominal de la planta.

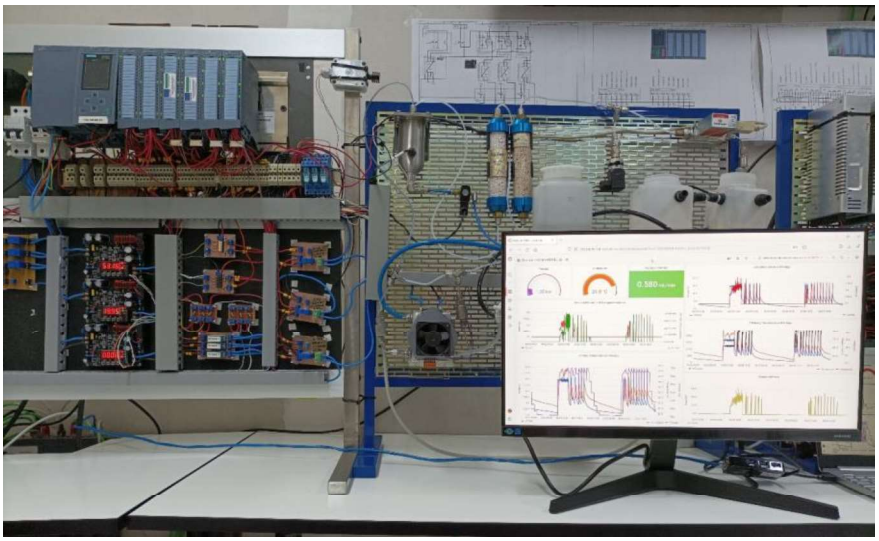

Figura 14. Instalación experimental junto a sistema de monitorización (Fuente: Fig.5 artículo 2)

4.3. Réplica digital

En el artículo 3 se describe el diseño y desarrollo de la réplica digital del electrolizador PEM integrado en el subsistema de apoyo de la smart microgrid. Los resultados mostrados en el artículo se agrupan en torno a 3 pilares: La instalación física donde se encuentra el electrolizador PEM, el desarrollo del modelo, y la validación del mismo.

El centro del sistema de generación de hidrógeno verde lo constituye un electrolizador PEM conformado por un stack de 6 celdas en serie. Dicho stack se encuentra alimentado con agua destilada y, a nivel eléctrico, mediante la corriente generada por el sistema primario de generación. El electrolizador se encuentra acompañado de sensores y actuadores que aseguran la correcta operación del sistema. A su vez, estos elementos garantizan la generación de hidrógeno de alta pureza (>99.9999%) para su posterior almacenamiento y uso en la pila de combustible tipo PEM. El diagrama de la Figura 15 ilustra el conjunto de elementos del sistema de generación de hidrógeno. De forma adicional, se observan los diversos flujos de productos y subproductos resultantes del proceso de electrólisis del agua.

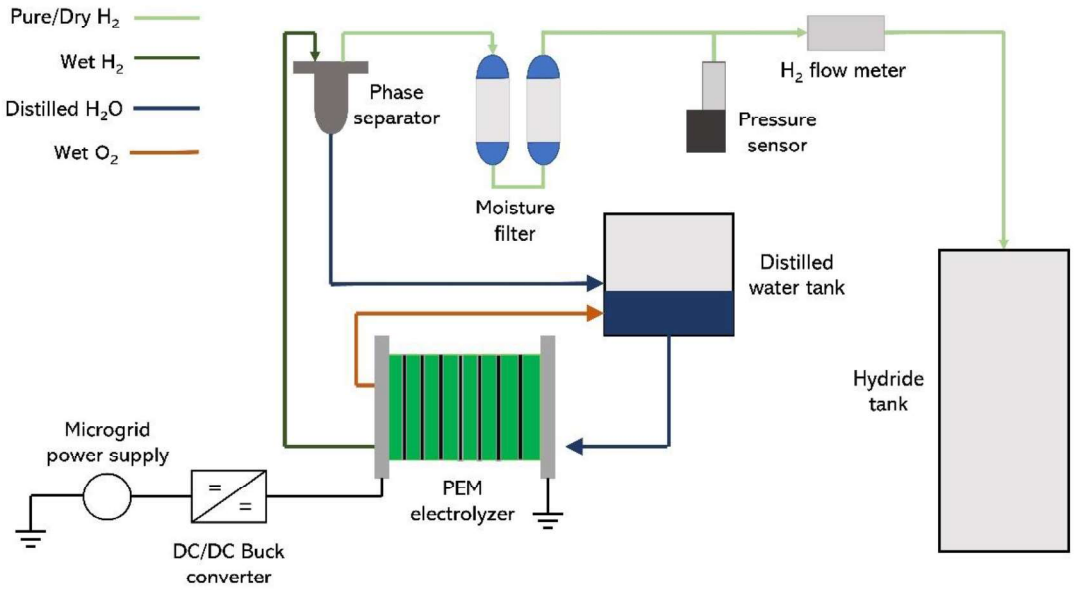

Figura 15. Sistema de generación de hidrógeno verde. Electrolizador PEM y elementos auxiliares. (Fuente: Fig.3 artículo 3)

La información proveniente de los sensores y actuadores de la instalación es recogida por un PLC que actúa como sistema de adquisición de datos. Seguidamente, dichos datos son enviados a una interfaz de usuario diseñada en LabVIEW que realiza las funciones de visualización en tiempo real de la planta y almacenamiento de datos mediante archivos de Excel. Esta comunicación es lograda mediante el protocolo *Open Platform Communications* (OPC). OPC es un protocolo de tipo cliente-servidor cuya tecnología es ampliamente utilizada en sistemas automatizados. El diagrama de la Figura 16 muestra el flujo de información desde los sensores en la instalación física hasta su almacenamiento en Excel.

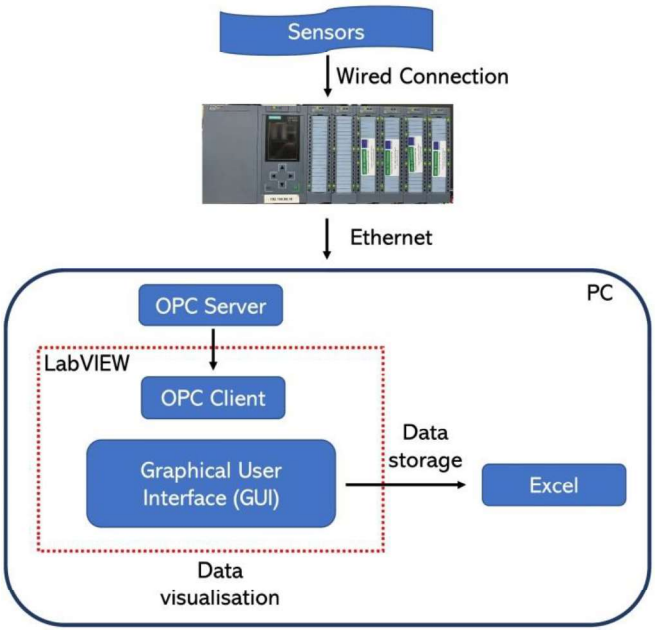

Figura 16. Sistema de adquisición de datos y flujo de información. (Fuente: Fig.5 artículo 3)

El modelo del electrolizador PEM ha sido desarrollado bajo una perspectiva a nivel de celda. Bajo este enfoque, el electrolizador es estudiado como un conjunto de celdas PEM interconectadas entre sí. Siguiendo esta premisa y, tras la revisión bibliográfica de diversos modelos, se plantea un modelo de circuito equivalente para una celda PEM. Dicho circuito simplificado está conformado por una fuente de corriente (I), una resistencia (R_{int}) y una fuente de tensión (V_{int}). En la Figura 17 se muestra el circuito equivalente de la celda PEM.

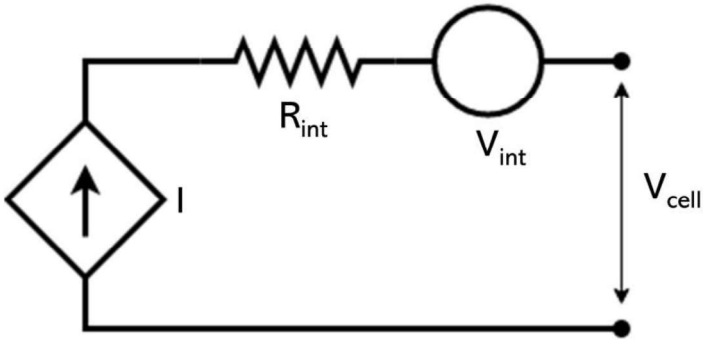

Figura 17. Modelo de circuito equivalente para celda PEM. (Fuente: Fig.6 artículo 3)

Donde:

- I hace referencia a la corriente consumida por la celda.
- R_{int} representa la disipación de potencia debido a la operación de la celda.
- V_{int} corresponde al voltaje ideal utilizado durante el proceso de electrólisis.
- V_{cell} indica el voltaje total entre los terminales de la celda.

La relación entre estos parámetros define el comportamiento de la celda PEM., permitiendo determinar otras variables clave como: la potencia total consumida ($P_{t,cell}$), la potencia útil empleada en la electrólisis ($P_{e,cell}$), el caudal de hidrógeno generado ($v_{H,cell}$), o la eficiencia de la celda (η_{cell}). Por un lado, las variables I y V_{cell} son medidas de manera directa por medio de sensores de corriente y voltaje, respectivamente. Por otro lado, las variables R_{int} y V_{int} son parámetros internos de la celda cuya medición directa resulta inviable. No obstante, dichas variables pueden ser calculadas de manera indirecta como relación de otros parámetros medibles.

Con objeto de definir y parametrizar el modelo propuesto para la celda PEM, se ha seguido una metodología secuencial basada en ensayos experimentales realizados sobre el stack de la instalación. Esta metodología tiene como objetivo principal el cálculo de la expresión, parametrizada para cada celda del stack, de la resistencia interna. A continuación, se enumeran los pasos o etapas seguidas en la metodología aplicada:

1. **Obtención de valores experimentales de $V_{cell}(T,I)$**. Ejecución de ensayos experimentales para obtener los valores de V_{cell} para todas las combinaciones de temperatura de trabajo (T) y corriente (I) dentro del rango nominal de operación del stack.
2. **Obtención de valores $R_{int}(T,I)$ para cada celda.** Cálculo de valores de resistencia interna (R_{int}) para todas las todas las combinaciones de temperatura de trabajo (T) y corriente (I) dentro del rango nominal de operación del stack.
3. **Determinación de la ecuación de ajuste general.** La representación gráfica de los valores de $R_{int}(T,I)$ revela un comportamiento similar de las celdas para un mismo punto de trabajo. Se emplea la herramienta ThreeDify XLGrapher de Excel para determinar la ecuación matemática de la superficie que mejor se ajusta a los datos experimentales obtenidos.
4. **Proceso de ajuste y obtención de ecuación parametrizada.** Se utiliza la herramienta o *toolbox* de MATLAB denominada *Curve Fitting* para obtener la expresión matemática parametrizada que define la resistencia interna de cada celda. Para ello, se hace uso de los valores experimentales obtenidos de $R_{int}(T,I)$ para cada celda, así como de la ecuación matemática determinada por la herramienta ThreeDify XLGrapher de Excel.

En la Figura 18 se resume de forma gráfica la metodología empleada mediante un diagrama de flujo.

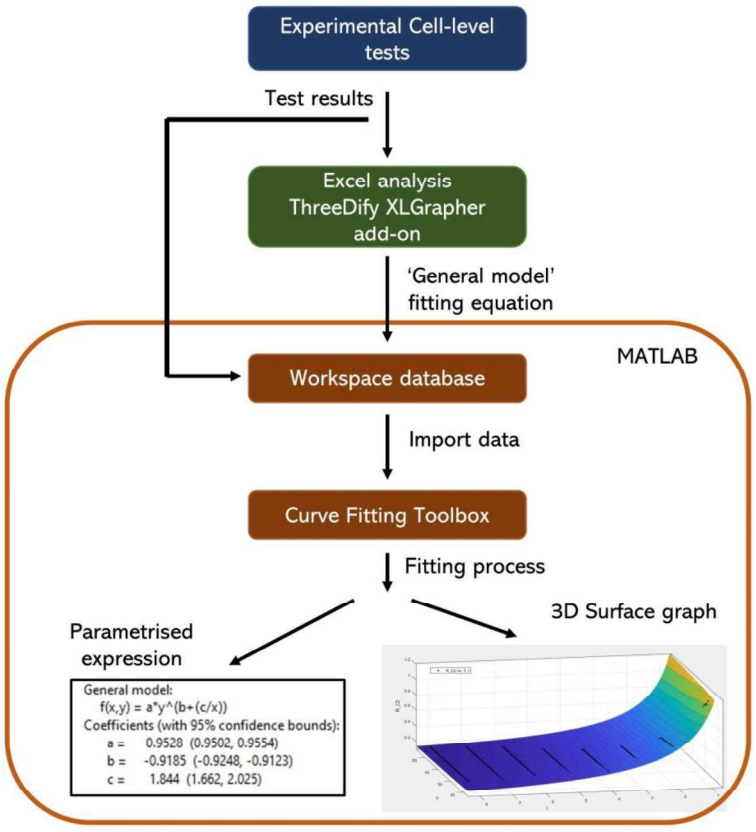

Figura 18. Metodología empleada para determinar la expresión de $R_{int}(T,I)$ para cada celda . (Fuente: Fig.10 artículo 3)

Tras obtener la expresión parametrizada que define la resistencia interna de cada celda, es posible calcular el resto de las variables clave que definen el modelo, como por ejemplo el voltaje de celda (V_{cell}). Las expresiones de $R_{int}(T,I)$ parametrizadas para cada celda han sido validadas mediante un proceso de comparación. Para este proceso se han comparado los valores experimentales de $R_{int}(T,I)$ obtenidos en los

ensayos, y valores teóricos calculados a partir de las expresiones determinadas por medio de la metodología seguida. De la misma forma, se ha realizado una comparación entre los valores experimentales de $V_{cell}(T,I)$, y los valores teóricos calculados mediante el modelo propuesto. Para ilustrar la idoneidad del proceso seguido, se muestra en la Figura 19 la comparación de valores realizada sobre la celda número 5 del stack PEM.

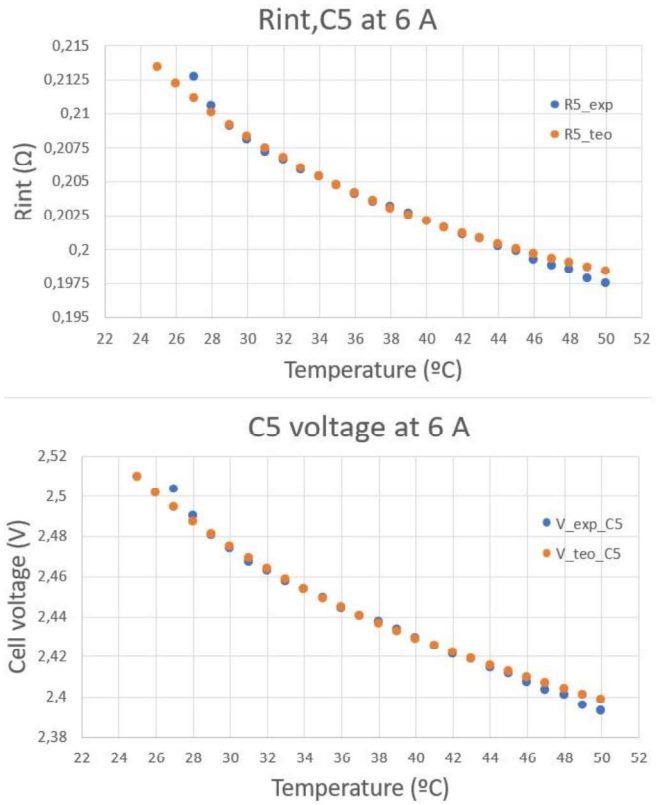

Figura 19. Comparación de valores experimental-teórico de $R_{int}(T,I)$ y $V_{cell}(T,I)$ para cada celda . (Fuente: Fig.11 (e) artículo 3)

Tras definir el modelo propuesto y obtener los parámetros clave a nivel de celda, se determinan las variables clave para el electrolizador PEM. Para ello, se ha tenido en cuenta la distribución y número de celdas del stack, así como la parametrización de cada una de estas. Como resultado se obtienen las curvas características del electrolizador. Estas curvas permiten visualizar la relación entre los parámetros clave del equipo y, por ende, definen el comportamiento del electrolizador. En la Figura 20 se muestra la curva característica V_{el}-I para todo el rango nominal de operación del electrolizador, donde se observa la similitud y proximidad entre los valores experimentales medidos y los obtenidos teóricamente por medio del modelo.

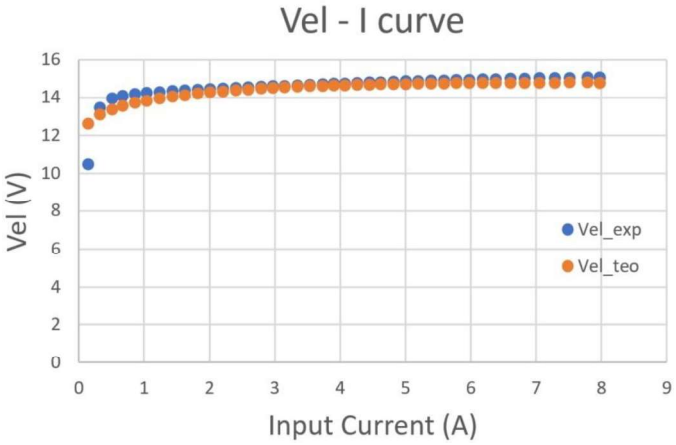

Figura 20. Curva característica V_{el}-I . (Fuente: Fig.12 artículo 3)

Los resultados mostrados en el artículo corroboran el correcto funcionamiento del modelo diseñado. Dicho modelo simula de manera eficaz y precisa el comportamiento del electrolizador PEM, así como el funcionamiento de cada una de las celdas que lo componen. De manera adicional, se describen en detalle la metodología, equipos y programas empleados en el desarrollo de la réplica digital. De esta forma se contextualiza el trabajo realizado y se facilita la reproducción del proceso seguido.

Capítulo 5. Conclusiones

En este capítulo se describen las conclusiones de la Tesis Doctoral y se exponen las posibles líneas de trabajo futuras derivadas de la investigación.

5.1. Conclusiones de la investigación

- Los trabajos realizados han supuesto una aportación significativa a los objetivos del Proyecto de investigación en el cual se encuentra enmarcada la Tesis Doctoral. El desarrollo de las herramientas planteadas, y con ello el estudio del electrolizador PEM integrado en la smart microgrid, ha facilitado el desarrollo de la réplica digital del subsistema de generación de hidrógeno verde. Con ello, se ha logrado replicar con éxito uno de los elementos clave de la microgrid.

- Se ha diseñado y desarrollado una plataforma de simulación multi-modelo dedicada al estudio de electrolizadores PEM. Dicha plataforma recoge un total de 4 modelos extraídos de la bibliografía científica, permitiendo la simulación, análisis y comparación del comportamiento de dichos modelos de manera individual o colectiva. Esta plataforma integra una interfaz de usuario donde se agrupan las funciones de configuración y simulación de los modelos, así como de visualización y comparación de los resultados obtenidos. La herramienta permite un control total sobre el modelo por parte del usuario, permitiendo la modificación de los parámetros que definen su comportamiento a través de la interfaz de usuario.

- Se ha diseñado y desarrollado un sistema de adquisición de datos y monitorización destinado al subsistema de generación de hidrógeno verde de la smart microgrid. Dicho sistema ha sido dedicado a la obtención de datos experimentales y visualización de la operación del electrolizador PEM integrado en el subsistema. El sistema se ha diseñado bajo una arquitectura IIoT de 4 capas mediante el uso de software de carácter IoT y *Open-Source*. La herramienta desarrollada destaca en aspectos como: Accesibilidad de implementación gracias al uso de software con bajos requisitos computacionales; facilidad de configuración y edición por medio de editores operados en web; integración de la información monitorizada en una interfaz de usuario sencilla y clara; versatilidad y ampliación de funciones mediante librerías.

- Se ha diseñado, desarrollado y validado una réplica digital del electrolizador PEM instalado en el subsistema de generación de hidrógeno de la smart microgrid. Para ello, se ha confeccionado un modelo a nivel de celda siguiendo una metodología basada en la determinación de la resistencia interna. Los datos requeridos para el diseño del modelo han sido obtenidos a partir de ensayos experimentales, los cuales han sido recopilados por medio de un sistema de adquisición de datos.

Los resultados obtenidos a nivel de celda y a nivel de stack han sido validados mediante un análisis comparativo gráfico y numérico. Dichos resultados muestran un funcionamiento satisfactorio y preciso de la réplica digital para todo el rango nominal de operación del electrolizador PEM físico.

- Durante el transcurso de la Tesis Doctoral, el Doctorando ha participado activamente en el desarrollo del proyecto de investigación donde se enmarca dicha Tesis Doctoral, así como en congresos de índole nacional e internacional. Esta actividad ha propiciado la búsqueda y experimentación con diversas tecnologías y aplicaciones, las cuales han facilitado el desarrollo de las herramientas objetivo de la presente Tesis Doctoral.

Como conclusión final del trabajo realizado se debe resaltar que se han cumplido los objetivos fundamentales que se pretendían alcanzar con la realización de esta Tesis Doctoral.

5.2. Trabajos futuros

- Ampliar el catálogo de modelos de electrolizador PEM disponibles en la plataforma multi-modelo. Con ello, se ampliaría la capacidad de análisis y comparación de la herramienta permitiendo visualizar resultados de un mayor número de modelos simulados.

- Añadir nuevas funcionalidades a la interfaz de usuario de la plataforma de simulación multi-modelo. Estas nuevas funciones podrían estar orientadas a mejorar la visualización de los resultados, permitiendo por ejemplo modificar el color de cada una de las curvas representadas en las gráficas. Otra funcionalidad podría dotar a la interfaz de la capacidad de exportar las gráficas representadas como archivos en formato de imagen. De esta manera, la plataforma permitiría exportar toda la información, ya sea numérica o gráfica, procedente de las simulaciones realizadas.

- Ampliar el sistema de adquisición de datos y monitorización implementado, haciéndolo extensible para todos los equipos integrados en la smart microgrid. La versatilidad de los programas IoT utilizados permiten la ampliación de la herramienta desarrollada para todos los elementos de la instalación física.

- Mejorar el comportamiento de la réplica digital diseñada mediante el estudio de la respuesta transitoria del electrolizador PEM físico. Con ello, se obtendría una réplica precisa y efectiva para el estado transitorio y estacionario del electrolizador PEM.

- Estudiar los efectos de degradación ocurridos en el electrolizador PEM. Existen diversas condiciones y modos de operación que afectan a la vida útil del electrolizador como, por ejemplo: la operación prolongada fuera de los rangos nominales de trabajo; el funcionamiento intermitente del equipo (apagado-encendido); el nivel de pureza del agua empleada en la electrólisis; o el número total de ciclos de operación. El uso de las herramientas desarrolladas y los resultados obtenidos pueden emplearse para estudiar los diversos mecanismos de degradación que ocurren en el electrolizador.

- Desarrollar las herramientas descritas en esta Tesis Doctoral para el estudio de otros equipos de la smart microgrid, como por ejemplo la pila de combustible tipo PEM o la batería de Ion-Litio.

A las líneas de investigación mencionadas habrá que añadir otras que surjan como consecuencia de nuevos avances en distintos ámbitos de la tecnología de los electrolizadores, de hardware y software IoT, de sistemas de adquisición de datos, y de sistemas o entornos de monitorización.

Anexo I

Referencia

Folgado F.J., González I., Calderón A.J., Simulation platform for the assessment of PEM electrolyzer models oriented to implement digital Replicas, Energy Conversion and Management, 2022; 267: 115917. DOI: 10.1016/j.enconman.2022.115917

Derechos de autor

Energy Conversion and Management 267 (2022) 115917

Contents lists available at ScienceDirect

Energy Conversion and Management

journal homepage: www.elsevier.com/locate/enconman

Simulation platform for the assessment of PEM electrolyzer models oriented to implement digital Replicas

Francisco Javier Folgado *, Isaías González, Antonio José Calderón

Department of Electrical Engineering, Electronics and Automation, Universidad de Extremadura, Avenida de Elvas, s/n, Badajoz 06006, Spain

ARTICLE INFO

Keywords:
Green hydrogen
PEM Electrolyzer
MATLAB/Simulink
Graphical user interface
Microgrid
Digital replica

ABSTRACT

This work presents the development and implementation of a simulation platform based on MATLAB/Simulink devoted to analysing the behaviour of Polymer Electrolyte Membrane (PEM) electrolyzer (PEMEL) models. A graphical user interface (GUI) designed in App Designer is included for controlling the platform and visualising simulation results. Through this GUI, the user is able to study the models hosted on the platform under various operating conditions, compare the results obtained and even modify the characteristic parameters of the models. The main objective of the platform is to facilitate the study of PEMEL for the development of a digital replica of a physical device housed in a smart microgrid. In these systems, PEMEL are integrated with renewable energy sources for the generation of green hydrogen, which is used as an energy carrier to cope with variations in demand in the medium and long term. The proposal overcomes the limitations identified in previous literature such as the absence of a GUI to facilitate model handling, model modification and the comparison and simulation of different models in the same application. The design and implementation of the simulation platform is reported along with a series of simulation cases to prove its feasibility and successful performance.

1. Introduction

In the last decade, hydrogen has taken a leading role in the development of multiple sectors [1]. The versatility of this element has led to an evolution in the technologies and applications associated with it, e.g. as a substitute for fossil fuels in the automotive sector [2]. The dependence on fossil fuels and the associated carbon emissions are also envisioned to be reduced with the utilization of hydrogen technology [3].

In the energy field, the integration of hydrogen as an energy carrier alongside renewable energies has encouraged the development of hydrogen-based systems together with smart grids and microgrids in recent years [4]. Hydrogen is applied to cope with the intermittency of renewable energies, as well as for long-term energy storage [5]. In this regard, the role of hydrogen is emphasised as a strategy within the Sustainable Development Goals of the UN. Namely, hydrogen is expected to support the achievement of the Goal 7, i.e. affordable and clean energy [6].

An electrolyzer is an electrochemical device that generates hydrogen by separating the elements of a compound. These devices are grouped according to their principle of operation, highlining alkaline, Polymer Electrolyte Membrane (PEM) and solid types. PEM electrolyzers (PEMEL) are widely used in combination with distilled water to produce high purity hydrogen. Moreover, this electrochemical process does not generate pollutant products, so by using a renewable energy source to power the PEMEL, the hydrogen generated is denoted as green hydrogen. PEMEL are integrated in renewable energy applications because of their high-speed response to changes in operating conditions [7].

Electrolyzer models are required to understand and study their electrochemical behavior as well as to evaluate their performance. In particular, Equivalent Circuit Models (ECM) are used in scientific literature to develop accurate models based on electrical laws and represent the behavior of complex equipment. In the scope of hydrogen generation, ECM are widely studied. Atlam and Kolhe [5] propose an ECM for PEMEL through experimental analysis on a single cell studied under steady-state conditions. The work in Awasthi et al. [8] depicts a MATLAB/Simulink-based model, separating the PEMEL into four parts: anode, cathode, membrane and voltage. For this purpose, the molar balance between cathode and anode is studied together with the Nest and Butler-Volmer equations. The behaviour of a PEMEL in a hybrid system of photovoltaic energy and hydrogen generation is studied in

* Corresponding author.
E-mail addresses: ffolgar@unex.es (F.J. Folgado), igonzp@unex.es (I. González), ajcalde@unex.es (A.J. Calderón).

https://doi.org/10.1016/j.enconman.2022.115917
Received 27 April 2022; Received in revised form 6 June 2022; Accepted 19 June 2022
Available online 25 June 2022

Table 1
Main features of previous literature.

Work	Type of model	Software	GUI	Customisation capabilities	Multiplicity of models
[5]	ECM	No	No	No	No
[8]	Equations without ECM	MATLAB/ Simulink	No	No	No
[9]	ECM/ Tafel's law	MATLAB	No	No	No
[10,11]	ECM/ Dynamic study	No	No	No	No
[13]	Equations without ECM	MATLAB/ Simulink	No	No	No
[12]	Equations without ECM	MATLAB/ Simulink	No	No	No
[37]	Equations without ECM	MATLAB	Yes	No	No
[38]	No	MATLAB	Yes	No	No
[39]	Faraday's law	MATLAB/ Simulink	Yes	No	No
Present	ECM	MATLAB/ Simulink	Yes	Yes	Yes

Ismail et al. [9]. In this context, the characteristic parameters of the electrolyzer are determined by means of an ECM and Tafel's law. In Guilbert and Vitale [10] and Guilbert et al. [11] models for PEMEL are developed and validated through experimental testing under dynamic operating conditions. The work described in Jansen et al. [12] implements Simulink models of hydrogen fuel cell and electrolyzer according to the Faraday's law in the context of an off-grid combination of PV generation, hydrogen and battery storage. In Virji et al. [13] a PEMEL model is implemented and simulated using MATLAB/Simulink.

Models are also required to develop Digital Replicas (DR) of physical equipment. The DR is framed within the Industry 4.0 paradigm and is referred to a virtual simulation that aims to mimic the real-time behaviour of the replicated device [14]. This virtual tool provides an ideal environment for testing the operating conditions of the device, isolating it from the rest of the components. DR are commonly model-driven approaches, i.e. they are based on mathematical models of the physical asset. As asserted in Mohammadshahi et al. [15], a virtualised model is the first step toward the implementation of a DR of the system.

In fact, DR are receiving a lot of attention from Academia and industry. The amount of works related to this paradigm is increasing daily [16,17], even in the form of patents [18]. It must be noted that most of publications are devoted to DR in industrial fields [19], whilst in energy-related systems there is a minor amount of research. Herein, recent works in the energy scenario are commented. DR of wind turbines are reported in Tao et al. [20] and González-González et al. [21]. Buildings are digitally mirrored in O'Dwyer et al. [22] from an energy perspective. A DR approach for microgrids is presented in Park et al. [23]. The work in Steindl et al. [24] proposes a general framework for DR in industrial energy systems. Applications of DR for energy services are reviewed in Onile et al. [25]. Digital replication of batteries under model-driven and data-driven approaches is studied in Wu et al. [26]. DR for electric vehicles are also studied in Van Mierlo et al. [27] and Bhatti et al. [28]. The use of DR to support decision making processes is presented in Granacher et al. [29] oriented towards energy systems design. However, there is not mention to hydrogen-related frameworks in the aforementioned works.

Therefore, there are very scarce works dealing with DR of PEMEL and fuel cells in literature. The most relevant ones are now briefly commented. Wang et al. [30] present a 3D model-based DR for PEM fuel cells. It uses a mathematical model which couples the heat and mass transport processes and the electrochemical kinetics. Also for PEM fuel cells, in Meraghni et al. [31] a data-driven replica is reported with prognostics purposes. In Ogumerem and Pistikopoulos [32] a DR of a PEMEL is presented using a mathematical model. The goal is to design a Model-based Predictive Controller (MPC) to regulate the thermal behavior of the electrolyzer. A DR of a 750 kW electrolyzer in a power Hardware in the Loop (HiL) scheme is developed in Jain et al. [33]. Among the future works in Jansen et al. [12], the authors point out the development of a DR of fuel cell and electrolyzer.

Consequently, there is a need of tools to model and simulate this type of complex device aiming at promoting the development and implementation of DR.

Moreover, when managing models of complex equipment, the models reported in literature are adjusted for specific system and simulated, without enabling customisation or edition. In this regard, such valuable models and simulation environments are closed in the sense that easy interaction with the user and customisation of the model parameters is not provided. This constitutes a drawback when the model must be adjusted to different devices, configurations or situations.

To overcome this limitation, a step beyond modeling consists of building a Graphical User Interface (GUI) to establish a user-friendly and intuitive interaction with the operator of the energy system. Commonly, a GUI is used to display graphical and numerical information of the facility, even with real-time capabilities. The role of GUI for energy-related applications is highlighted in recent literature [4,34–36]. In the case of simulation approaches, the GUI facilitates the adjustment and customisation of parameters as well as the graphical illustration of the simulated results.

This paper presents a simulation platform based on MATLAB/ Simulink for the study of various models of PEMEL. To achieve this purpose, a set of well-known PEMEL models are implemented and simulated in Simulink environment. Furthermore, the App Designer toolbox has been used to develop a GUI to visualise and customise the parameters of the different models and the generated results. Both environments are hosted and interconnected by MATLAB, sharing information during their operation.

Concerning energy-related approaches, MATLAB has been reported as versatile and powerful tool to deploy GUI but there are scarce works in literature about GUI related to PEMEL models. Particularly, MATLAB-based GUI for equipment devoted to generation and consumption of hydrogen are even scarcer. Illustrative examples of using MATLAB to implement GUI together with simulation capabilities are now commented. MATLAB GUI is used in Smaoui and Krichen [37] to deploy a simulation interface for a hybrid system combining PV and wind generation with hydrogen (fuel cell and electrolyzer). The user can simulate different time intervals but is not able to modify the implemented models. In Jafari and Malekjamshidi [38] MATLAB is applied to implement a GUI which displays and records data of a prototype of microgrid (PV and fuel cell). However, simulation is not considered in such research. A valuable contribution in the field of hydrogen equipment simulation is found in Vivas et al. [39], where MATLAB is used to make up a simulator for the hybridization of renewable energy sources with hydrogen. This simulator includes the model of an alkaline electrolyzer based on Faraday's law as well as a GUI.

For a clearest overview of previous research about PEMEL models and GUI, Table 1 summarizes the main features of the aforesaid literature and of the present work. Five categories have been considered, namely type of model, used software, implementation of GUI, availability of customisation capabilities and multiplicity of models.

According to the review of previous papers conducted by the authors, as can be checked in Table 1, to date there are no works that simulate and compare different models under a GUI with capabilities of easy interaction and fully customisation of the models. Consequently, the proposal constitutes a novelty in literature.

It must be remarked that the goal of this proposal is not to develop an own model of PEMEL, but to present a tool and methodology to facilitate analyses and comparisons between different models, widely tested and

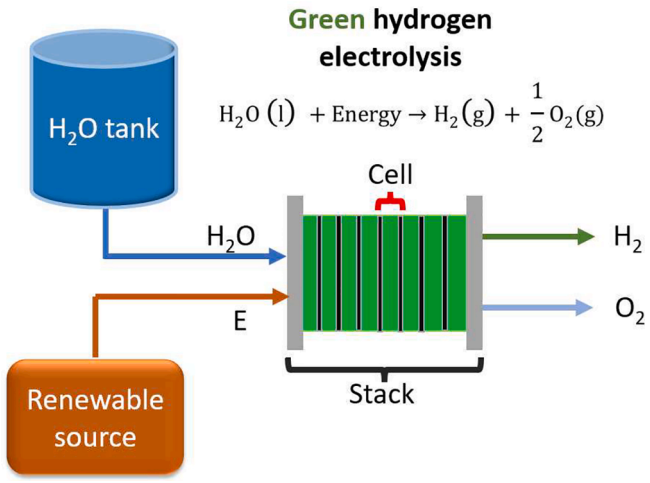

Fig. 1. Green hydrogen generation through PEM electrolyzer.

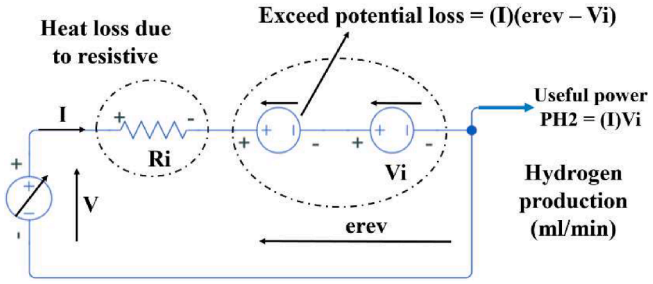

Fig. 2. ECM described in [5]. (Source: Own design).

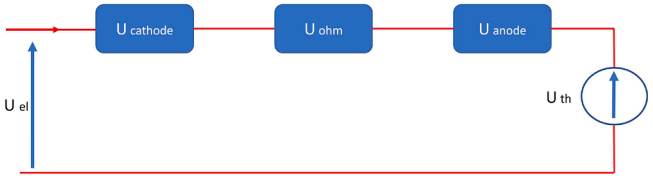

Fig. 3. ECM described in [9]. (Source: Own design).

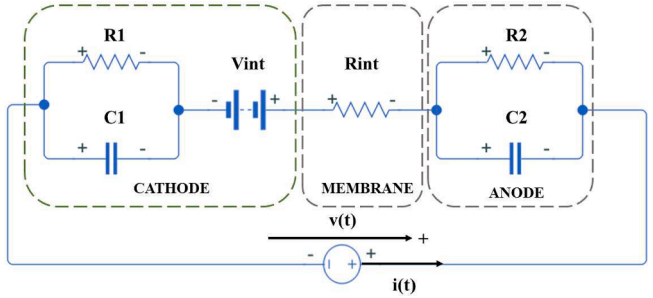

Fig. 4. ECM described in [10]. (Source: Own design).

validated in the literature, in order to select the most suitable one to implement DR of experimental equipment. Indeed, the motivation arises from the fact that this work is framed in an on-going R&D project devoted to the digital replication of a hybrid microgrid which combines photovoltaic power and hydrogen for off-grid applications.

The structure of the rest of the paper is as follows. The second section explains the principle of operation of PEMEL and describes the models selected for the development of the simulation platform. Section 3 reflects the design of the simulation platform, focusing on the structure and operation of the GUI through App Designer. Section 4 details the implementation of the platform through a set of simulations on the described models, displaying the functionalities provided by the proposed work. Finally, the most relevant conclusions of the work are depicted.

Table 2
Experimental values of the electrical components of the model in [10].

Electrical component	Value
R_1	0.035 Ω
C_1	37.26F
V_{int}	4.38 V
R_2	0.318 Ω
C_2	37.26F
R_{int}	0.088 Ω

2. PEM electrolyzer: Operation and models

This section describes the working principle of the PEMEL as well as the models selected for the design and implementation of the simulation platform.

2.1. Working principle

The electrolysis is an electrochemical reaction that allows to split a compound into its fundamental components by means of electricity. Electrolyzers use this working principle for generating hydrogen by splitting various compounds. There are three main types of electrolyzers: PEM, solid oxide and alkaline. Focusing on the PEM type, this device is water-powered and uses a proton exchange membrane and a solid polymeric electrolyte for the electrolysis process. After that process, the results are oxygen and hydrogen gas, as shown in Eq. (1):

$$H_2O(l) + Energy \rightarrow H_2(g) + \frac{1}{2}O_2(g) \quad (1)$$

Particularly, when the PEMEL is powered by a renewable energy source, e.g. photovoltaic or wind energy, the resulting hydrogen is called green hydrogen [40]. This designation is given by the fact that the whole process does not generate any kind of pollutant product, either in obtaining the input energy from the electrolyzer, or to obtain the hydrogen produced. In terms of structure, all electrolyzers consist of basic units called cells. These cells are responsible for the electrolysis and can be arranged in series, forming a stack, or in parallel. Each cell consists of three parts, the anode, the cathode and the membrane. The diagram in Fig. 1 shows an example of a green hydrogen generator using a PEMEL consisting of 8 cells in series.Fig. 2.

2.2. Selected PEM electrolyzer models

This section gives a brief description of the PEMEL models available in the literature that have been used for the development of the simulation platform. These models are based on ECM, where each electrical component forming the circuit refers to effects associated with the internal operation of the electrolyzer. The aim of the work is to implement the models selected from the literature in the simulation platform. Therefore, the following subsections illustrate the behaviour of each model through the same expressions described in the works [5,8–10].

The objective of these models is to determine the relationship between the input current *I* and the voltage measured at the electrolyzer terminals *V*. The *V-I* curve resulting from this relationship represents the characteristic curve that defines the operation of the electrolyzer. This curve is particularly illustrative for determining the behaviour of the PEMEL and is therefore used in the models and tests carried out in the literature as a starting point for studying this device [5,8–10]. The

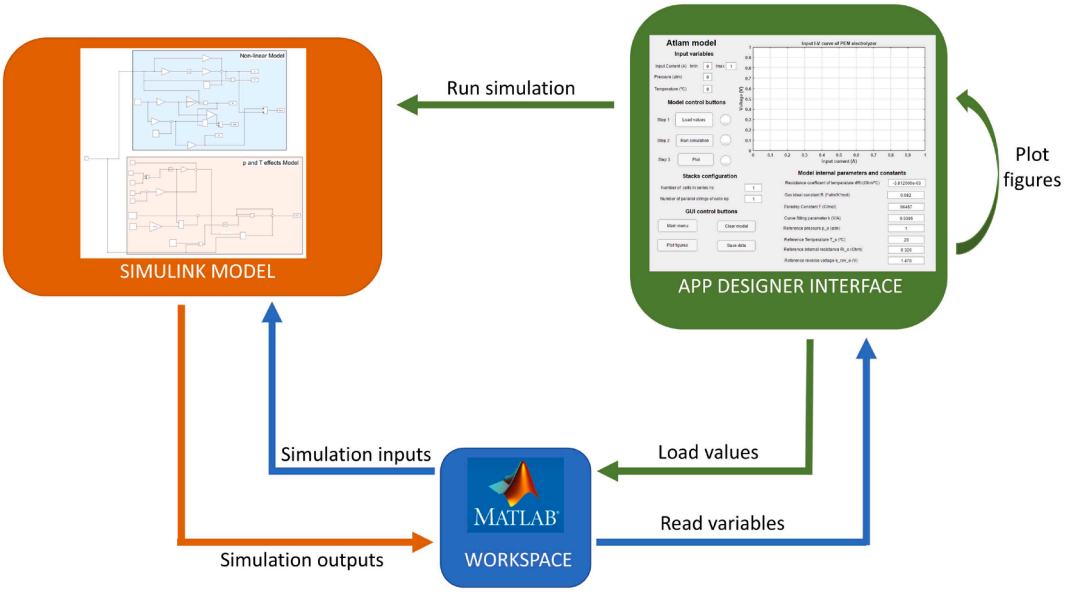

Fig. 5. Relationship between environments involved with the simulation platform.

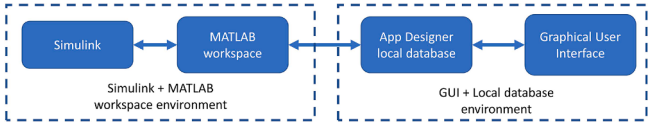

Fig. 6. Environment and database interaction.

remaining parameters of the electrolyzer, such as power or efficiency, are derived from this curve. To achieve this objective, each model develops a different methodology, studying the behaviour of the complete electrolyzer or of an individual cell.

2.2.1. Model for a PEM electrolyzer under steady-state conditions

An ECM for PEMEL is developed and validated in the reference [5] and this model is used in the present work to study the behaviour of the PEMEL under steady-state conditions. The equations and derivations below are cited and summarized from Atlam and Kolhe [5].

As can be seen in the figure, the behaviour of the electrolyzer is represented by a reversible voltage e_{rev} in series with a resistance R_i. e_{rev} is the voltage of the electrolyzer without considering the losses. This potential groups the ideal electrochemical potential V_i, along with the activation over-potential, meanwhile R_i represents the over potential during the operation of the electrolyzer.

Vi is defined as the useful volage for the electrolysis process and is obtained from the increase of the Gibbs free energy according to Eq. (2).

$$V_i = \frac{\Delta G}{2F} \tag{2}$$

Being:

$$\Delta G = 285,840 - 163.2(273 + T) \tag{3}$$

The study of the model is started by analysing the electrolyzer under nominal operating temperature and pressure conditions ($T = 20$ °C, $p = 1$ atm). Under these conditions, the cell voltage is determined by the non-linear expression in Eq. (4), where $e_{rev} = 1.4676$ V, $V_i = 1.233$ V and $R_i = 0.3264$ Ω.

$$V = 1.46760 - 1.4760e^{-\frac{5}{0.02}I} + 0.3264I \tag{4}$$

The hydrogen flow rate generated v_H (ml min^{-1}) for the operating point of the electrolyzer/cell is determined from Faraday's law

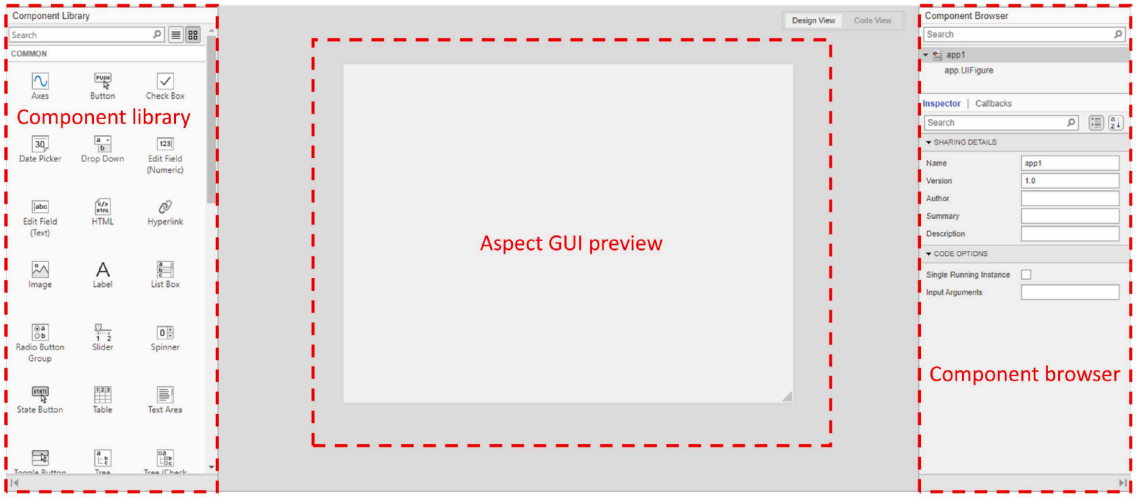

Fig. 7. Design view tab appearance.

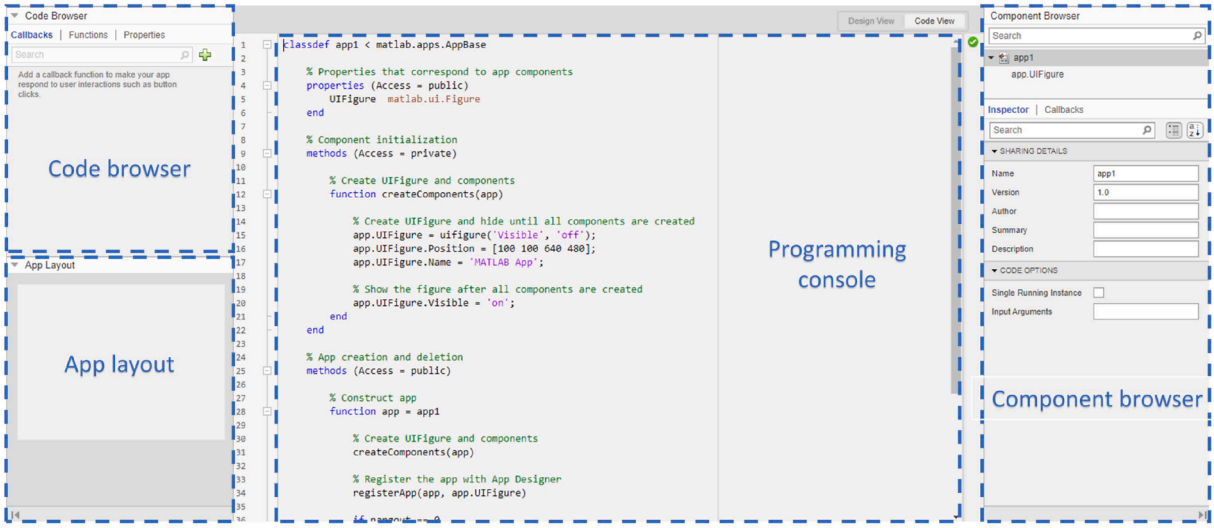

Fig. 8. Code view tab appearance.

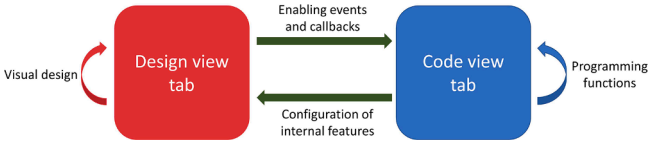

Fig. 9. Synergy between the tabs of the App Designer environment.

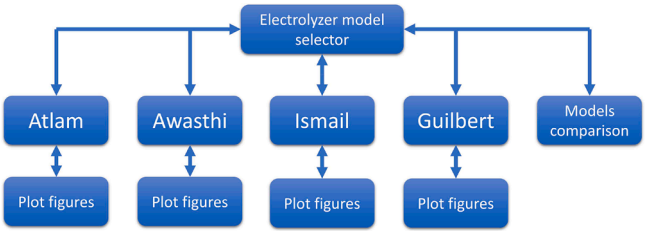

Fig. 10. Navigation map of the GUI.

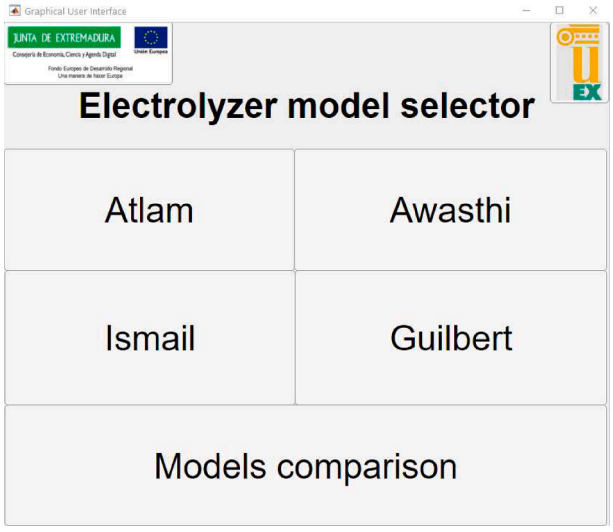

Fig. 11. *Main menu* tab appearance.

according to the Eq. (5).

$$v_H = v_M(l)\left(\frac{10^3 ml}{l}\right)\left(\frac{60s}{min}\right)\left(\frac{I\left(\frac{C}{s}\right)}{2F(C)}\right) = v_M(10^3)(60)\frac{I}{2F} \tag{5}$$

The useful electrochemical power of hydrogen P_{H2} can be derived from V_i as indicated in the Eq. (6).

$$P_{H2} = v_H\left(\frac{ml}{min}\right)\frac{\Delta G\left(\frac{J}{mol}\right)}{v_m\left(\frac{l}{mol}\right)\left(\frac{10^3 ml}{l}\right)\left(\frac{60s}{min}\right)} = IV_i \tag{6}$$

The total power consumed P by the cell is defined in Eq. (7).

$$P = VI = I^2R_i + Ie_{rev} \tag{7}$$

Finally, the cell efficiency η_e is defined by Eq. (8) as the ratio of the electrochemical power of hydrogen P_{H2} to the total power consumed P.

$$\eta_e = \frac{P_{H2}}{P} = \frac{V_i I}{VI} = \frac{V_i}{V} \tag{8}$$

After this analysis under nominal conditions, the performance of the cell is generalised for any operating temperature and pressure range. For this purpose, R_i and e_{rev} are modelled as a function of T and p.

$$R_i(T,p) = R_{io} + kln\left(\frac{p}{p_o}\right) + dR_t(T - T_o) \tag{9}$$

$$e_{rev}(T,p) = e_{rev_o} + \frac{R(273+T)}{2F} ln\left(\frac{p}{p_o}\right) \tag{10}$$

Derived from Eq. (9) and Eq. (10), the cell voltage expression is defined in Eq. (11).

$$V(T,p) = e_{rev}(T,p) - e_{rev}(T,p)e^{-\frac{s}{0.02}I} + IR_i(T,p) \tag{11}$$

Finally, in Atlam and Kolhe [5] an expression is given to determine the electrolyzer voltage as a function of the distribution of the cells in the electrolyzer, where n_s and n_p are the number of cells in series or in parallel respectively.

$$V(T,p) = I\frac{n_s}{n_p}R_i(T,p) + n_s e_{rev}(T,p) \tag{12}$$

2.2.2. *Modelling by varying temperature and pressure*

In Awasthi et al. [8] the model of a PEM cell is developed based on its physical structure. Under this approach, the cell model is divided into

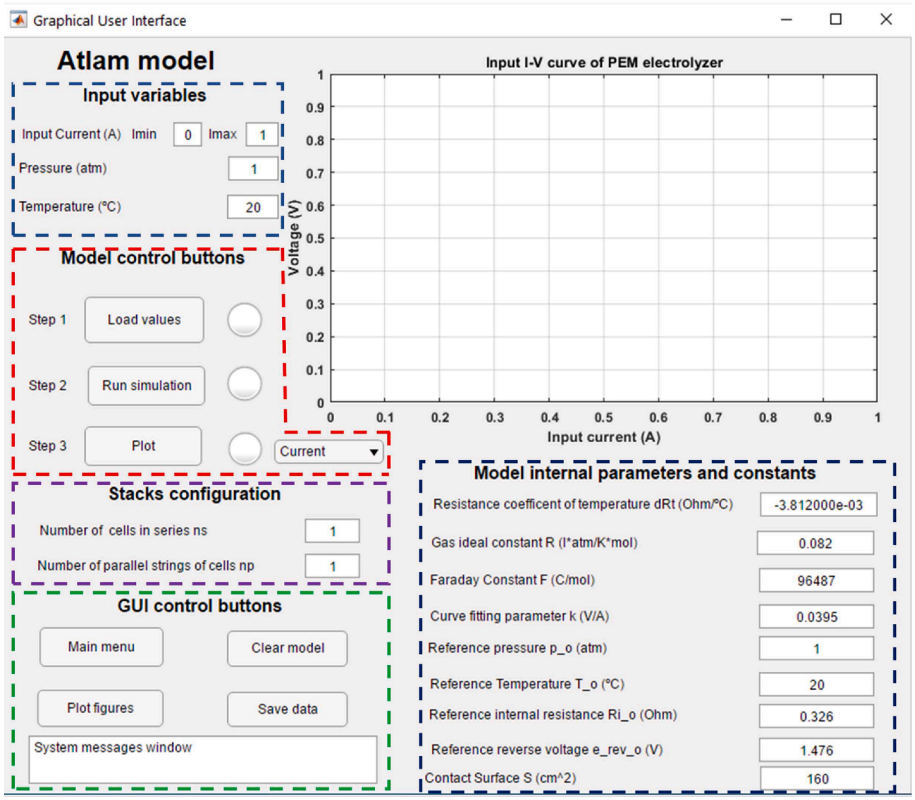

Fig. 12. *Atlam model* tab appearance.

four components: anode, cathode, membrane and voltage. The equations and derivations below are cited and summarized from Awasthi et al. [8]. Based on the abovementioned structure, the model describes the operation of the cell considering variations in operating temperature T and pressure p, as well as variations in ambient temperature T_{amb}. In this case, the relationship between the input current and the cell voltage is determined by a set of over voltages and the open circuit voltage E. This open circuit voltage is calculated by the Nernst equation expressed in Eq. (13).

$$E = E^0_{rev} + \frac{RT}{nF} ln\left(\frac{p_{H_2} p_{O_2}^{1/2}}{p_{H_2O}}\right) \tag{13}$$

As indicated in Eq. (13). E is a function of T and p. In this expression, the pressure is decomposed into the various partial pressures of the compounds involved in the electrolysis. In this expression, the E^0_{rev} term is determined through Eq. (14), whose value is dependent on the difference between T and T_{amb}.

$$E^0_{rev} = 1.229 - 0.9 \times 10^{-3}(T - T_{amb}) \tag{14}$$

The activation overvoltage η_{act} is defined in terms of current density i by the Butler-Volmer equation as given in Eq. (15).

$$\eta_{act} = \frac{RT}{\alpha_{an} F} arcsinh\left(\frac{i}{2i_{o,an}}\right) + \frac{RT}{\alpha_{cat} F} arcsinh\left(\frac{i}{2i_{o,cat}}\right) \tag{15}$$

The ohmic overvoltages η_{ohm} are associated with the resistive effects present in the electrolyzer cell and are calculated by Eq. (16).

$$\eta_{ohm} = \frac{\delta_m I}{A\sigma_m} \tag{16}$$

2.2.2.1. Model based on Tafel's law. The model presented in Ismail et al. [9] results from the experimental study of a PEM type cell serving as the load of a photovoltaic powered system. The equations and derivations below are cited and summarized from Ismail et al. [9]. In this context, the behaviour of the cell is represented by the diagram in Fig. 3, where the cell voltage is expressed in Eq. (17) as a function of four terms: the theoretical voltage V_{th}, the anodic overvoltage V_{anode}, the cathode overvoltage $V_{cathode}$, and the ohmic voltage drop V_{ohm}.

$$V_{cell} = V_{th} + V_{anode} + V_{cathode} + V_{ohm} \tag{17}$$

In this case, the relationship between the input current and the cell voltage is determined through Tafel's law, from which Eq. (18) is obtained.

$$V_{cell} = a + b \times log(I) + c \times I \tag{18}$$

The parameters a, b and c are defined according to the characteristics of the electrolyzer cell, such as geometry, materials or working temperature and pressure. These parameters are determined by means of an experimental test carried out at an operating temperature of 80 °C, obtaining the values of $a = 1.8018$, $b = 0.0632$ and $c = 0.0482$.

Derived from Eq. (18), the voltage of the electrolyzer is obtained as a function of the distribution of its component cells.

$$V_{el} = s\left(a + blog\left(\frac{I_e}{p}\right)\right) \tag{19}$$

Where s and p refer to the number of cells in series and in parallel, respectively.

The volume of total hydrogen generated by the electrolyzer is calculated according to the ideal gas law by Eq. (20).

$$Q_{H_2} = \frac{N_{cell} \times R \times I_f \times T}{Z \times F \times p} = \frac{N_{cell} \times 8.32 \times I_f \times T}{2 \times 96500 \times 0.1013} \tag{20}$$

Where N_{cell} is the total number of cells making up the electrolyzer ($s \times p$).

The electrolyzer efficiency is given by the Eq. (21).

$$\eta_{el} = \frac{1.23 \times s}{V_F} \tag{21}$$

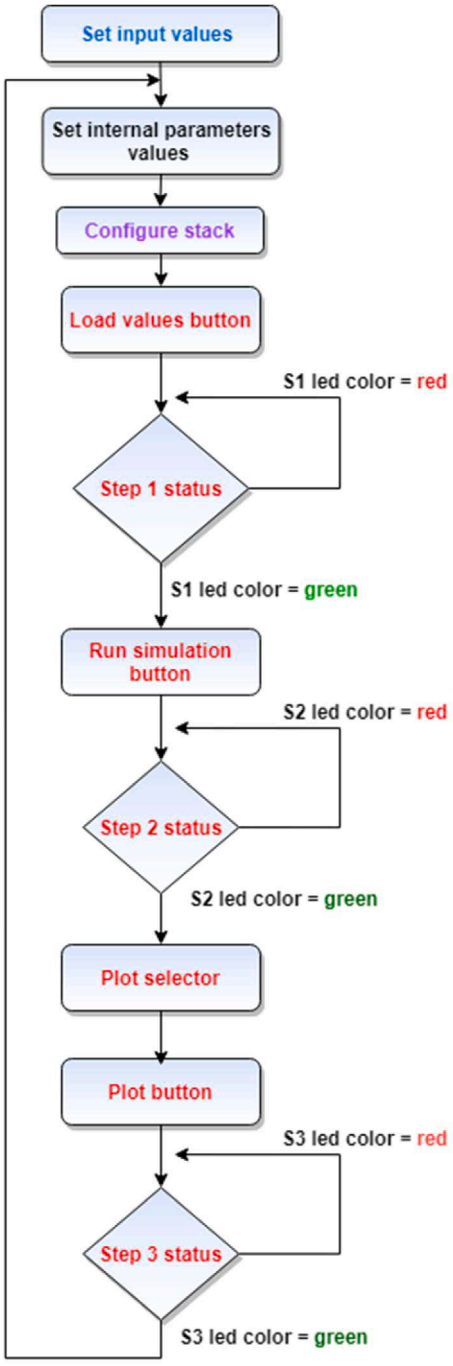

Fig. 13. GUI management flowchart.

2.2.2.2. Dynamic emulation of a PEM electrolyzer. The model developed in Guilbert and Vitale [10] defines an ECM whose components are determined by the dynamic study of a stack consisting of three cells in series. This electrical model is shown in the Fig. 4. The equations and derivations below are cited and summarized from Guilbert and Vitale [10].

This model separates the electrolyzer into three parts: anode, cathode and membrane. The electrical elements representing them are associated with local effects of the electrolyzer behaviour. On the one place, the group R_1C_1 represents the cathode operation. In particular, R_1 simulates the Gibbs free energy and heat losses at the cathode. The V_{int} voltage reproduces the useful power used for hydrogen production. On the second place, the group R_2C_2 represents the operation of the anode. In this group, R_2 simulates only the heat losses at the cathode. Between anode and cathode, the R_{int} resistance is located representing the losses in the membrane.

The values of these parameters are determined through a series of laboratory experiments where dynamic operating conditions for the electrolyzer are established. These values are shown in Table 2.

Using the calculated parameters, the expressions defining the behaviour of the electrolyzer are determined. Firstly, the voltage of the electrolyzer is given by the Eq. (22).

$$V = R_{tot}I + V_{int} \tag{22}$$

Where R_{tot} is the sum of the resistances R_1, R_2 and R_{int}.

The useful power used for the generation of hydrogen P_H is calculated by Eq. (23).

$$P_H = IV_{int} \tag{23}$$

The total power consumed or input power P_{in} is determined by Eq. (24).

$$P_{in} = IV_{int} + I^2(R_1 + R_2 + R_{int}) \tag{24}$$

Finally, the efficiency of the electrolyzer is defined in Eq. (25) as the ratio of useful power to input power.

$$\eta = \frac{P_H}{P_{in}} \tag{25}$$

3. Simulation platform and GUI

This section describes the development of the simulation platform used to study the different PEMEL models. At the same time, a GUI has been designed to facilitate the control of the platform and the visualisation of the results obtained in the simulations.

3.1. Operation of the simulation platform

The simulation platform designed in MATLAB is based on the interaction between three different environments: App Designer, Simulink, and Workspace.

On the first place, App Designer is a specific toolbox dedicated to the design of applications and GUI. This plugin has been used to design the GUI aimed to control the simulation platform. On the second place, Simulink is an environment for systems modelling and simulations. The studied models have been replicated using block diagrams to carry out the simulations. Finally, the default MATLAB database, called Workspace, has been used as a bridge to transmit data between Simulink and the GUI, while acting as a temporary database.

Through the GUI, the user takes control over all aspects of the models: setting parameters, running the simulation, displaying results, saving data, and so on. All of this is done through commands that the interface sends to Simulink and MATLAB. The diagram in Fig. 5 depicts the communication between the environments and the exchange of data together with the execution of commands.

The operation of Simulink and the GUI is linked to the exchange of data between these environments. On the one hand, Simulink requires user-set input data to simulate the behaviour of models. On the other hand, the GUI uses the simulation output data to represent the simulation results.

Each of these environments uses a different database. Applications and interfaces created in App Designer define their variables locally in a stand-alone database. In contrast to this toolbox, Simulink can read and store data in any defined database. Due to this discrepancy, it has been decided to use the MATLAB Workspace as a common database for data exchange. This one provides several advantages in the functioning of the application: Simulink uses this database by default, no pre-configuration of the database is necessary, and GUI can export and read variables to the database easily through specific commands. Fig. 6 shows the

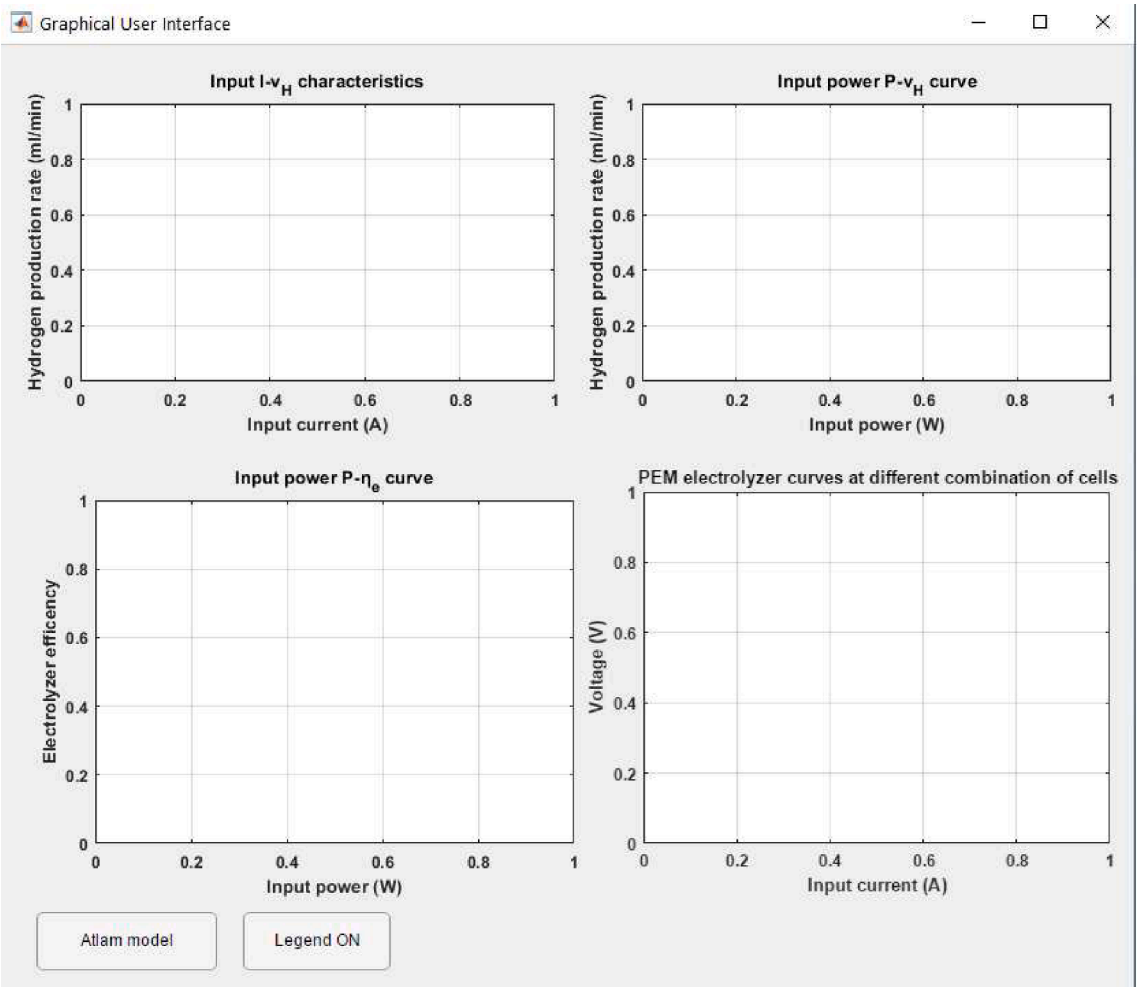

Fig. 14. *Atlam Plot figures* tab appearance.

interaction between the different environments abovementioned and the databases.

3.2. App Designer structure

The graphical appearance and functionalities provided by the GUI are conditioned by those used in the App Designer environment. This toolbox provides a series of tools for the development of a GUI through the simultaneous management of two different tabs: *Design view* and *Code view*.

Firstly, the *Design view* tab allows the graphical configuration and customisation of the interface through the use of a component library that facilitates the interaction between the GUI and the operator. Its layout, shown in Fig. 7, consists of the component library, a central area where the GUI appearance is previewed, and a browser where the components used are sorted and their internal characteristics are presented.

The other screen called *Code view* is intended for programming the actions performed by the interface during its execution, as well as modifying internal properties of the components, such as their display. Regarding its distribution, shown in Fig. 8, it consists of a column where the different events and callbacks used to programme the GUI operation are presented, a central area where the interface actions are programmed by means of codes, and finally, the component browser, maintaining the same qualities as in the *Design view* tab.

The key to the functioning of the App Designer environment is based on the interaction between these two windows. To begin with, each programmable event in the *Code view* tab is linked to an element in the *Design view* tab. In this way, the actions that the GUI can perform depend primarily on the elements placed in the *Design view* screen. In turn, the *Code view* tab allows the modification of internal features not accessible from the component browser. The diagram in Fig. 9 indicates the different interactions between the *Design view* and *Code view* tabs.

3.3. Graphical appearance of the GUI and navigation map

In terms of the graphical aspect presented by the GUI, its operation is based on navigation through tabs. The use of tabs allows the information to be presented to the user in an ordered and grouped manner, facilitating its visualisation and interpretation. The diagram in Fig. 10 presents the navigation map of the developed GUI, where the relations between the different screens are depicted.

The GUI starts with a main menu screen called *Electrolyzer model selector*, from which to access a set of tabs by means of buttons. The second level of the interface contains specific windows for each studied model that can be accessed via the buttons under the names of each of the models (*Atlam*, *Awasthi*, *Ismail* or *Guilbert*). Furthermore, the *Models comparison* button on the main screen provides access to a tab dedicated to the analysis and comparison of the results obtained by simulating the different models. As the last depth layer, within each model tab, there is a plot figures button, which changes the displayed screen to one dedicated to the representation of the operating curves of each model.

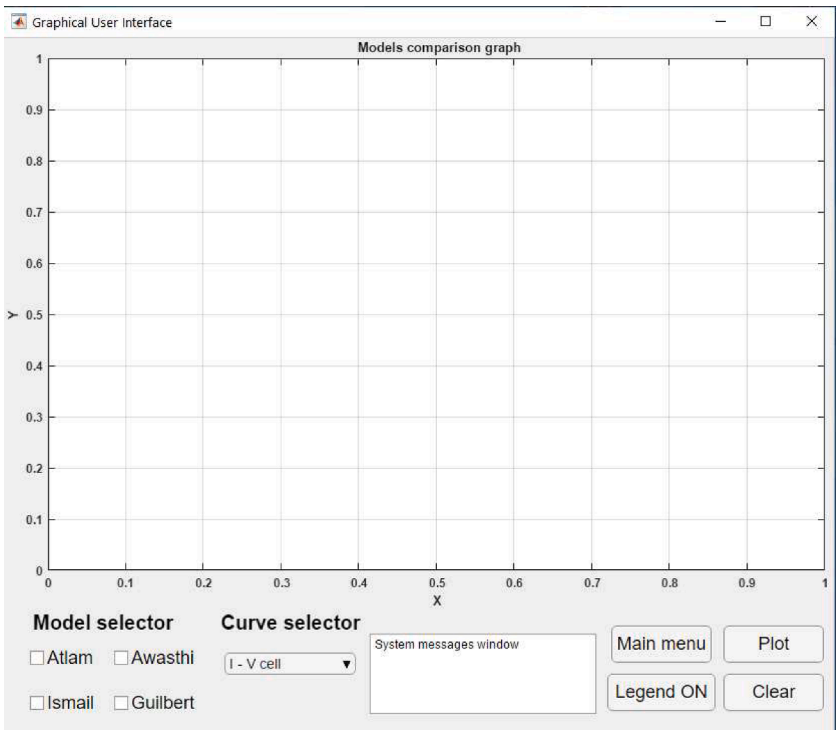

Fig. 15. *Models comparison* tab appearance.

Table 3
GUI buttons and actions.

Category	Button	Action
Navigation	Model	Shows the model tab
	Plot figures	Displays the plot figures tab of the model
	Models comparison	Shows the models comparison tab
Data management	Load values	Saves simulation input data in Workspace
	Save data	Export simulation data to Excel file
Simulation control	Run simulation	Execute the simulation of the model in Simulink
Visualisation	Plot	Plots the curves of the model
	Clear	Erase represented curves
	Legend ON/OFF	Enable/disable legend visibility

3.3.1. Main menu screen

The *Electrolyzer model selector* tab contains the buttons to access the model screens and the *Models comparison* tab. Due to the graphical similarity of the model screens, the main menu serves as a starting point to the interface, as well as a transit screen when switching between model tabs. Fig. 11 shows the appearance of this main window.

3.3.2. Model tabs

The model tab constitutes the main core of the GUI. Through this screen, the operator has control over the configuration of the digital model and its simulation. To explain the performance and layout of this tab, the Atlam model [5] has been selected as an example (Fig. 12).

As can be observed in the figure, the elements that make up the tab are distributed in different areas according to their purpose. To begin with, there are three areas dedicated to the configuration of the simulation: *Input variables* (blue dotted line), *Model internal parameters and constants* (black dotted line) and *Stack configuration* (purple dotted line). These areas contain numerical input fields that modify the input variables of the digital model in Simulink. Modifying these input variables results in a variation of its performance in the simulation. Concerning the control of the model, the *Model control buttons* (red dotted line) contains three sequential buttons and one selector for the execution of the simulation and results representations process. The *GUI control buttons* area (green dotted line) contains a series of buttons associated with different GUI functionalities and navigation options. In turn, a dynamic text window guides the actions performed by the user during tab operation, indicating whether a specific action is in progress or has been completed. Finally, a graphic space has been reserved in this tab for the representation of the characteristic *I-V* curve of the electrolyzer. This curve defines the operation of the electrolyzer by showing the voltage variation in response to input current variations.

The flowchart in Fig. 13 shows the sequence of actions to be performed by the operator to archive a successful simulation of the model and representation of its results. The colours used in the flowchart are associated with the different areas explained in Fig. 12. The loop of actions represented in the flowchart illustrates the ability of the GUI to perform consecutive simulations while operating on the model tab.

3.3.3. Plot figures tabs

The *Plot figures* tabs of the models represent the bottom level of the GUI navigation map. These screens are dedicated to the graphical representation of the results obtained in the simulations through curves. The layout of the elements and the appearance of these tabs are identical for all models implemented in the GUI. Due to this fact, this window can only be accessed through the model tab to which it is associated, to avoid confusing the user during the execution of simulations. Fig. 14 shows the appearance of the *Plot figures* tab. The axes associated with each of the graphic spaces indicate the represented variable and its corresponding unit. In turn, due to the adjusted size of the graphic spaces, the axes are auto-scaled according to the range represented to cover the entire curve.

Almost the entire window is occupied by four charts, intended to represent the characteristic curves of the electrolyzer. At the bottom, the *Atlam model* button allows navigation between the model tab and this one. Below is the button calls *Legend ON/OFF* that enables and disables the display of the legends in each of the graphs, facilitating the display of curves when running multiple simulations.

3.3.4. Models comparison tab

The last window of the interface is the *Models comparison* tab. This

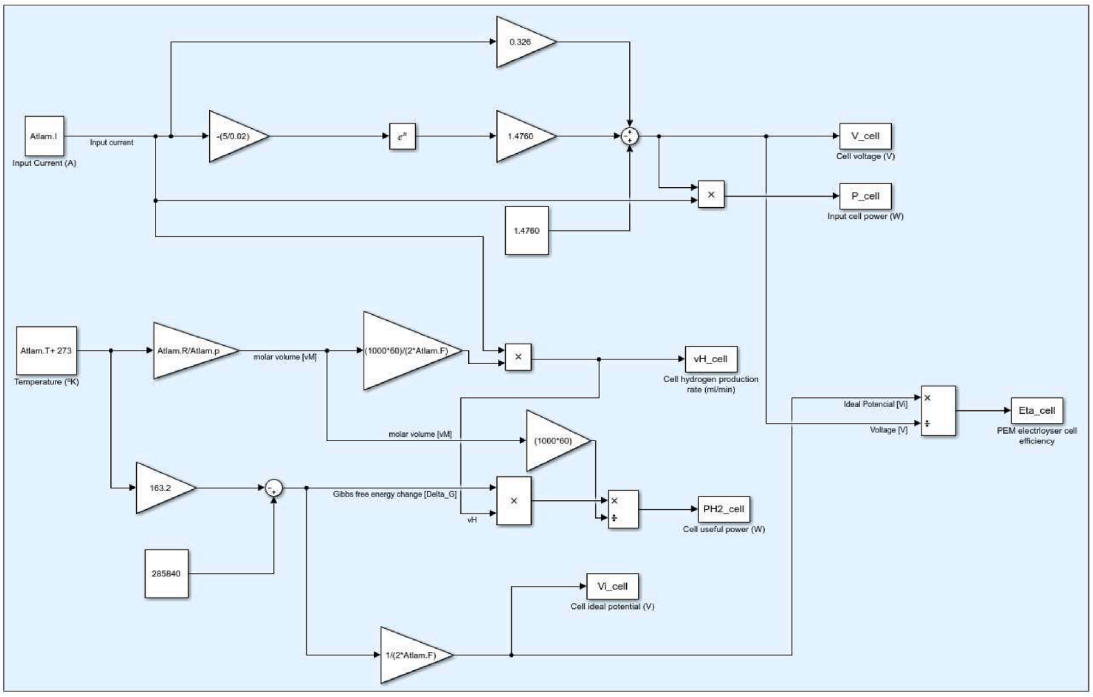

Fig. 16. Part of the Simulink block diagram of the Atlam model.

Table 4
Parameters and values used in the simulation case.

Parameter	Value
Internal parameters of the model	
Resistance coefficient of temperature dRt (Ω/°C)	−3.812e-03
Curve fitting parameter k (V/A)	0.0395
Reference pressure p_o (atm)	1
Reference temperature T_o (°C)	20
Internal reference resistance Ri_o (Ω)	0.326
Stack configuration	
Number of cells in series ns	3
Number of cells in parallel np	1
Input variables	
Input current I (A)	[0–1]
Working pressure (atm)	1
Working temperature (°C)	60

screen is accessible via the main screen. Its purpose is to provide the user with a graphical space to compare the curves resulting from the various simulations of the digital models. This helps the operator to carry out the study of the electrolyzer and its models.

Regarding the elements that make it up, the window is almost entirely occupied by a single graphic. In contrast to the *Plot figures* tabs, this screen seeks to analyse a single curve from different models, thus focusing attention on the differences between the curves represented. The compared models are selected by means of the check boxes in the *Model selector* area. In turn, the curve represented in the graphic space is selected by means of a drop-down selector in the area *Curve selector*. The remaining elements of the tab perform similar functions to their counterparts in the other tabs seen above. Fig. 15 shows the appearance of the *Models comparison* tab and its elements.

3.4. Features and functionalities of the GUI

As seen in the GUI design section, the tabs that constitute the interface are made up of elements with distinct functions. LED indicators or numeric fields, serve as visual indicators or data input fields for the user, respectively. In contrast, buttons are complex components that allow the execution of actions previously programmed in the interface code. Each button is identified by its name, which makes it possible to differentiate it from the rest and to indicate its function to the user. Depending on their specific function, each button can be categorised into *Navigation* buttons, *Data management* buttons, *Simulation control* buttons or *Visualisation* buttons. Table 3 summarizes the buttons abovementioned according to a classification by category and action performed.

4. Results and discussion

This section illustrates the operation of the simulation platform designed. For this purpose, a representative simulation case is run on one of the models presented previously and the results obtained are represented on the GUI.

4.1. Simulation case

For the simulation case, the Atlam model [5] is selected as an example of electrolyzer performance. As indicated above, the behaviour of these models is replicated by means of block diagrams in the Simulink environment. Fig. 16 depicts a part of the block diagram of the Atlam model, where the different parameters used in it can be observed.

During this study, the values associated with the internal parameters of the model have been kept constant in order not to alter the model described. On the other hand, the stack configuration, input variables, temperature and working pressure conditions have been modified in order to test the model operation. The set of parameters and values used in this simulation are shown in Table 4.

As shown in Table 4, the simulated electrolyzer consists of a stack of 3 cells in series. Through this configuration, it is possible to compare the performance between the stack and a single cell.

4.2. Simulation results

After determining the conditions of the simulation case, the GUI is

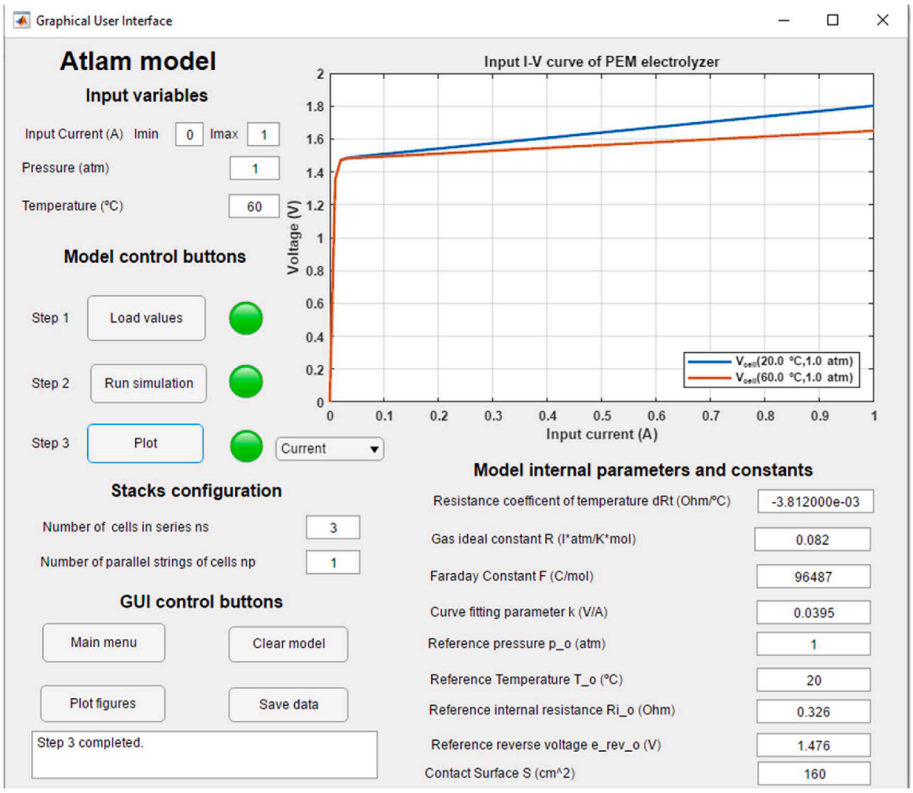

Fig. 17. *Model tab* with simulation case.

applied. Within the tab of the selected model, the steps explained in section 3 are executed to perform a successful simulation of the model. The simulation process uses the input values specified in the GUI and executes the block diagram of the model, obtaining the output values through the expressions specified in subsection 2.2.1. After running the simulation, the GUI plots the output values of the model through the specific charts: the *I-V* characteristic curve in the *model* tab, and the rest of the curves in the *plot figures* tab.

Fig. 17 shows the model tab together with two different coloured *I-V* curves. For this particular curve, blue represents the nominal conditions used in Atlam and Kolhe [5] and red indicates the simulated conditions in this case.

The *I-V* curve has a non-linear shape with two distinct zones. This form is homologous to those described in the literature models [8–10]. At low current ranges (from 0 to 0.05 A), the curve resembles a step ramp, which represents the threshold voltage that the cell must overcome to start electrolysis. In later current ranges (higher than 0.05 A), the curve takes the form of a straight line whose slope is modified by variations in temperature and working pressure. In the case of the curves shown in the figure, for a current of 0.5 A, $v_{cell}(20\ ^{\circ}C) = 1.639$ V while $v_{cell}(60\ ^{\circ}C) = 1.563$ V, where a downward trend of the slope is observed with increasing temperature.

Fig. 18 shows the appearance of the *Plot figures* tab after the simulation, where the rest of the curves are displayed. In this window, a comparison is made between the behaviour of the electrolyzer and that of a single cell. In this way, the effects of modifying the parameters of the stack configuration on the operation of the PEMEL can be observed. For this purpose, the cell curves are graphed in blue and the electrolyzer curves in red, all of them under the conditions of the simulation case.

The $I\text{-}v_H$ curve shows an increase in hydrogen generation due to an increment in the number of cells that compound the stack. For the case of $I = 0.6$ A, $v_{H\_cell} = 5$ ml/min while $v_{H\_el} = 15$ ml/min, tripling hydrogen production due to the number of cells in the stack. Comparison of the $I\text{-}V_{el}$ and $I\text{-}V_{cell}$ curves reflects a higher total electrolyzer voltage as a result of the increased number of cells in series, as defined by the model in Eq. (12). Taking as an example the value of $I = 0.6$ A, the value of $V_{cell} = 1.563$ V while $V_{el} = 4.689$ V, thus affirming the relationship between electrolyzer voltage and cell number. This voltage increase translates into an increase in the total power consumed, as seen in the $P\text{-}v_H$ and $P\text{-}\eta$ curves.

Section 3 highlights the ability of the GUI to perform successive simulations on the same model, being able to represent all the results obtained in the graphs. To demonstrate this feature, an additional simulation case has been run on the model by modifying the temperature and pressure conditions to $T = 20\ ^{\circ}C$ and $p = 4$ atm. The results obtained from this simulation are presented together with the previous simulation in Fig. 19 and Fig. 20.

The $I\text{-}V_{cell}$ curve resulting from this new simulation allows to determine an upward trend of the cell voltage with increasing working pressure, as can be seen from the voltage values for $I = 1$ A: $V_{cell}(20\ ^{\circ}C, 1\ atm) = 1.802$ V, $V_{cell}(60\ ^{\circ}C, 1\ atm) = 1.649$ V and $V_{cell}(20\ ^{\circ}C, 4\ atm) = 1.857$ V. Fig. 20 shows the rest of the electrolyzer and cell curves for each of the simulations, together with a common legend for each graphical chart. The effects associated with the increase in working pressure are visualised in these graphs, where the $I\text{-}v_H$ and $P\text{-}v_H$ curves describe a reduction in hydrogen generation and an increase in power consumption respectively. Due to this, the $P\text{-}\eta$ curve shows a worsening of the efficiency of the electrolyzer, according to the values given for the cell efficiency at $I = 1$ A: $\eta_{cell}(20\ ^{\circ}C, 1\ atm) = 0.685$, $\eta_{cell}(60\ ^{\circ}C, 1\ atm) = 0.727$ and $\eta_{cell}(20\ ^{\circ}C, 4\ atm) = 0.664$.

4.3. Comparison of models

Through the *Models comparison* tab, the user is able to perform a combined representation of the last cases simulated in each model in order to compare the curves obtained. To show the applicability of this window, an identical simulation case is carried out for all the models described, configuring a stack formed by 3 cells in series working under

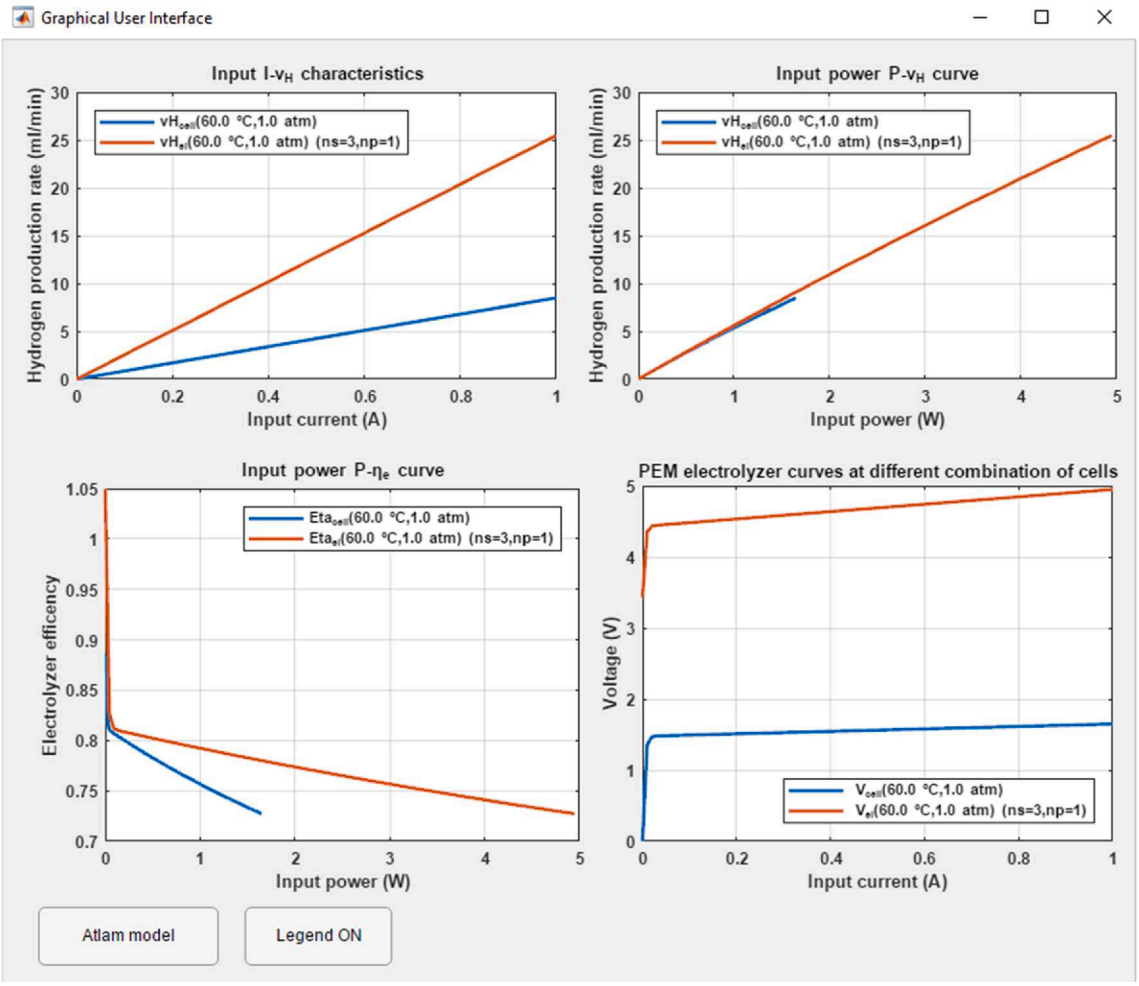

Fig. 18. *Plot figures* tab with simulation case.

operating conditions of $T = 80$ °C and $p = 1$ atm. The *I-V*, *P-I* and *P-* η curves for a single cell and for the stack are shown in Fig. 21, Fig. 22 and Fig. 23, respectively.

Fig. 21 depicts the *I-V* curves of a single cell and the stack of each of the models. From this information it is determined that the behaviour of the Atlam, Awasthi and Guilbert models are similar, with minor differences in voltage. On the contrary, the Ismail model presents a higher voltage value than the rest. To put this statement into context, the cell voltage values of the models at I = 1 A are presented: $V_{cell\_Atlam} = 1.573$ V, $V_{cell\_Awasthi} = 1.544$ V, $V_{cell\_Guilbert} = 1.607$ V and $V_{cell\_Ismail} = 1.85$ V.

The Atlam and Awasthi model curves have an identical step-like shape, with the voltage difference increasing as cells are added in series to the stack. This discrepancy between the models is due to the fact that Awasthi considers the ambient temperature as well as the anode and cathode partial pressures in determining the electrolyzer voltage. In contrast, the Guilbert model gives a curve with a linear shape, due to Eq. (22). This approach is indicated in Atlam and Kolhe [5] as a viable solution for the study of electrolyzer operation. The curve obtained from the Guilbert model gives similar values to the Atlam and Awasthi model without taking into account the factors of temperature or working pressure.

Fig. 22 shows the model *P-*v_H curves comparing the single cell and stack values. This figure shows the effects of the voltages observed in Fig. 21 and the differences between the models. Thus, the Ismail model stands out in power consumption due to the high voltage value determined by Eq. (19). The rest of the models present similar curves with very approximate values. In turn, the figure highlights the relationship between hydrogen production and the number of cells in the electrolyzer, where a significant increase in the generated flow rate is observed before due to the increase in the cells in series of the stack. This behaviour is identical in all the models, with discrepancies in the power consumed in each of them due to the differences in the calculated voltages.

Fig. 23 shows a comparison of the efficiency of the electrolyzer versus its power consumption. To determine the efficiency, the models relate the values of the ideal voltage used for electrolysis and the electrolyzer voltage. For the Guilbert case, the value of V_{int} is considered as a constant unrelated to variations in temperature or pressure. Comparing the cell efficiency values for the models at $I = 1$ A, it can be seen that the Guilbert model has the highest value: $\eta_{cell\_Atlam} = 0.752$, $\eta_{cell\_Awasthi} = 0.766$, $\eta_{cell\_Guilbert} = 0.909$ and $\eta_{cell\_Ismail} = 0.665$.

The Atlam and Awasthi models present close efficiency values through they both study the effects associated with the ideal voltage due to variations in the working temperature and pressure. In particular, Awasthi includes the ambient temperature parameter in its model, which affects the ideal voltage and differentiates it from the Atlam model.

The simulated values in Ismail's model are the smallest of all those represented in the graph. Ismail's model takes a constant ideal voltage value ($V_{i\_Ismail} = 1.23$ V), as in the Guilbert model, but its cell voltage value is much higher than in the other models ($V_{cell\_Ismail} = 1.85$ V), as shown in Fig. 21.

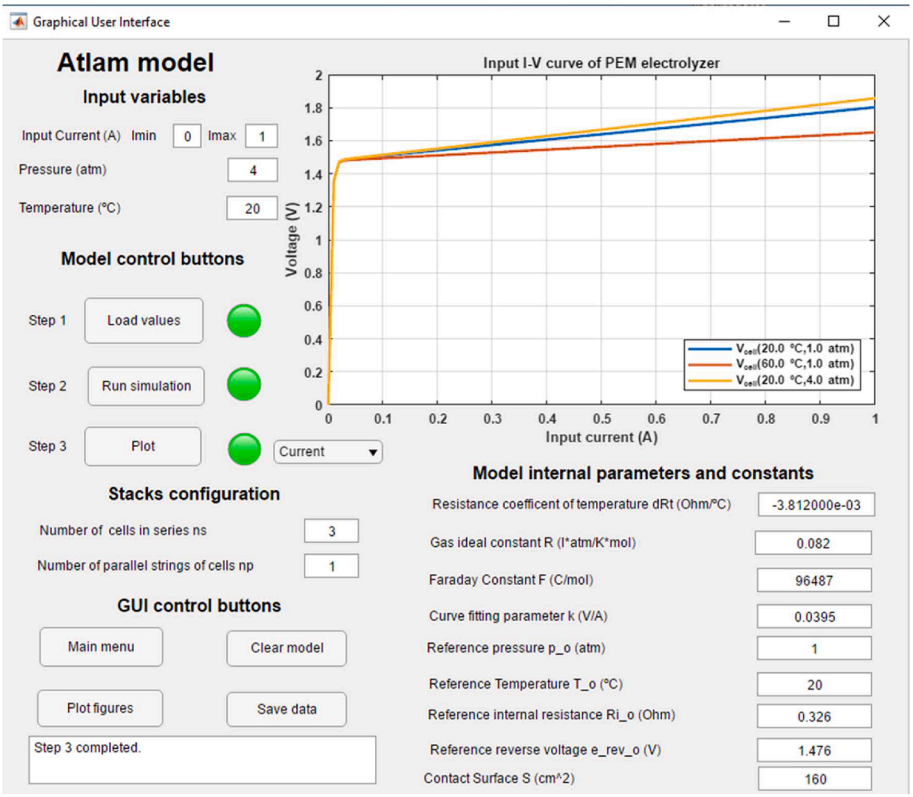

Fig. 19. *Model tab* with additional simulation.

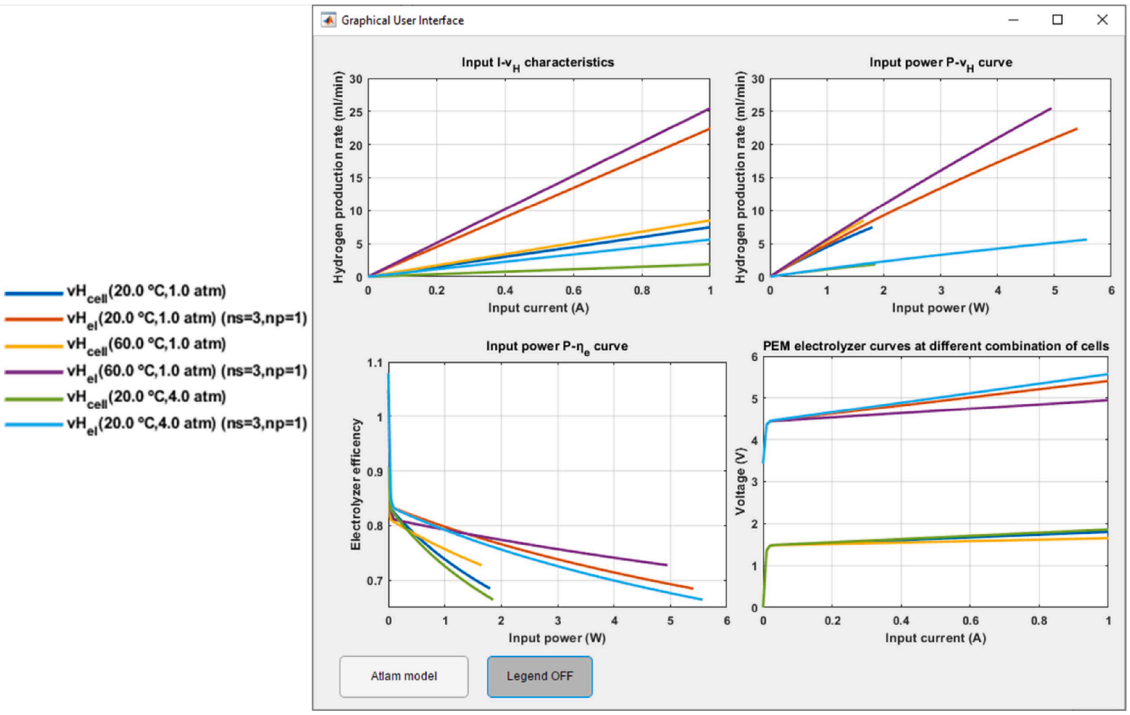

Fig. 20. *Plot figures* tab with additional simulation.

4.4. Discussion

The previous section highlights the potential of the platform to undertake the analysis of PEMEL models, either locally through the specific tabs for each model, or through a comparison of different simulation cases. In the latter case, it is illustrated a common behaviour of the PEMEL, differing numerically between them due to the expressions taken into consideration to define the model parameters. These differences are key to determine which model is closer to the behaviour of an experimental PEMEL. For this purpose, the platform facilitates the

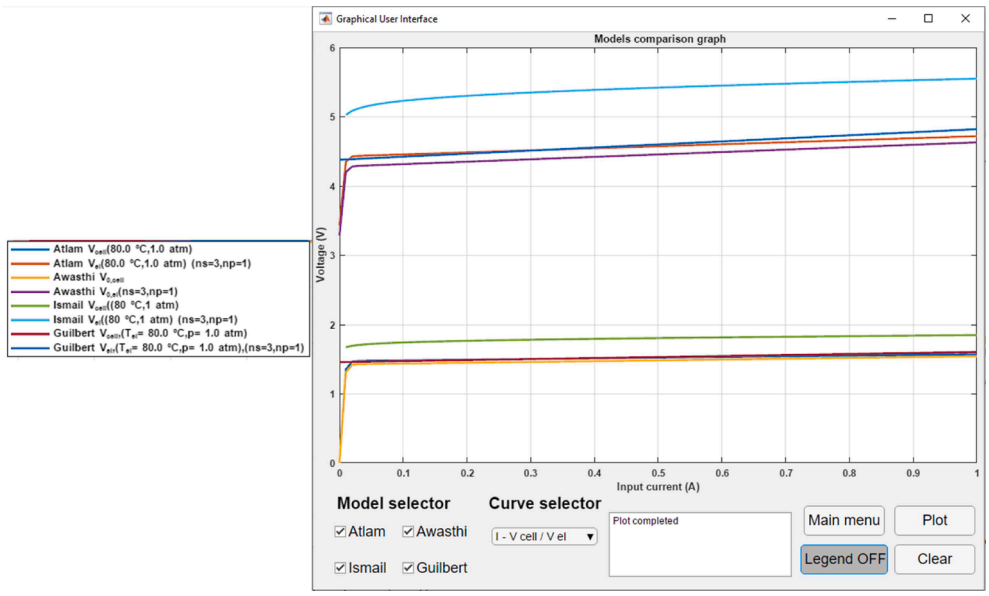

Fig. 21. Models comparison tab with I-V curves.

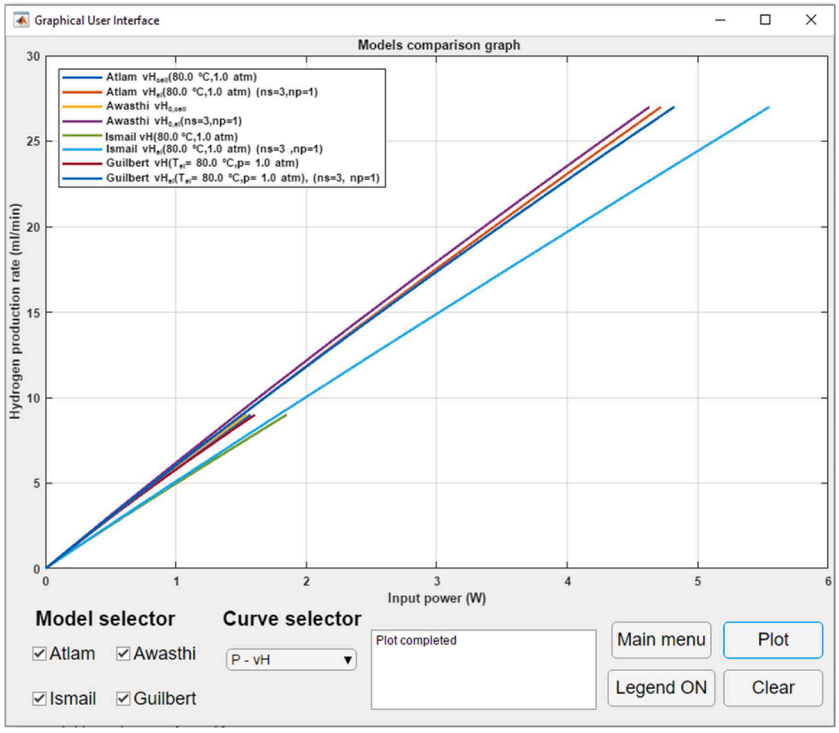

Fig. 22. Models comparison tab with P-v_H curves.

export of data to Excel in order to manage the results of the simulations carried out and compare them with experimental data collected from the electrolyzer.

The simulation platform designed is an innovative tool for the simulation and analysis of multiple PEMEL models, facilitating the study of these devices through an intuitive and user-friendly GUI. This interface gives the user full access to each model to modify and experiment with it, allowing the user to visualise the effects associated with these changes. This customisation implies a novelty compared to the literature, which present pre-set and closed models and the user is only allowed to enter input variables, thus limiting the ability to analyse and understand the results represented. At the same time, the functions presented in the GUI can be easily modified or extended thanks to the App Designer toolbox, whose programming nature allows further modifications to the GUI. Furthermore, the interconnected environment-based structure of the simulation platform allows the catalogue of models available for the interface to be extended, and may include not only PEM, but also alkaline and solid models, acquiring a more generalist character. To do so, it is only necessary to include the new model in Simulink and create a new tab in the GUI according to the new model. In this way, the application acquires the capacity to evolve and improve according to the user's needs.

In a similar sense, an interesting aspect to consider is the interaction between water transport and PEMEL operation. In this context, some

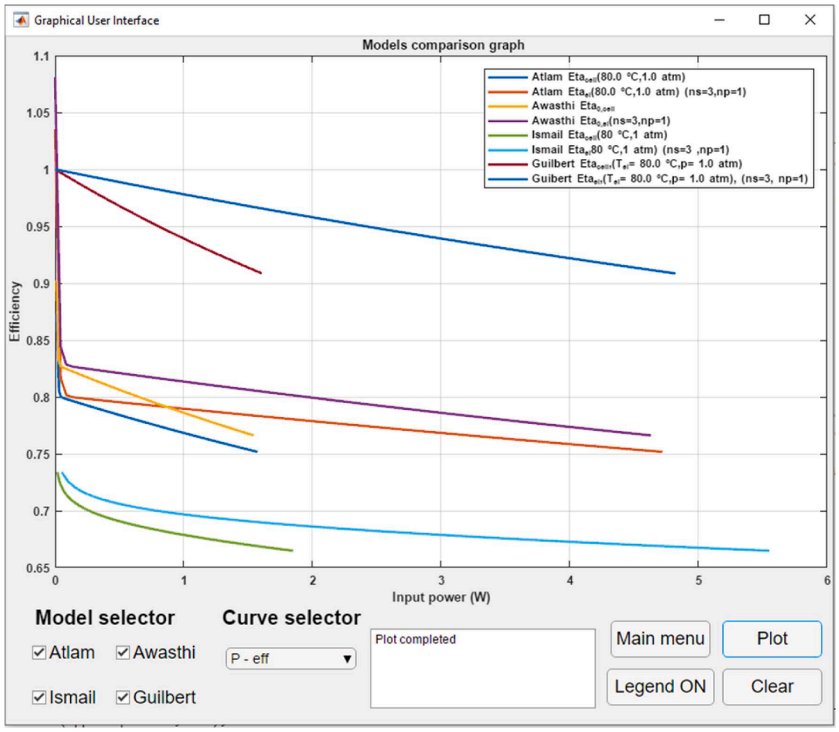

Fig. 23. Models comparison tab with P- η curves.

models study internal water flow as a key factor in the PEMEL performance, resulting in effects associated with degradation mechanisms and influence in internal model parameters, such as ohmic losses. The implementation of this type of models in the presented simulation platform is possible thanks to its versatility and ease of use, enriching the catalogue of available models and the results of the obtained comparisons.

As indicated in the introduction, the described platform has been conceived with the aim of studying the behaviour of PEMEL in order to develop a DR of a physical device. Beyond this, the characteristics of the described platform highlight its versatility. As a result, this tool can be used for various purposes such as the study and analysis of the behaviour of PEMEL in the field of research, with the aim of characterising physical devices. In the academic field, the application provides a virtual environment to teach about the operation of PEMEL in a visual and interactive way.

5. Conclusions

This work has presented the design, operation and implementation of a simulation platform based on MATLAB/Simulink for the study of PEMEL models. The application is intended to facilitate the study and analysis the behaviour of this device with the aim of developing a DR of an experimental PEMEL framed in a smart microgrid. The information provided by the simulation platform allows the identification of the most suitable model for the behaviour of the experimental electrolyzer.

A GUI has been developed using the App Designer toolbox for the control of the platform, as well as for the representation of the curves resulting from the simulations and the comparison between the models. The interaction of these three environments constitutes the working principle of the simulation platform. The proposal allows fully customisation of the model parameters and working conditions through the GUI, which constitutes a novelty in literature.

Regarding the GUI, the handling of App Designer has been described, as well as the structure and performance of the interface, highlighting the functionalities of each of the elements that compose it.

The models implemented in the platform have been described and compared by means of a series of simulations executed through the GUI, where the differences between the models can be appreciated due to the expressions used in each one of them.

Future work will use the data collected from the simulations performed through the platform to develop a DR of an experimental PEMEL. To this end, the models hosted on the platform will be used as a starting point to develop the replica model that matches the operation of the physical device. Another future guideline will deal with the study of models focussed on the water transport influence in PEMEL operation, and their implementation in the simulation platform.

CRediT authorship contribution statement

Francisco Javier Folgado: Conceptualization, Software, Investigation, Data curation, Writing – review & editing. **Isaías González:** Methodology, Investigation, Writing – original draft, Writing – review & editing. **Antonio José Calderón:** Conceptualization, Methodology, Validation, Investigation, Data curation, Writing – review & editing, Supervision.

Declaration of Competing Interest

The authors declare that they have no known competing financial interests or personal relationships that could have appeared to influence the work reported in this paper.

Data availability

The authors are unable or have chosen not to specify which data has been used.

Acknowledgments

This project was co-financed by European Regional Development Funds FEDER and by the Junta de Extremadura (IB18041).

References

[1] Okolie JA, Patra BR, Mukherjee A, Nanda S, Dalai AK, Kozinski JA. Futuristic applications of hydrogen in energy, biorefining, aerospace, pharmaceuticals and metallurgy. Int J Hydrogen Energy 2021;46:8885–905. https://doi.org/10.1016/j.ijhydene.2021.01.014.

[2] He H, Wang X, Chen J, Wang Y-X. Regenerative fuel cell-battery-supercapacitor hybrid power system modeling and improved rule-based energy management for vehicle application. J Energy Eng 2020;146(6). https://doi.org/10.1061/(asce)ey.1943-7897.0000708.

[3] Neuwirth M, Fleiter T, Manz P, Hofmann R. The future potential hydrogen demand in energy-intensive industries - a site-specific approach applied to Germany. Energy Convers Manage 2022;252:115052.

[4] González I, Calderón AJ, Andújar JM. Novel remote monitoring platform for RES-hydrogen based smart microgrid. Energy Convers Manage 2017;148:489–505. https://doi.org/10.1016/j.enconman.2017.06.031.

[5] Atlam O, Kolhe M. Equivalent electrical model for a proton exchange membrane (PEM) electrolyser. Energy Convers Manage 2011;52:2952–7. https://doi.org/10.1016/j.enconman.2011.04.007.

[6] Sánchez A, Zhang Qi, Martín M, Vega P. Towards a new renewable power system using energy storage: an economic and social analysis. Energy Convers Manage 2022;252:115056.

[7] Feng Qi, Yuan X, Liu G, Wei B, Zhang Z, Li H, et al. A review of proton exchange membrane water electrolysis on degradation mechanisms and mitigation strategies. J Power Sources 2017;366:33–55.

[8] Awasthi A, Scott K, Basu S. Dynamic modeling and simulation of a proton exchange membrane electrolyzer for hydrogen production. Int J Hydrogen Energy 2011;36:14779–86. https://doi.org/10.1016/j.ijhydene.2011.03.045.

[9] Ismail TM, Ramzy K, Elnaghi BE, Abelwhab MN, El-Salam MA. Using MATLAB to model and simulate a photovoltaic system to produce hydrogen. Energy Convers Manage 2019;185:101–29. https://doi.org/10.1016/j.enconman.2019.01.108.

[10] Guilbert D, Vitale G. Dynamic emulation of a PEM electrolyzer by time constant based exponential model. Energies 2019;12(4):750.

[11] Guilbert D, Sorbera D, Vitale G. A stacked interleaved DC-DC buck converter for proton exchange membrane electrolyzer applications: design and experimental validation. Int J Hydrogen Energy 2020;45:64–79. https://doi.org/10.1016/j.ijhydene.2019.10.238.

[12] Jansen G, Dehouche Z, Corrigan H. Cost-effective sizing of a hybrid Regenerative Hydrogen Fuel Cell energy storage system for remote & off-grid telecom towers. Int J Hydrogen Energy 2021;46:18153–66. https://doi.org/10.1016/j.ijhydene.2021.02.205.

[13] Virji M, Randolf G, Ewan M, Rocheleau R. Analyses of hydrogen energy system as a grid management tool for the Hawaiian Isles. Int J Hydrogen Energy 2020;45:8052–66. https://doi.org/10.1016/j.ijhydene.2020.01.070.

[14] Novák P, Vyskočil J, Wally B. The digital twin as a core component for industry 4.0 smart production planning. IFAC-PapersOnLine 2020;53(2):10803–9.

[15] Mohammadshahi SS, Boulaire FA, Love J, Gorji SA, Mackinnon IDR. A flexible analytical model for operational investigation of solar hydrogen plants. Int J Hydrogen Energy 2022;47:782–808. https://doi.org/10.1016/j.ijhydene.2021.10.072.

[16] Liu M, Fang S, Dong H, Xu C. Review of digital twin about concepts, technologies, and industrial applications. J Manuf Syst 2021;58:346–61. https://doi.org/10.1016/j.jmsy.2020.06.017.

[17] Qi Q, Tao F, Hu T, Anwer N, Liu A, Wei Y, et al. Enabling technologies and tools for digital twin. J Manuf Syst 2021;58:3–21.

[18] Wang KJ, Lee TL, Hsu Y. Revolution on digital twin technology—a patent research approach. Int J Adv Manuf Technol 2020;107:4687–704. https://doi.org/10.1007/s00170-020-05314-w.

[19] José A, Godoy C, González Pérez I. Design and Implementation of Smart Micro-Grid and Its Digital Replica: First Steps. Proc. 16th Int. Conf. Informatics Control. Autom. Robot. (ICINCO 2019) , (2019), p. 715–21.

[20] Tao F, Zhang M, Liu Y, Nee AYC. Digital twin driven prognostics and health management for complex equipment. CIRP Ann 2018;67:169–72. https://doi.org/10.1016/j.cirp.2018.04.055.

[21] González-González A, Jimenez Cortadi A, Galar D, Ciani L. Condition monitoring of wind turbine pitch controller: a maintenance approach. Measurement 2018;123:80–93.

[22] O'Dwyer E, Pan I, Acha S, Shah N. Smart energy systems for sustainable smart cities: current developments, trends and future directions. Appl Energy 2019;237:581–97. https://doi.org/10.1016/j.apenergy.2019.01.024.

[23] Park H-A, Byeon G, Son W, Jo H-C, Kim J, Kim S. Digital twin for operation of microgrid: optimal scheduling in virtual space of digital twin. Energies 2020;13(20):5504.

[24] Steindl G, Stagl M, Kasper L, Kastner W, Hofmann R. Generic digital twin architecture for industrial energy systems. Appl Sci (Switzerland) 2020;10:1–20. https://doi.org/10.3390/app10248903.

[25] Onile AE, Machlev R, Petlenkov E, Levron Y, Belikov J. Uses of the digital twins concept for energy services, intelligent recommendation systems, and demand side management: a review. Energy Rep 2021;7:997–1015. https://doi.org/10.1016/j.egyr.2021.01.090.

[26] Wu B, Widanage WD, Yang S, Liu X. Battery digital twins: Perspectives on the fusion of models, data and artificial intelligence for smart battery management systems. Energy and AI 2020;1:100016.

[27] Van Mierlo J, Berecibar M, El Baghdadi M, De Cauwer C, Messagie M, Coosemans T, et al. Beyond the state of the art of electric vehicles: a fact-based paper of the current and prospective electric vehicle technologies. World Electric Vehicle J 2021;12(1):20.

[28] Bhatti G, Mohan H, Raja Singh R. Towards the future of smart electric vehicles: digital twin technology. Renew Sustain Energy Rev 2021;141:110801. https://doi.org/10.1016/j.rser.2021.110801.

[29] Granacher J, Nguyen T-V, Castro-Amoedo R, Maréchal F. Overcoming decision paralysis—A digital twin for decision making in energy system design. Appl Energy 2022;306:117954. https://doi.org/10.1016/j.apenergy.2021.117954.

[30] Wang B, Zhang G, Wang H, Xuan J, Jiao K. Multi-physics-resolved digital twin of proton exchange membrane fuel cells with a data-driven surrogate model. Energy and AI 2020;1:100004. https://doi.org/10.1016/j.egyai.2020.100004.

[31] Meraghni S, Terrissa LS, Yue M, Ma J, Jemei S, Zerhouni N. A data-driven digital-twin prognostics method for proton exchange membrane fuel cell remaining useful life prediction. Int J Hydrogen Energy 2021;46:2555–64. https://doi.org/10.1016/j.ijhydene.2020.10.108.

[32] Ogumerem GS, Pistikopoulos EN. Parametric optimization and control for a smart Proton Exchange Membrane Water Electrolysis (PEMWE) system. J Process Control 2020;91:37–49. https://doi.org/10.1016/j.jprocont.2020.05.002.

[33] Jain R, Nagasawa K, Veda S. Power-to-gas systems for active load management at EV charging sites with high der penetration. IEEE Transp Electrification Conf Expo, ITEC 2021;2021(2021):601–6. https://doi.org/10.1109/ITEC51675.2021.9490110.

[34] Vale Z, Morais H, Faria P, Ramos C. Distribution system operation supported by contextual energy resource management based on intelligent SCADA. Renewable Energy 2013;52:143–53. https://doi.org/10.1016/j.renene.2012.10.019.

[35] Calderón A, González I, Calderón M, Segura F, Andújar J. A new, scalable and low cost multi-channel monitoring system for polymer electrolyte fuel cells. Sensors (Switzerland) 2016;16(3):349.

[36] González I, Calderón AJ, Folgado FJ. IoT real time system for monitoring lithium-ion battery long-term operation in microgrids. J Storage Mater 2022;51:104596.

[37] Smaoui M, Krichen L. Control, energy management and performance evaluation of desalination unit based renewable energies using a graphical user interface. Energy 2016;114:1187–206. https://doi.org/10.1016/j.energy.2016.08.051.

[38] Jafari M, Malekjamshidi Z. Optimal energy management of a residential-based hybrid renewable energy system using rule-based real-time control and 2D dynamic programming optimization method. Renewable Energy 2020;146:254–66. https://doi.org/10.1016/j.renene.2019.06.123.

[39] Vivas FJ, De las Heras A, Segura F, Andújar JM. H2RES2 simulator. A new solution for hydrogen hybridization with renewable energy sources-based systems. Int J Hydrogen Energy 2017;42(19):13510–31.

[40] Hosseini SE. Design and analysis of renewable hydrogen production from biogas by integrating a gas turbine system and a solid oxide steam electrolyzer. Energy Convers Manage 2020;211:112760. https://doi.org/10.1016/j.enconman.2020.112760.

Anexo II

Referencia

Folgado F.J., González I., Calderón A.J., Data acquisition and monitoring system framed in Industrial Internet of Things for PEM hydrogen generators, Internet of Things, 2023; 22: 100795. DOI: 10.1016/j.iot.2023.100795

Derechos de autor

Internet of Things 22 (2023) 100795

Contents lists available at ScienceDirect

Internet of Things

journal homepage: www.sciencedirect.com/journal/internet-of-things

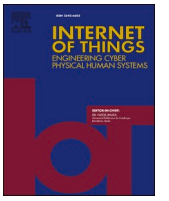

Research article

Data acquisition and monitoring system framed in Industrial Internet of Things for PEM hydrogen generators

Francisco Javier Folgado *, Isaías González, Antonio José Calderón

Department of Electrical Engineering, Electronics and Automation, Universidad de Extremadura, Avenida de Elvas, s/n, Badajoz 06006, Spain

ARTICLE INFO

Keywords:
Industrial IoT
Data acquisition
Monitoring
Hydrogen
PEM electrolyzer
Renewable energy

ABSTRACT

Hydrogen is an energy carrier with increasing relevance in the current energy scenario since it contributes to reduce fossil fuels dependence and carbon emissions for a sustainable development. For its generation, Polymer Electrolyte Membrane (PEM) technology uses water and electricity to produce hydrogen and oxygen, avoiding pollutants. In this paper, a novel data acquisition and monitoring system for PEM hydrogen generators is presented. The main magnitudes of the PEM electrolyzer (PEMEL) such as current, voltage, pressure, hydrogen flow, etc., are sensed and acquired by an industrial controller. A middleware layer gathers the measurements through a communication network and stores them in a database. The user accesses online to this information in real time through a web-based interface. All components and functions are orchestrated according to an Industrial Internet of Things (IIoT) architecture, integrating industrial equipment, IoT software and sensing devices, which constitutes a novelty in literature. Experimental data of a PEMEL under real operating conditions are reported to prove the feasibility and successful performance of the developed system.

1. Introduction

The utilization of hydrogen as an energy carrier, which is devoid of any environmental pollutants, has emerged as an indispensable alternative for the prospective developments of power systems in all countries worldwide [1]. The adoption of hydrogen technology is anticipated to mitigate the reliance on fossil fuels and its related carbon emissions [2]. Furthermore, the deployment of hydrogen technologies is encouraged to attain the United Nations' Sustainable Development Goals, particularly in the context of goal 7, which pertains to affordable and clean energy [3]. The hydrogen applications are strategically aligned with the advancement of the aforementioned goal.

The technologies related to hydrogen production are categorized based on their fundamental operating principle, namely Polymer Electrolyte Membrane (PEM), alkaline, and solid types. In particular, membrane-based electrolysis has attracted increasing research attention over the past decade [4]. This method offers certain advantages, such as the absence of net carbon emission into the atmosphere during operation (with only hydrogen, oxygen, and water generated) and the ability to replicate and combine multiple single-unit membrane electrodes into a stack [4]. Moreover, the integration of PEM electrolyzers with renewable energies is fostered due to their high-speed response to changes in operating conditions [5]. According to Kumar and Himabindu [6], PEM water electrolysis is one of the favorable methods for conversion of renewable energy into high pure hydrogen. As asserted in [4], the application

* Corresponding author.
E-mail address: ffolgar@unex.es (F.J. Folgado).

https://doi.org/10.1016/j.iot.2023.100795
Received 17 January 2023; Received in revised form 29 March 2023; Accepted 17 April 2023
Available online 25 April 2023

of membrane-based electrolysis allowing the use of hydrogen in transportation and industrial activities will be of significant interest over the next 5 to 10 years.

Concerning the architecture of a PEM electrolyzer (PEMEL), it comprises of cells arranged in series, forming a stack, to perform the electrolysis process. The electrochemical process for water involves the separation of water molecules into hydrogen and oxygen, as represented by Equation 1:

$$2H_2O\ (l) + E = 2H_2\ (g) + O_2\ (g) \quad (1)$$

where E denotes the amount of electrical energy needed to drive the electrolysis reaction.

Due to the critical role of hydrogen production in the energy scenario, numerous research papers investigate various aspects of electrolysis processes [6], materials for enhancing performance [7], modeling approaches [8–10] and techno-economic considerations [11]. Nevertheless, there are very few works on data acquisition (DAQ) and monitoring tasks concerning hydrogen generators according to the conducted literature review as expounded in the second section.

In this regard, automated DAQ, logging and visualization are required for the continuous monitoring and surveillance of processes [12]. In particular, for energy-related facilities, the relevance of DAQ and monitoring is highlighted in recent literature [13]. Monitoring systems are deemed crucial infrastructure for the transition towards a decentralized generation energy framework [14]. In the context of intelligent power grids, such as smart grids and microgrids, monitoring is of utmost importance [15,16]. For microgrids that incorporate hydrogen generation, the DAQ and monitoring system is a critical component of the energy management system [17], which is essential for the efficient operation of the microgrid.

Concerning hydrogen generators, it is crucial to provide the user with continuous updates on the status and progress of hydrogen production, along with the associated metrics. Therefore, efficient supervision systems are required to aid users in identifying any malfunctioning or healthy condition of the generator [18]. The monitoring system contributes to detect sensor/actuator faults and scheduling maintenance tasks to prevent system failure [18]. As asserted in [1], further research is necessary to monitor the operation and aging process of hydrogen-based systems to fulfill industrial demands and enhance the durability and reliability of hydrogen systems.

However, despite this importance of these systems, they are scarcely studied in previous literature. In fact, some works mention a system for DAQ and/or monitoring, but there is a lack of details regarding the configuration, architecture, or communication protocols employed. This issue is highlighted in the second section of the manuscript where the literature background is given.

Consequently, there is a research gap to address the development of DAQ and monitoring systems for the real deployment of hydrogen generation and to foster the green hydrogen paradigm. The term green hydrogen denotes the output obtained from electrolysis without producing any pollutants and utilizing renewable energy, such as photovoltaic energy.

Aiming at overcoming such a research gap, this paper proposes a DAQ and monitoring system based on Industrial Internet of Things (IIoT) for a hydrogen generator of PEM type. The main parameters of the PEMEL are sensed and acquired by an industrial controller. A middleware layer gathers the measurements through a communication network and stores them in a database. Online remote access to real time information of these magnitudes is provided by means of a web-based interface programmed with IoT software. According to the conducted literature review, this proposal constitutes a novel contribution to the existing literature on the topic.

The motivation of the present work arises in a R&D project about green hydrogen generation in a photovoltaic (PV)-powered microgrid. In such a scenario, sensing, DAQ and monitoring of a PEMEL was required and it was decided to develop a system based on IIoT technologies. The main contributions of the work are listed:

- Hydrogen generation is monitored through real-time visualization of parameters such as current, voltage, pressure, hydrogen flow, etc.
- Configuration and customization features are provided, including details about hardware and software components.
- Online remote access is achieved through web-based interface.
- IIoT technologies are successfully orchestrated and applied.
- Experimental results validate the developed system.

The structure of the rest of the paper is as follows. The second section provides a brief literature review to contextualize the presented research. Section 3 provides a detailed description of the developed DAQ and monitoring system, including information on the hardware and software components, data exchange mechanisms, and IIoT architecture configurations. Experimental results are reported and discussed in Section 4. Finally, the main conclusions of the work are expounded.

2. Literature background

There is an abundance of literature about PEMEL that use software simulation [19], emulators [20] and hardware in the loop [21]. However, research papers that report experimental measurements, data handling (acquisition, storage and transmission) and operation under real conditions over time are scarce. In this regard, experimental tests and demonstrative projects are essential means to develop new methods and tools to address the challenges of the future energy grid [22]. Concerning hydrogen facilities, further experimental work is still required [19]. Although simulation-based approaches are valuable, they cannot fully replicate real-world conditions and therefore cannot replace experimental research, which is essential to study and evaluate the operation of hydrogen-related equipment.

Table 1
Main features of related publications.

Work	DAQ device	Data storage (Database)	Middleware	Communication protocols	Visualization software	IoT	H_2 device
[23]	PLC	NA	NA	NA	NA	No	Yes (PEMEL)
[24]	NA	NA	NA	RS232	LabVIEW	No	Yes (Alkaline EL)
[25]	NA	NA	NA	CAN bus + OPC	iFIX	No	Yes (PEMEL)
[26]	PLC, power meter	NA	Python	Modbus	Python	No	Yes (Alkaline EL)
[21]	PLC	NA	NA	NA	LabVIEW	No	Yes (PEMEL)
[12]	PLC	Yes (localfile)	LabVIEW	OPC+TCP/IP	Easy Java Simulations	No	Yes (FC, PEMEL)
[27]	NA	NA	NA	NA	LabVIEW	No	Yes (PEMEL)
[30]	PLC	Yes (SQL)	NA	NA	NA	No	Yes (EL)
[31]	PLC	NA	NA	NA	NA	No	Yes (PEMEL)
[29]	PLC	NA	NA	NA	NA	No	Yes (PEMEL)
[32,33]	DAQ unit	NA	LabVIEW	NA	LabVIEW	No	Yes (PEMEL)
[28]	PLC	NA	NA	NA	TIA Portal (WinCC)	No	Yes (PEMEL)
[34]	PLC	NA	NA	Modbus TCP/IP	Matlab	No	Yes (PEMEL)
[35]	PLC	NA	NA	NA	LabVIEW	No	Yes (PEMEL)
[38]	Arduino	Yes (MySQL)	Python	Radio	HTML5	Yes	No
[39]	Smart meter, inverters	Yes (MySQL)	LabVIEW	OPC+Modbus TCP/IP	LabVIEW/Grafana	Yes	No
[40]	PLC	Yes (MySQL)	Node-RED	OPC UA	Grafana	Yes	No
[16]	Arduino	Yes (mariaDB)	Python	1-wire+TCP/IP	Grafana	Yes	No
[41]	PLC,BMU	Yes (mariaDB)	Python	Modbus TCP/IP, CAN, PROFINET	Grafana	Yes	No
[13]	Battery management unit/BMU	Yes (mariaDB)	Python	Modbus TCP/IP	Grafana	Yes	No
Present	PLC	Yes (mariaDB)	Node-RED	Modbus TCP/IP	Grafana	Yes	Yes (PEMEL)

Regarding to electrolyzers, relevant previous works are now commented. In [18] the importance of monitoring systems for PEMEL is emphasized and a model of the PEMEL is proposed to facilitate the detection of faults. In [23], a theoretical model and experimental analysis of a high pressure PEMEL is presented. Regarding DAQ, it is indicated that a Programmable Logic Controller (PLC) collects data from sensors and control the actuators; there is no mention to monitoring or visualization of the hydrogen generator operation. In [24] a DAQ system based on LabVIEW and RS232 connection is applied for monitoring an alkaline electrolyzer. The automation and monitoring system for a solar-hydrogen production unit is described in [25]. Data from a PEMEL is managed by a supervisory system, developed with iFIX of General Electric, enabling visualization of data transmitted over the Controller Area Network (CAN) protocol. Some screens of the Human-Machine Interface (HMI) are provided, but only instant values of the whole system are displayed. The work in [26] analyzes the operation of a grid-connected hydrogen buffer which includes an alkaline EL. A power meter and a PLC are responsible of DAQ and Python-based software displays the information transmitted over the protocol Modbus. A remote monitoring platform is developed in [12] to track the operation of a microgrid including renewable energies and hydrogen. Easy Java Simulations is the software used to carry out the visualization task whereas a PLC acquires data from sensors. Simulation based on a HIL scheme is reported in [21], where LabVIEW and a PLC are used to gather sensors measurements. In a similar sense, [27] develops a model for PEMEL cells including experimental analysis. Information about DAQ and monitoring is not reported, only LabVIEW running on a computer can be seen in a figure. The research in [28] develops an optimized balance of plant for a mid-size PEMEL including a PLC and a supervisory system programmed with the software TIA Portal of Siemens. In this case, a number of screens of the Supervisory Control and Data Acquisition (SCADA) system are reported. Sood et al. [29] propose dynamical model for PEMEL under intermittent sources like wind and solar. A laboratory-scale electrolyzer is described where a PLC is used to acquire sensor signals. An HMI can be observed in a photograph of the experimental setup, but the monitoring interface is not shown. The study of an electrolyzer in a fueling station is reported in [30], using a PLC and a SCADA system together with a Search Query Language (SQL) database to monitor its operation. The utilization of hydrogen generation as grid management tool for islands is studied in [31]. The control and monitoring of a PEMEL is performed with a PLC and a HMI. In [32] and [33] a DAQ unit NI PXI together with LabVIEW software is used to collect data from a set of microscopic sensors applied to a PEMEL. A remote HIL measurement system is proposed in [34], using a PLC for DAQ and Matlab linked through Modbus Transmission Control Protocol/Internet Protocol (TCP/IP). A model and real-time controller for PEMEL are designed by Flamm et al. [35]. The control approach includes a PLC for DAQ and LabVIEW.

The majority of the abovementioned literature does not provide detailed information on DAQ and monitoring concerning communication, data storage and graphical interfaces. Notably, monitoring interfaces are not reported in [18,21,23,24,26,30–35], whereas information about data communication and storage are not addressed in [18,21,23,26–33,35]. It must be remarked that these publications are not focused on monitoring tasks but contribute to advancements in aspects like modeling, simulation or operation issues. Therefore, according to the conducted literature review, there are no publications dealing with monitoring systems for hydrogen generators despite the importance of such systems.

At present, the utilization of IoT hardware and software constitutes a prevalent scientific and technological trend in the design of monitoring systems [13]. In fact, recent literature concerning open-source applications of IoT evinces a wide range of benefits, such as versatility, applicability, usability, affordability, and the availability of support, among others [36]. Alternatively, the IIoT is regarded as a sub-domain of IoT that encompasses the application of industrial and machine-to-machine (M2M) communication technologies employed in smart factories or within automation fields [37]. In this sense, a distinct cluster of publications that address monitoring systems featuring IoT or IIoT technologies, but without specific reference to hydrogen generation or consumption, are presently being expounded. The supervision of microgrid magnitudes is solved through Hyper Text Markup Language version 5 (HTML5) and a remote database in [38]. In [39] a real-time monitoring platform for distributed energy resources in microgrids is deployed using MySQL databases and software such as LabVIEW and Grafana. In the context of industrial digital twins, a framework to integrate physical assets and software twins is presented in [40]. The framework uses Node-RED to interface PLC and MySQL database, while Grafana is employed for data visualization. Grafana, SQL databases and Python as middleware are applied for monitoring purposes of PV generation and Lithium-ion battery in [16,41] and [13].

In order to reflect the reviewed literature in the scope of DAQ and monitoring systems for electrolyzers, Table 1 summarizes the main features of such literature considering seven categories. It must be noted that with the term Middleware we refer to the software entity dedicated to read data from the DAQ device and write to database, enabling data abstraction. NA stands for Not Available, for the information that is not found in the reference. As it can be checked in Table 1, the works that deal with hydrogen generators do not use IoT technologies, whereas those that use IoT equipment do not apply it to hydrogen generation processes. Consequently, there is no work addressing the DAQ and monitoring of hydrogen generators integrating IIoT technologies and providing information about configuration, data storage and communications.

3. Developed IIoT architecture for the DAQ and monitoring system

The developed system is expounded together with the conceptual IIoT architecture over which it relies. To begin with, it must be remarked that conceptual architectures allow establishing layers or levels to perform different functionalities. This type of architectures or frameworks are critical in distributed systems and networks to facilitate the understanding of roles, locations, and levels of abstraction of different hardware, software, and networking components [42]. Therefore, the orchestration of hardware and software nodes within the IoT and the IIoT is accomplished by adhering to layered architectures. In fact, various architectures have been outlined in literature, ranging from the fundamental three-tiered architecture to proposals comprising seven layers [43]. As stated in [44], there is no singular reference architecture, and devising one is a complex task, despite the multitude of standardization endeavors. In-depth reviews about IoT architectures can be found in [45] and [46]; for the scope of IIoT architectures, refer to [37].

Specifically, in the industrial field, there exist numerous heterogeneous components such as sensors, PLC, and HMI which must collaborate within an IIoT system [37]. Among the architectures for IoT and IIoT available in literature, there are abstract models which do not address the integration of things from the industrial environment, mainly communication fieldbuses endowed with real-time monitoring capabilities [37].

Under this perspective, the DAQ and monitoring system for PEMEL has been developed integrating equipment and protocols commonly employed in industrial environment. Namely, a PLC has been designated for DAQ operations, being connected to a set of sensors that measure the PEMEL parameters. Furthermore, the industrial communication protocol Modbus TCP/IP has been selected for data exchange between the PLC and the middleware.

The system has been orchestrated and deployed according to a four-layered architecture as proposed in [37,47,48]. Fig. 1 illustrates the architecture particularized for the developed DAQ and monitoring system for PEMEL. Subsequently, the functions of each layer and the technology selected for the PEMEL are described.

3.1. Perception/sensing layer

Concerning the Perception/Sensing layer, also referred to as Objects layer, it represents the physical layer and encompasses objects and devices that engage with each other and the physical environment via the exchange of data [49]. In industrial facilities, this layer is materialized by field devices such as sensors and actuators which gather information regarding the process, as well as computing devices, and other monitoring and automation objects [47].

In particular, to inform about the hydrogen generation, a number of magnitudes are acquired and displayed by the developed system. To begin with, the current consumed by the stack is measured by a Hall Effect sensor, whereas the voltage is sensed by means of a potentiometric voltage divider. A temperature probe type Resistance Temperature Detector (RTD) PT-100 [50] is applied to gage the stack temperature. Regarding fluidic magnitudes, hydrogen flow rate corresponds to the hydrogen generated over time, being sensed by a thermal mass flow rate meter. The hydrogen pressure is gathered by two pressure transmitters that determine both the pressure of the generated hydrogen and the stored gas. The water level within the gas-liquid phase separator is detected by means of an electro-optic switch. These sensors and their key characteristics are summarized in Table 2. Moreover, Fig. 2 depicts a fluidic diagram of the PEMEL where the sensors can be appreciated.

In addition, this layer transforms the acquired analog data into digital signals to ensure compatibility with other layers of the system [43]. In the reported system, the PLC acts as DAQ device, and hence, it is situated within the Perception/Sensing layer. A PLC is a device equipped with digital and analog Input/Output (I/O) modules that facilitate the interfacing of sensors and actuators. Modern PLC are equipped with communication capabilities that support several protocols, which enables data sharing over communication networks. In the present case, the PLC is devoted to acquiring data from the aforementioned sensors. In particular, a PLC S7–1500 family of the manufacturer Siemens is used, which incorporates in-built RJ45 ports for Ethernet-based networked communications [51].

3.2. Network/transportation layer

The Network/Transportation layer, also referred as Transmission or Connectivity layer, is accountable for data routing and transmission [49]. This layer facilitates the communication of data between the Perception/Sensing layer and the

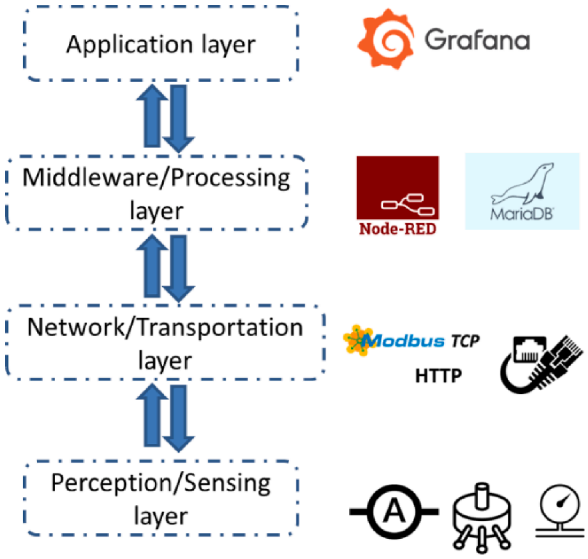

Fig. 1. IIoT architecture for the measurement and monitoring system for PEMEL.

Table 2
Sensors devoted to measure hydrogen production magnitudes.

Magnitude	Sensor
Hydrogen flow rate (ml/min)	Thermal Mass Flow Meter for gases (model Bronkhorst, range 0–1000 ml/min)
Current (A)	Hall effect sensor (model LEM LTS15-NP)
Voltage (V)	Potentiometric voltage divider
Pressure (bar)	Pressure transmitter (4–20 mA, 0 – 10 bar, model WIKA A-10)
Stack temperature (ºC)	RTD PT-100
Water level	Electro-optic switch (5 V, model ELS-900)

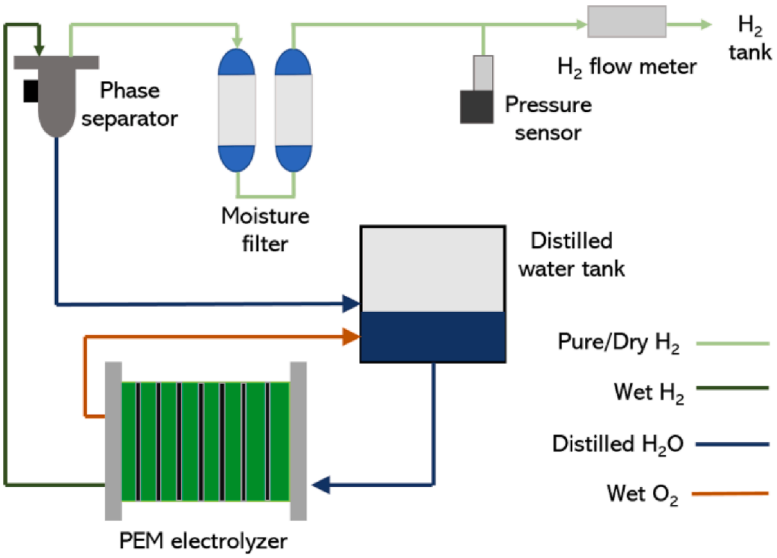

Fig. 2. Fluidic diagram of the PEMEL including sensors from the perception/sensing layer.

Middleware/Processing layer through various networks [52]. This layer comprises all the technologies and protocols that enable the establishment of such connections [44].

A number of communication protocols can be handled in this layer such as TCP/IP, Radio-Frequency Identification (RFID), Wi-Fi, Message Queuing Telemetry Transport (MQTT), etc. In the present case, this layer comprises Modbus TCP/IP, Hypertext Transfer Protocol (HTTP) and Ethernet. Regarding the first one, Modbus is a protocol considered as a de facto standard for industrial communications, being its first version developed in 1979 by Modicon [53]. Nowadays, the TCP/IP version is considered as an IoT protocol [54] resulting from its evolution and adaptation to newer decentralized frameworks [41]. The client/server model is implemented and both types of nodes establish their linkage using the IP address. An interesting feature of this communication interface is that it is supported by both proprietary and IoT open-source hardware/software, facilitating a seamless data exchange [41]. As indicated in [55], with the aid of Modbus TCP/IP protocol, reliable operations can be supported and applied in IoT systems. For PEMEL monitoring, Modbus TCP/IP is employed to exchange data between the aforementioned PLC and a middleware platform placed in the upper layer.

Next in order, HTTP was initiated in 1989 by Tim Berners-Lee for data transfer across the web [56]. HTTP is a request-response protocol under the client/server model. A web browser can play the role of client, whereas a computing node hosting a website acts as server. This protocol corresponds to the application layer of the Open Systems Interconnection (OSI) reference model for networked communications. Within the context of IIoT and Industry 4.0, HTTP is pointed as a reliable communication in [57]. In the developed system, this protocol is utilized by the software application Grafana to fetch information from the database for visualization purposes.

Finally, Ethernet aligns with the IEEE standard 802.3 and operates within the two lower levels of the OSI model, the physical level (layer 1) and the link level (layer 2). Ethernet-based networks have witnessed a surge in popularity owing to their numerous benefits, such as high speed, ample bandwidth, and seamless integration with both the Internet and office networks [58]. Ethernet is recognized as the foundation for advancements in industrial communications and the standardization of industrial protocols [59]. In fact, Ethernet-based networks are the prevalent trend for Information Technology (IT), IoT-enabled equipment and modern automation systems [58,60]. Indeed, wired Ethernet network is the preferred choice in industrial settings due to its enhanced reliability and heightened security features [61].

3.3. Middleware/processing layer

The Middleware/Processing layer provides a number of critical functionalities such as storage, filtering, aggregation, analysis and processing of data coming from the Network/Transportation layer [44,49,52]. Data is collected from heterogeneous devices by means of various communication protocols, so the middleware layer enables interoperability among connected devices [49]. Within the middleware layer, the specifics of various technologies are concealed, and standard interfaces are employed to offer an abstraction that sits between IoT technologies and applications. Furthermore, a crucial decision in the process of designing IoT-based systems is the selection of open-source or proprietary middleware solutions. Open-source middleware offers greater flexibility, cost advantages, and ease of deployment [52]. Consequently, in the present proposal, open-source tools have been selected.

Regarding data storage, a relational database deployed with the package mariaDB handles information accumulation in SQL format, being fed by the middleware entity (Node-RED). The different magnitudes are recorded including the corresponding time-stamp with a sample time of 1 min. This sampling interval is deemed sufficient for visualizing the PEMEL response and operation. However, it can be readily adjusted if shorter sampling periods are required.

With respect to data interoperability and abstraction, according to Lombardi et al. [44], some noteworthy advantages provided by middleware are execution on various operating systems; distributed computing and interaction of services among heterogeneous networks, devices, and applications; and support for standard protocols. In this sense, Node-RED fulfills these features and is considered as suitable for acting as middleware platform in the developed system. Node-RED is a multiplatform flow-based visual programming tool built on Node.js and started in 2013 [62]. It is a user-friendly software that offers a visually intuitive design through the use of drag-and-drop blocks and connections [40]. Node-RED allows wiring together hardware devices, Application Programming Interfaces (API) and online services [63]. The middleware boasts extensive programming capabilities, featuring a large node library with built-in support for IoT protocols. This enables the wiring together of field and automation devices with cloud services and databases [40]. Besides, it has the added advantage of being multi-client accessible, lightweight, robust and easy to access via the cloud for developers in Industry 4.0 and IoT connectivity fields [40].

Fig. 3a depicts the flow defined to perform the tasks required for processing the PEMEL data. Firstly, a node for reading through Modbus TCP/IP collects the sensor measurement stored in the PLC memory. Next in order, a function node processes the read data using JavaScript code (Fig. 3b). A statement for SQL writing is the last instruction of this node. Finally, a SQL configuration node is required for accessing the database.

The configuration of Modbus operation in Node-RED is briefly commented and illustrated in Fig. 4. In order to access the Modbus server in Node-RED, the following parameters must be configured: the function code, which in this case is FC3 (Read Holding Register), and the address of the variable within the PLC memory. Additionally, the IP address of the Modbus server and the logic port used for transmission must also be specified. By default, the port used for Modbus transmission is 502. These parameters are illustrated in Fig. 4.

3.4. Application layer

The Application layer, also referred as Services layer, represents the highest level of the system and provides the output formats, applications and services requested by the final users [49]. This layer leverages all the functionalities of the middleware layer and encompasses all the software components required to provide a specific service. As a result, data becomes accessible to IoT applications

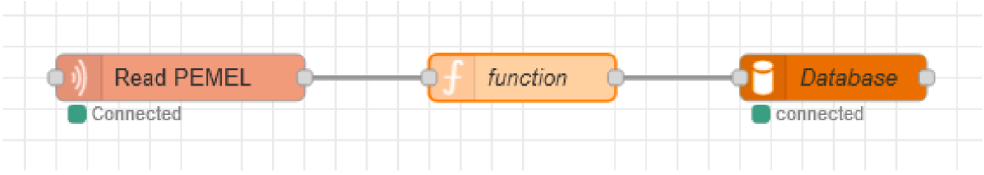

(a)

```
1  var Current = msg.payload[4];
2  var Voltage = msg.payload[5];
3  var Temp = msg.payload[6];
4  var Pressure = msg.payload[21];
5  var HFlow = msg.payload[23];
6  msg.payload = [Current, Voltage, Temp, Pressure, HFlow];
7  msg.topic = "INSERT INTO electrolizador_stack1('CurrentACC','VoltageACC','Temperature') VAL
8  msg.topic = "INSERT INTO general_values('Presion','Caudal') VALUES("+Pressure+","+HFlow+")"
9  return msg;
```

(b)

Fig. 3. . a) Flow defined in Node-RED for data retrieving and storage tasks. b) JavaScript code for processing data.

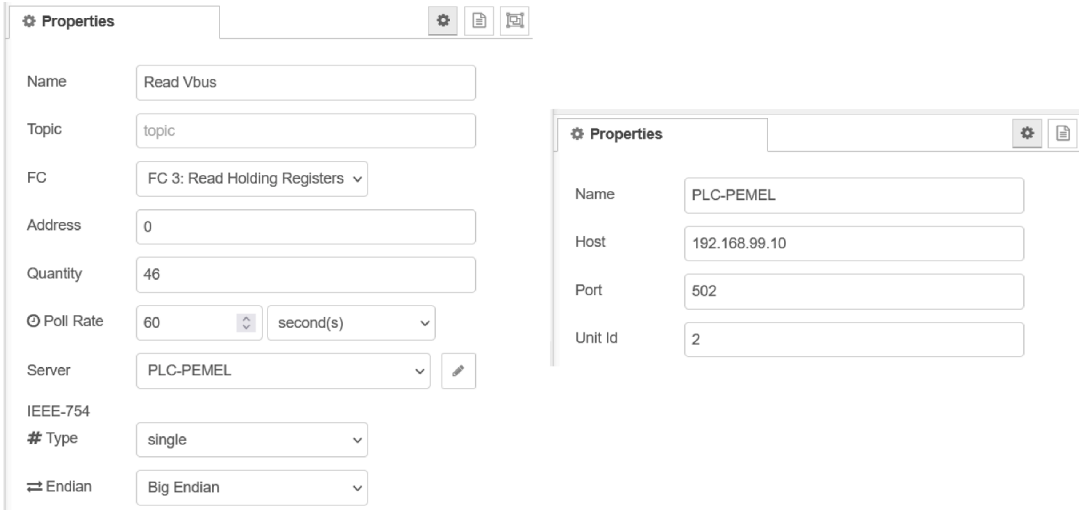

Fig. 4. Configuration of modbus TCP/IP communication in node-RED.

[44]. At this layer, software solutions and applications for remote monitoring and control of things in the industrial environment can be designed and developed [37]. Hence, visualization of data acquired from the process representing the evolution over time can be performed at this layer by means of HMI, SCADA systems and graphical interfaces [37].

In particular, the Grafana IoT software suite has been selected for the visualization of the PEMEL operation. This web-based application provides data query and real-time display of data through time-series charts as well as instant values in user-created dashboards. The visual features and interactivity of the graphical dashboards contribute to the surveillance of the monitored process [13] and aids in understanding complex scenarios and improved decision making [40]. It is open-source, multi-platform, lightweight and incorporates built-in connectivity with a number of databases, which makes it suitable for the purposes of the PEMEL monitoring system. In fact, a Grafana server gathers information from the mariaDB database of the Middleware/Processing layer and provides a set of customized dashboards that display the hydrogen generator main parameters over time, as it will be described in the next section.

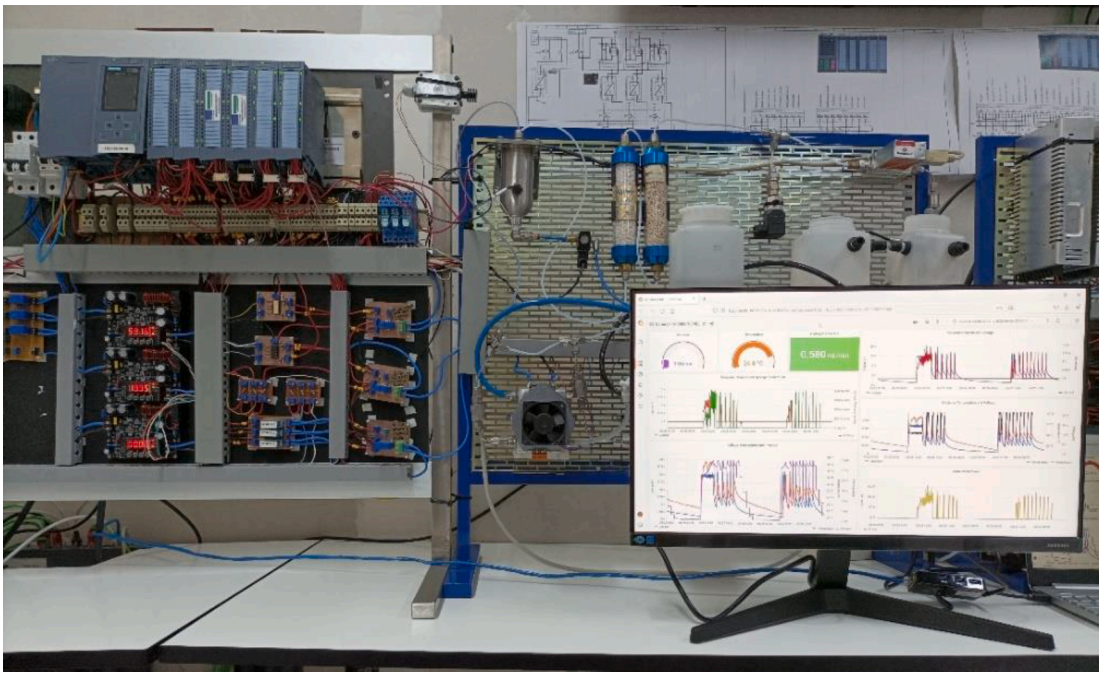

Fig. 5. Physical aspect of the PEMEL in the laboratory setup.

4. Experimental results and discussion

This section reports on the experimental results obtained from the implementation of the developed system and IIoT architecture in an experimental PEMEL, in order to demonstrate its suitability. The laboratory setup and graphical interfaces are described, followed by a discussion of the results and the main findings in the third subsection.

4.1. Results

4.1.1. Physical deployment in laboratory setup

As depicted in Fig. 5, the PEMEL and its associated sensors are physically deployed in the laboratory setup. The PLC is mounted on a metal sheet panel and connected to the sensors through I/O modules. Meanwhile, the PEM stack is placed on another panel along with the other associated elements, such as the phase separator or the thermal mass flow meter. Table 3 summarizes the key features of this hydrogen generator.

4.2. Graphical interfaces

The Grafana dashboard has been designed to facilitate the user a rapid inspection of the key parameters involved in the operation of PEMEL through numerical values and graphical elements (Fig. 6). Regarding the structure of the dashboard, the upper portion displays instantaneous values of working pressure and temperature, along with the hydrogen flow rate generated, conveyed through numerical and gauge-type indicators. The remaining section of the dashboard comprises graphs that depict various PEMEL variables. Each graph displays a set of variables, considering the interrelation of these variables in the operation of the electrolyzer. The time interval for data display can be modified by the user, allowing for short- or long-term visualization, as well as real time display. Another notable feature is the capability to zoom in or display the dashboard elements in full screen, providing a comprehensive view of the information exhibited. Additionally, Grafana offers the possibility to export the data represented in the selected time interval through a local download.

4.2.1. ECM electrolyzer model

In the literature, various Equivalent Circuit Models (ECM) are available to represent the behavior of electrolyzer cells and stacks [64]. Among them, in order to analyze the operation of the experimental PEMEL through the developed system, the ECM proposed in [8] has been utilized as a reference to identify the key parameters of the PEMEL and their relationship, in order to develop the dashboard graphs and to group the relevant parameters. In Atlam and Kolhe [8], a series of expressions based on the ECM are described, which relate PEMEL parameters such Voltage V, Current I, hydrogen flow rate v_H, working temperature T, working pressure p or efficiency η_e. These expressions are presented below.

Firstly, Eq. (2) shows the relationship between the PEMEL voltage and the current consumed, as well as the operating temperature and pressure conditions.

$$V(T,p) = I\frac{n_s}{n_p}R_i(T,p) + n_s e_{rev}(T,p) \tag{2}$$

Where n_s and n_p represent the number of cells in series or parallel, respectively, that comprise the PEMEL stack. Furthermore, R_i and e_{rev} denote the internal resistance and reversible voltage of the electrolyzer, respectively. These parameters refer to internal properties of the PEMEL as a function of T and p.

The power consumed by the PEMEL is defined in Eq. (3):

$$P = VI \tag{3}$$

Regarding hydrogen production, the hydrogen flow rate v_H is expressed in Eq. (4) and is directly dependent on the current consumed by the PEMEL.

$$v_H = v_M(l)\left(\frac{10^3\ ml}{l}\right)\left(\frac{60\ s}{min}\right)\left(\frac{I\left(\frac{C}{s}\right)}{2F(C)}\right) = v_M\left(10^3\right)(60)\frac{I}{2F} \tag{4}$$

Table 3
Main features of the PEMEL used in the experimental setup.

Feature	Value
Number of cells	6
Input current range	0 – 10 A
Operating temperature	Up to 60 °C
Operating pressure	Up to 6 bar
Hydrogen flow production	750 ml/min
Hydrogen purity	>99.9999%

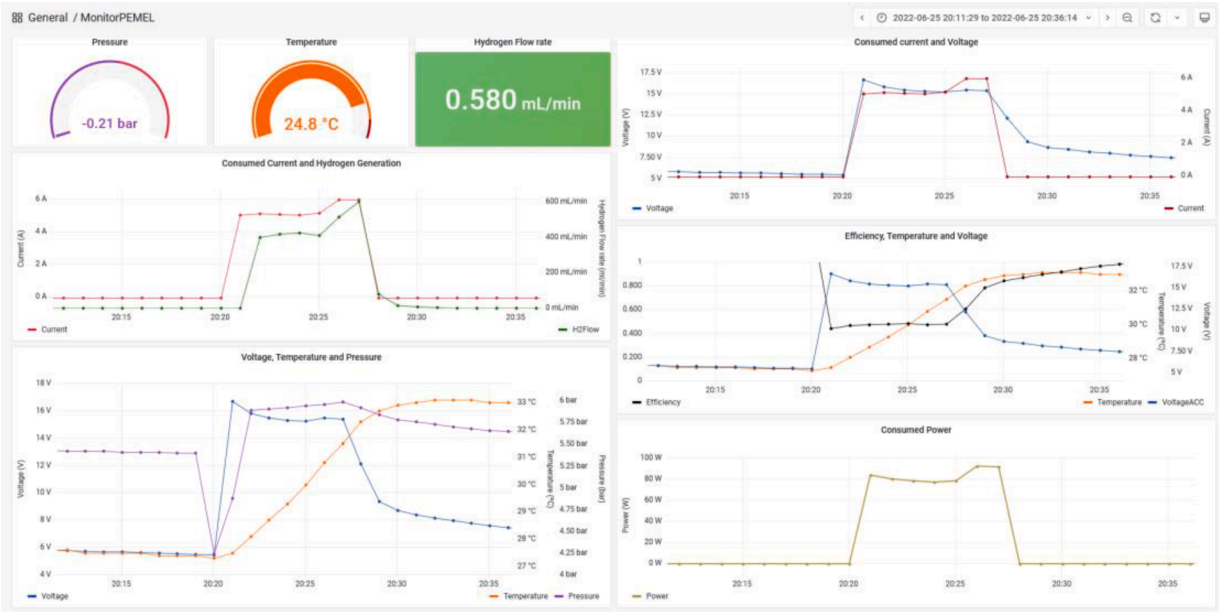

Fig. 6. General view of the Grafana interface for PEMEL monitoring.

Where v_M is the molar volume generated and F is the Faraday constant.

Finally, the electrolyzer efficiency η_e is defined in Eq. (5) as the ratio between the ideal voltage V_i used in the electrolysis process and the total voltage V presented by the PEMEL. V_i is calculated per cell, so in the expression it is accompanied by n_s to obtain the total ideal voltage of the PEMEL.

$$\eta_e = \frac{n_s V_i}{V} \tag{5}$$

4.2.2. *Consumed current and hydrogen flow*

The correlation between the current consumed and the hydrogen flow produced illustrates the working principle of the PEMEL. Fig. 7 depicts the direct relationship between the two parameters, as indicated in Eq. (4). This figure displays three different sections of

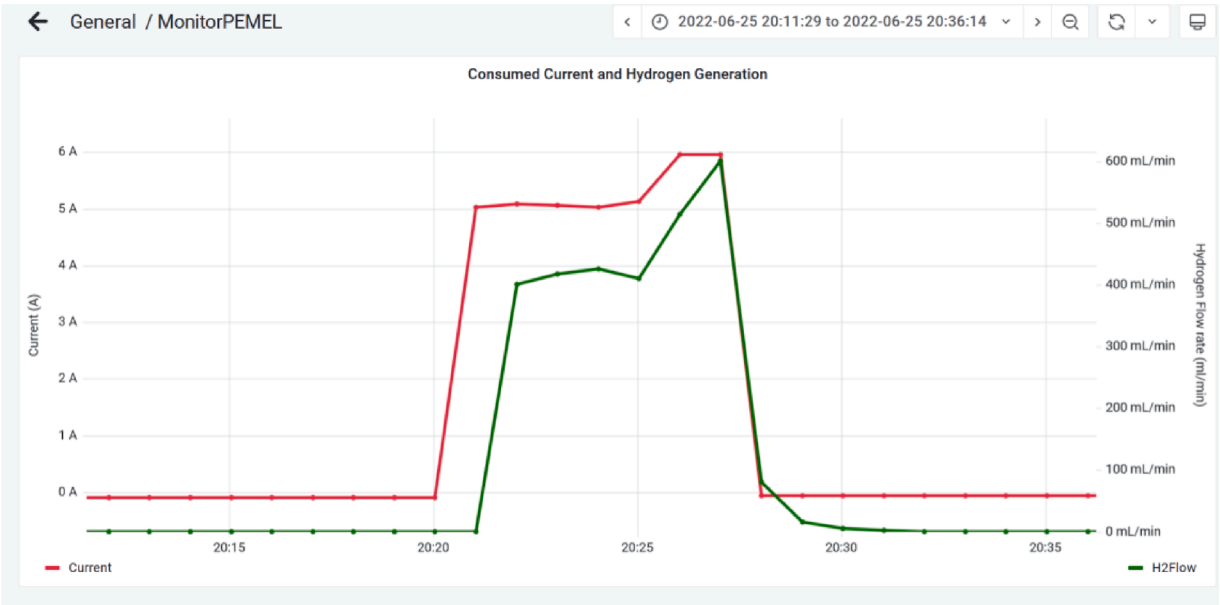

Fig. 7. Consumed current (red line) and hydrogen flow (green line) graph.

increasing and decreasing current, respectively. Consequently, the generated hydrogen flow rate exhibits the same variations as the current. In the first section, a current increase of 5 A is performed, which results in a hydrogen flow rate of 400 ml/min with a delay of one minute after reaching the setpoint current. Subsequently, an additional current increase is executed until 6 A is reached. As a result, the flow rate is raised to a maximum point value of 600 ml/min. Finally, the PEMEL is halted by reducing the current consumption to 0 A, resulting in an immediate and delay-free drop in hydrogen production to 0 ml/min.

4.2.3. Consumed current and voltage

The voltage measured at the electrolyzer terminals is dependent on the current consumed. Fig. 8 illustrates the direct relationship between both parameters, where it is observable that an increase in current (from 0 A to 5 A) instantaneously results in an increase in voltage (from 6 V to 16 V). In contrast, when the current consumed decreases (from 6 A to 0 A), the voltage drop in the electrolyzer is not immediate, but instead there is a gradual decrease. This effect derives from the structure of the cells that comprise the stack, which essentially consists of interconnected capacitors, leading to electrical accumulation. When the PEMEL is below the operating threshold current, a self-discharge mechanism occurs, which causes a continuous and gradual decrease in voltage. Regarding this particular case, it can be observed that the self-discharge phenomenon causes a reduction in voltage from 15 V to 8 V in approximately 7 min. This voltage drop occurs in two stages, from 5 V to 10 V, and from 10 V to 8 V. In the experimental PEMEL setup employed, the voltage level of 10 V represents the threshold voltage of the stack at the minimum operating current. The initial stage occurs rapidly due to the fact that the PEM electrolyzer is designed to operate with sudden variations in current and to adjust its parameters at a comparable rate, while still operating within its designated nominal range. During the second stage, the cells of the stack do not receive sufficient current to operate, thereby triggering the self-discharge effect, which results in a gradual reduction in voltage. This phenomenon is illustrated in Fig. 8 as a variation in the slope of the voltage curve.

4.2.4. Power and hydrogen flow

The total power consumed by the PEMEL is a function of the voltage and consumed current, as depicted in Eq. (3). Nonetheless, hydrogen generation is solely dependent on the current, as indicated by Eq. (4) and demonstrated by the curves in Fig. 9. These curves exhibit an analogous pattern to those observed in Fig. 7. In the situation depicted in Fig. 9, an initial level of flow generated at 400 ml/min under a power consumption of 80 W is illustrated. Subsequently, as the parameters are increased for a second time, a 10 W increase in the consumed power results in a notable increase of 200 ml/min in the generated flow rate. This behavior represents a 50% improvement in the hydrogen generated compared to a minimum increment of power consumption.

4.2.5. Voltage, temperature and pressure

As indicated in Eq. (2), the PEMEL voltage is dependent on temperature and working pressure due to R_i and e_{rev}. Regarding temperature, an elevation in this parameter leads to a decrease in voltage, while conversely, a reduction in temperature results in an increase in voltage. The impact of pressure on the PEMEL is opposite to that of temperature; an increase in pressure leads to an increase in voltage, while a decrease in pressure results in a decrease in voltage. The situation depicted in Fig. 10 illustrated a reduction in voltage (from 16 V to 15 V) due to an increase in temperature (from 27.5 ºC to 33 ºC), at a slight fluctuation in pressure (0.20 bar).

Fig. 8. Consumed current (red line) and voltage (blue line) graph.

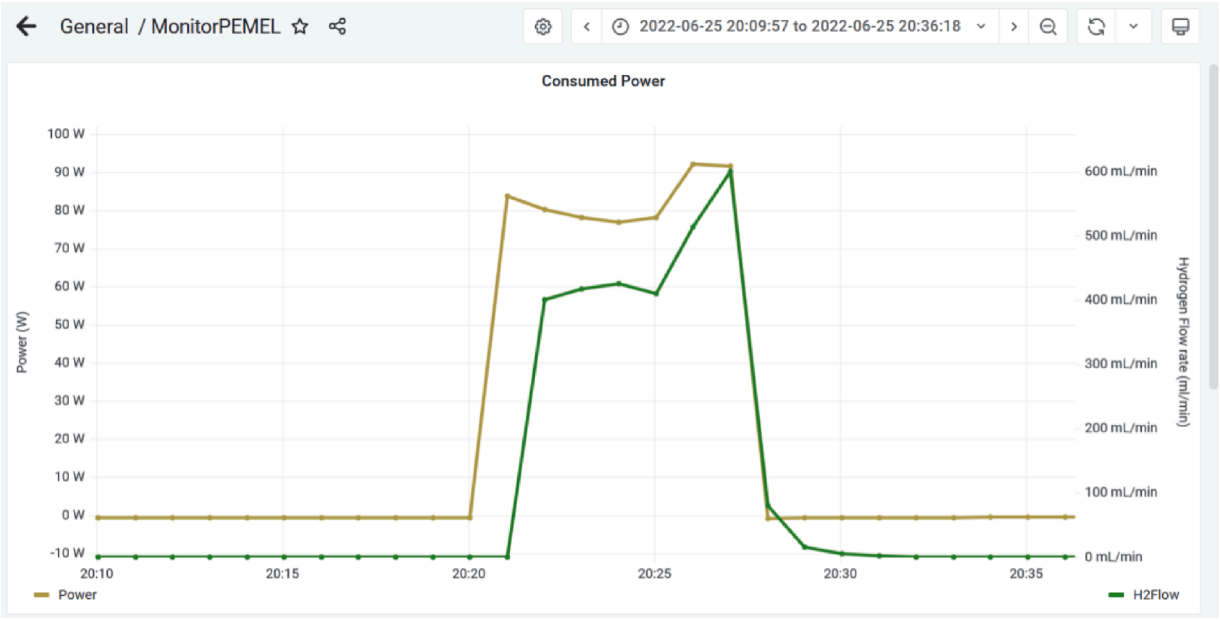

Fig. 9. Consumed power (yellow line) and hydrogen flow (green line) graph.

Concerning the pressure curve, this parameter undergoes a sharp initial drop from 5.40 bar to 4.20 bar due to a purging process executed in the system. The purpose of this process is to eliminate the water content in the hydrogen generated by means of a solenoid valve. Subsequent to the purging process, the working pressure promptly increases and stabilizes at approximately 5.60 bar.

4.2.6. *Efficiency, temperature and voltage*

The efficiency of the PEMEL is calculated as the ratio between V_i and V. Moreover, the electrolyzer voltage is affected by temperature variations, as illustrated in Fig. 10. This results in a correlation between efficiency and working temperature. Fig. 11 displays the PEMEL in operation, showcasing an increase in temperature (from 27.5 ºC to 33 ºC) that leads to a drop in voltage (from 16 V to 15 V). Both variations lead to an upward trend in the efficiency curve, with a nominal value of approximately 45% for these specific conditions. Analogously, an increase in voltage causes an instantaneous reduction in the efficiency of the equipment.

4.2.7. *Characterization essay*

An additional functionality of the dashboard implemented in Grafana is the utilization of the graphical elements provided to analyze the results derived from tests or trials for the characterization of the PEMEL. As an illustration of this, a test for the study of the self-discharge effect is depicted in Fig. 12. For this purpose, the PEMEL is operated at different current consumption points, from 5 A to 8 A. In order to conduct this test, the electrolyzer is subjected to cycles of starting, operating and shutting down at different current points. In each of the cycles it can be observed that, regardless the current point, the maximum voltage reached after start-up is 16 V. After one minute of operation, the power consumption is interrupted and it is observed that, for all the cycles carried out, the self-discharge effect described in Section 4.2.3 starts for a voltage level of 8 V. In this instance, the duration of the phenomenon is not pertinent, since the objective is to investigate the self-discharge phenomenon and its correlation with the level of voltage and current consumed. Nevertheless, in the last cycle performed, a reduction in voltage was observed due to self-discharge, which caused the voltage to drop from 8 V to 2 V over a period of 6 h.

It is worthy to remark that long-term intermittent operation results in a deterioration of the lifetime of the PEMEL and its repetition over long operating cycles leads to degradation mechanisms associated with the permanent increase of the operating voltage of the cells for the same current point [65].

4.3. *Discussion*

DAQ and monitoring of a PEMEL have been properly achieved, following an IIoT architecture consisting on four layers. The reported results correspond to an experimental setup operating under real conditions. Furthermore, a significant number of the IIoT architecture proposals found in literature are solely conceptual, based on theoretical knowledge without performing experimental validation [66].

User-friendly and responsive interfaces facilitate the inspection of the PEMEL operation. The observation of instant values and time-series of the most relevant magnitudes of the hydrogen generation are achieved. Moreover, the developed interfaces are reported together with equations based on well-known ECM to validate the displayed curves.

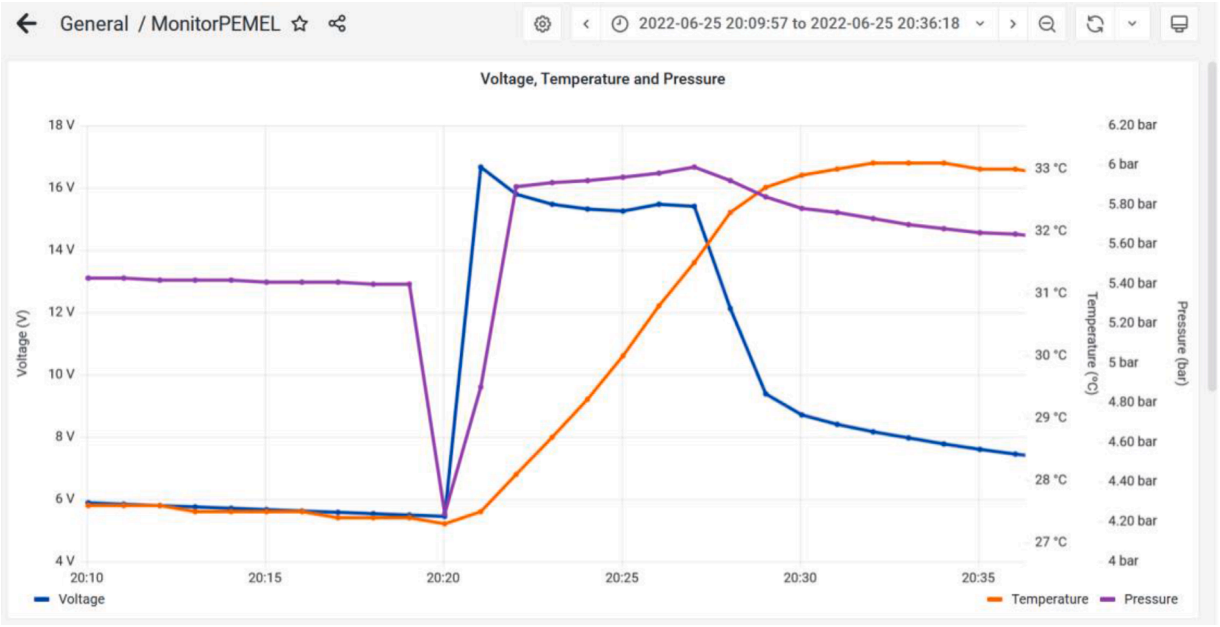

Fig. 10. Voltage (blue line), working temperature (orange line) and working pressure (purple line) graph.

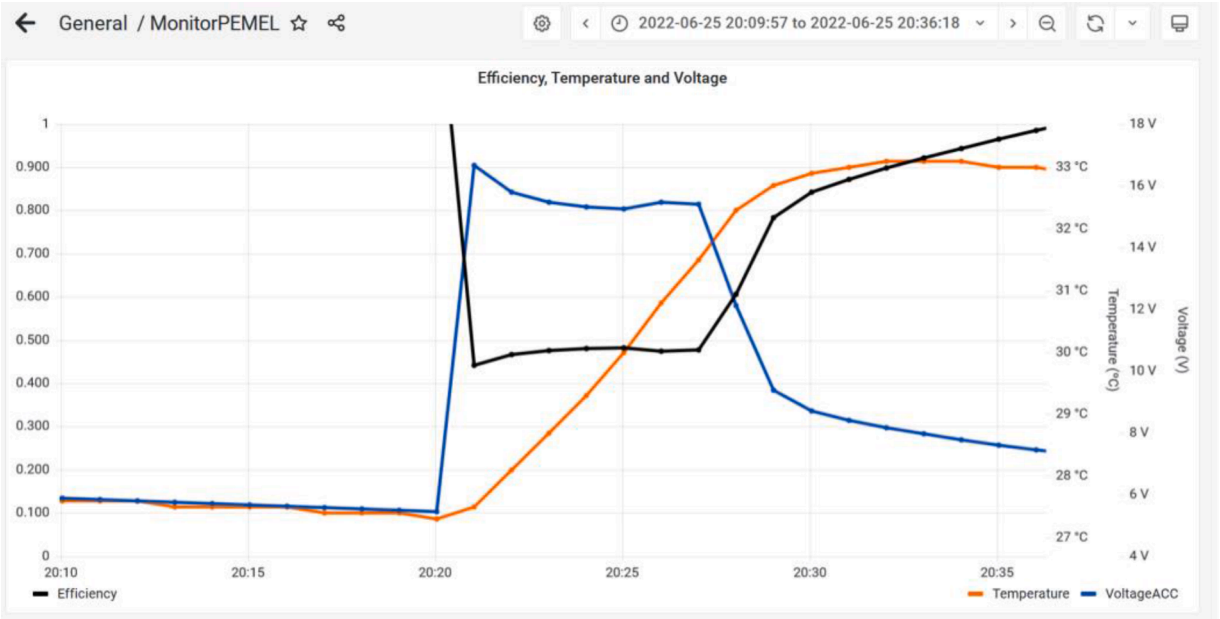

Fig. 11. Efficiency (black line), working temperature (orange line) and voltage (blue line) graph.

The wide availability of communication protocols that can be handled by Node-RED contributes to manage the heterogeneity of communication protocols and devices (sensors, controllers, HMI, etc.) industrial environment. In fact, easy configuration of data communication between nodes is achieved due to Node-RED features, which acts as middleware. Moreover, Modbus TCP/IP has been selected as it is a widely applied and supported communication interface. Nonetheless, other modern protocols like MQTT and Open Platform Communications-Unified Architecture (OPC-UA) can also be used for data transmission.

Proprietary and IoT open source equipment have been seamlessly integrated under the developed system, which is required to manage interoperability and heterogeneity of components [41,67].

The low-cost nature of IoT software decreases the investments required for managing hydrogen-related equipment, mainly generators, contributing to spread their deployment. This aspect is relevant concerning scientific equipment as highlighted in recent

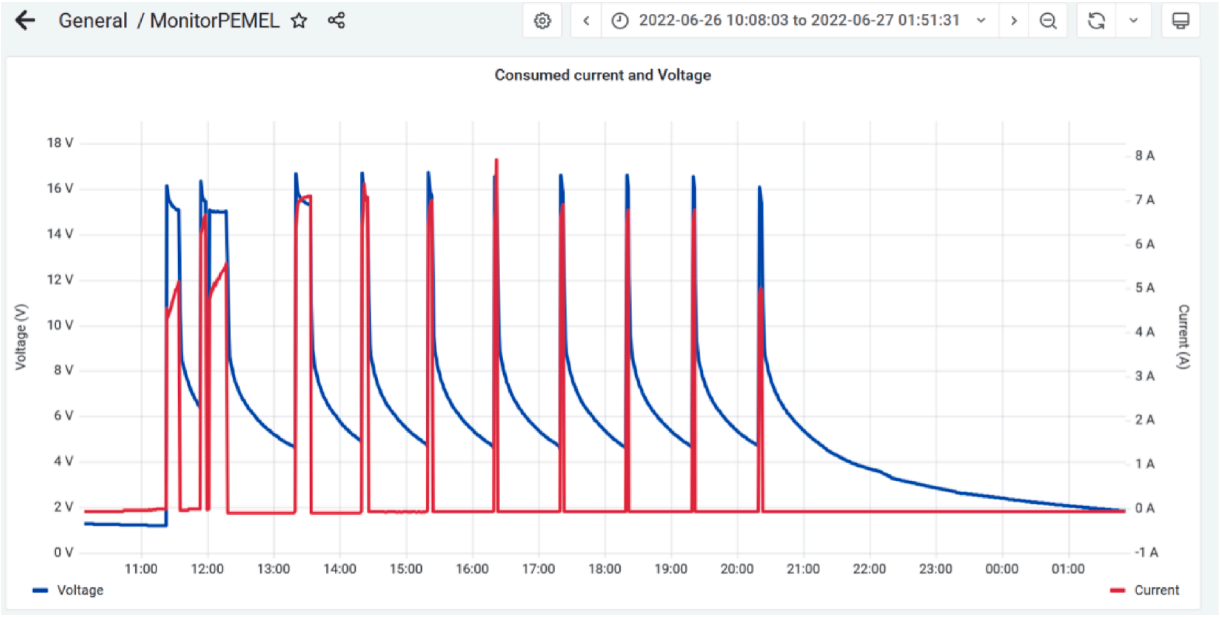

Fig. 12. Consumed current (red line) and voltage (blue line) graph in self-discharge essay.

literature [68].

The visualized and acquired data could be used for degradation effects diagnostics through the use of the stored values and the implemented graphical interface. Another relevant feature of the Grafana IoT software is its ability to operate with stored data, which enables the integration of models validated in the literature for comparative analysis of electrolyzer performance.

The system can be reconfigured and fully customized by the developer without the restrictions typical of commercial data-logging and monitoring systems. For instance, characterization processes of stacks can be conducted and the monitoring system facilitates data storage and visualization of the associated phenomena. This feature is particularly appealing for research-related frameworks as well as for testing new industrial-oriented facilities. Other potential customization options could involve adapting the proposal to different types of EL, such as alkaline or even PEM fuel cells. The sensing devices and the visualization interfaces should be particularized for the specific equipment to monitor.

5. Conclusions

This paper has presented a novel DAQ and monitoring system for hydrogen generators of PEM type. Successful experimental results prove the validity of the proposal.

An IIoT architecture is proposed and the system is deployed according to it, integrating industrial equipment, IoT software and sensing devices appropriate to the PEMEL. As it was stated in the second section, the present work constitutes a novelty in literature. There is no previous work that develops a DAQ and monitoring system framed into the IIoT paradigm for electrolyzers. The proposal provides complete information about configuration of both hardware and software as well as communication and data storage.

The developed research is envisioned to promote hydrogen production, storage and utilization in energy industry through the integration and application of IIoT technologies.

Future works deal with developing a digital twin of the PEMEL utilizing the acquired data. Furthermore, the acquired information is highly valuable to face the design and implementation of energy management strategies for hydrogen-based microgrids.

Declaration of Competing Interest

The authors declare that they have no known competing financial interests or personal relationships that could have appeared to influence the work reported in this paper.

Data availability

The authors are unable or have chosen not to specify which data has been used.

Acknowledgements

Project co-financed by European Regional Development Funds FEDER and by the Junta de Extremadura (IB18041).

References

[1] M. Yue, H. Lambert, E. Pahon, R. Roche, S. Jemei, D. Hissel, Hydrogen energy systems: a critical review of technologies, applications, trends and challenges, Renew. Sustain. Energy Rev. 146 (2021), 111180, https://doi.org/10.1016/j.rser.2021.111180.
[2] M. Neuwirth, T. Fleiter, P. Manz, R. Hofmann, The future potential hydrogen demand in energy-intensive industries - a site-specific approach applied to Germany, Energy Convers. Manage. 252 (2022), https://doi.org/10.1016/j.enconman.2021.115052.
[3] A. Sánchez, Q. Zhang, M. Martín, P. Vega, Towards a new renewable power system using energy storage: an economic and social analysis, Energy Convers. Manage. 252 (2022), https://doi.org/10.1016/j.enconman.2021.115056.
[4] M.F. Ahmad Kamaroddin, N. Sabli, T.A. Tuan Abdullah, S.I. Siajam, L.C. Abdullah, A. Abdul Jalil, et al., Membrane-based electrolysis for hydrogen production: a review, Membranes 11 (2021) 1–27, https://doi.org/10.3390/membranes11110810.
[5] Q. Feng, X.Z. Yuan, G. Liu, B. Wei, Z. Zhang, H. Li, et al., A review of proton exchange membrane water electrolysis on degradation mechanisms and mitigation strategies, J Power Sources 366 (2017) 33–55, https://doi.org/10.1016/j.jpowsour.2017.09.006.
[6] S. Shiva Kumar, V. Himabindu, Hydrogen production by PEM water electrolysis – a review, Mater. Sci. Energy Technol. 2 (2019) 442–454, https://doi.org/10.1016/j.mset.2019.03.002.
[7] S. Wang, A. Lu, C.J. Zhong, Hydrogen production from water electrolysis: role of catalysts, Nano Convergence 8 (2021), https://doi.org/10.1186/s40580-021-00254-x.
[8] O. Atlam, M. Kolhe, Equivalent electrical model for a proton exchange membrane (PEM) electrolyser, Energy Convers. Manage. 52 (2011) 2952–2957, https://doi.org/10.1016/j.enconman.2011.04.007.
[9] A. Awasthi, K. Scott, S. Basu, Dynamic modeling and simulation of a proton exchange membrane electrolyzer for hydrogen production, Int. J. Hydrogen Energy 36 (2011) 14779–14786, https://doi.org/10.1016/j.ijhydene.2011.03.045.
[10] D.S. Falcão, A.M.F.R. Pinto, A review on PEM electrolyzer modelling: guidelines for beginners, J. Clean. Prod. 261 (2020), https://doi.org/10.1016/j.jclepro.2020.121184.
[11] D. Jang, J. Kim, D. Kim, W.B. Han, S. Kang, Techno-economic analysis and Monte Carlo simulation of green hydrogen production technology through various water electrolysis technologies, Energy Convers. Manage. 258 (2022), 115499, https://doi.org/10.1016/j.enconman.2022.115499.
[12] I. González, A.J. Calderón, J.M. Andújar, Novel remote monitoring platform for RES-hydrogen based smart microgrid, Energy Convers. Manage. 148 (2017) 489–505, https://doi.org/10.1016/j.enconman.2017.06.031.
[13] I. González, A.J. Calderón, F.J. Folgado, IoT real time system for monitoring lithium-ion battery long-term operation in microgrids, J. Energy Storage 51 (2022), 104596, https://doi.org/10.1016/j.est.2022.104596.
[14] Z. Vale, H. Morais, P. Faria, C. Ramos, Distribution system operation supported by contextual energy resource management based on intelligent SCADA, Renew. Energy 52 (2013) 143–153, https://doi.org/10.1016/j.renene.2012.10.019.
[15] C. Vargas-Salgado, J. Aguila-Leon, C. Chiñas-Palacios, E. Hurtado-Perez, Low-cost web-based Supervisory Control and Data Acquisition system for a microgrid testbed: a case study in design and implementation for academic and research applications, Heliyon 5 (2019), https://doi.org/10.1016/j.heliyon.2019.e02474.
[16] J.M. Portalo, I. González, A.J. Calderón, Monitoring system for tracking a pv generator in an experimental smart microgrid: an open-source solution, Sustainability (Switzerland) 13 (2021), https://doi.org/10.3390/su13158182.
[17] Y.E.G. Vera, R. Dufo-López, J.L. Bernal-Agustín, Energy management in microgrids with renewable energy sources: a literature review, Appl. Sci. (Switzerland) 9 (2019), https://doi.org/10.3390/app9183854.
[18] M.E. Lebbal, S. Lecœuche, Identification and monitoring of a PEM electrolyser based on dynamical modelling, Int. J. Hydrogen Energy 34 (2009) 5992–5999, https://doi.org/10.1016/j.ijhydene.2009.02.003.
[19] H.A.Z. Al-Bonsrulah, M.J. Alshukri, L.M. Mikhaeel, N.N. Al-Sawaf, K. Nesrine, M.V. Reddy, et al., Design and simulation studies of hybrid power systems based on photovoltaic, wind, electrolyzer, and pem fuel cells, Energies 14 (2021), https://doi.org/10.3390/en14092643.
[20] B. Yodwong, D. Guilbert, W. Kaewmanee, M. Phattanasak, Energy efficiency based control strategy of a three-level interleaved DC-DC buck converter supplying a proton exchange membrane electrolyzer, Electronics (Switzerland) 8 (2019), https://doi.org/10.3390/electronics8090933.
[21] V. Ruuskanen, J. Koponen, K. Huoman, A. Kosonen, M. Niemelä, J. Ahola, PEM water electrolyzer model for a power-hardware-in-loop simulator, Int. J. Hydrogen Energy 42 (2017) 10775–10784, https://doi.org/10.1016/j.ijhydene.2017.03.046.
[22] S. Bracco, F. Delfino, F. Pampararo, M. Robba, M. Rossi, A dynamic optimization-based architecture for polygeneration microgrids with tri-generation, renewables, storage systems and electrical vehicles, Energy Convers. Manage. 96 (2015) 511–520, https://doi.org/10.1016/j.enconman.2015.03.013.
[23] F. Marangio, M. Santarelli, M. Calì, Theoretical model and experimental analysis of a high pressure PEM water electrolyser for hydrogen production, Int. J. Hydrogen Energy 34 (2009) 1143–1158, https://doi.org/10.1016/j.ijhydene.2008.11.083.
[24] V. Pérez-Herranz, M. Pérez-Page, R. Beneito, Monitoring and control of a hydrogen production and storage system consisting of water electrolysis and metal hydrides, Int. J. Hydrogen Energy 35 (2010) 912–919, https://doi.org/10.1016/j.ijhydene.2009.11.096.
[25] C. Ziogou, D. Ipsakis, F. Stergiopoulos, S. Papadopoulou, S. Bezergianni, S. Voutetakis, Infrastructure, automation and model-based operation strategy in a stand-alone hydrolytic solar-hydrogen production unit, Int. J. Hydrogen Energy 37 (2012) 16591–16603, https://doi.org/10.1016/j.ijhydene.2012.02.179.
[26] C. Sánchez, D. González, Experimental characterization of a grid-connected hydrogen energy buffer: hydrogen production, Int. J. Hydrogen Energy 38 (2013) 9741–9754, https://doi.org/10.1016/j.ijhydene.2013.05.096.
[27] V. Liso, G. Savoia, S.S. Araya, G. Cinti, S.K. Kær, Modelling and experimental analysis of a polymer electrolyte membrane water electrolysis cell at different operating temperatures, Energies 11 (2018), https://doi.org/10.3390/en11123273.
[28] J.J.C. Mancera, F.S. Manzano, J.M. Andújar, F.J. Vivas, A.J. Calderón, An optimized balance of plant for a medium-size PEM electrolyzer. Design, control and physical implementation, Electronics (Switzerland) (2020) 9, https://doi.org/10.3390/electronics9050871.
[29] S. Sood, O. Prakash, M. Boukerdja, J.Y. Dieulot, B. Ould-Bouamama, M. Bressel, et al., Generic dynamical model of PEM electrolyser under intermittent sources, Energies 13 (2020), https://doi.org/10.3390/en13246556.
[30] M. Genovese, D. Blekhman, M. Dray, P. Fragiacomo, Hydrogen losses in fueling station operation, J. Clean. Prod. 248 (2020), 119266, https://doi.org/10.1016/j.jclepro.2019.119266.
[31] M. Virji, G. Randolf, M. Ewan, R. Rocheleau, Analyses of hydrogen energy system as a grid management tool for the Hawaiian Isles, Int. J. Hydrogen Energy 45 (2020) 8052–8066, https://doi.org/10.1016/j.ijhydene.2020.01.070.
[32] C.Y. Lee, C.H. Chen, G. Bin Jung, S.C. Li, Y.Z. Zeng, Internal microscopic diagnosis of accelerated aging of proton exchange membrane water electrolysis cell stack, Micromachines (Basel) 11 (2020) 1–12, https://doi.org/10.3390/mi11121078.
[33] C.Y. Lee, C.H. Chen, G. Bin Jung, Y.X. Zheng, Y.C. Liu, Persistent effect test and internal microscopic monitoring for pem water electrolyzer, Micromachines (Basel) 12 (2021) 1–14, https://doi.org/10.3390/mi12050494.
[34] A. Mazza, A. Estebsari, G. Morandi, E. Bompard, H. Lok, Remote hardware-in-the-loop measurement system for electrolyser characterization, in: Proceedings - 2019 IEEE International Conference on Environment and Electrical Engineering and 2019 IEEE Industrial and Commercial Power Systems Europe, EEEIC/I and CPS, Europe, 2019, https://doi.org/10.1109/EEEIC.2019.8783587, 2019.
[35] B. Flamm, C. Peter, F.N. Büchi, J. Lygeros, Electrolyzer modeling and real-time control for optimized production of hydrogen gas, Appl. Energy 281 (2021), 116031, https://doi.org/10.1016/j.apenergy.2020.116031.

[36] R.I.S. Pereira, I.M. Dupont, P.C.M. Carvalho, S.C.S. Jucá, IoT embedded linux system based on Raspberry Pi applied to real-time cloud monitoring of a decentralized photovoltaic plant, Measure. J. Int. Measure. Confeder. 114 (2018) 286–297, https://doi.org/10.1016/j.measurement.2017.09.033.
[37] I. Ungurean, N.C. Gaitan, A software architecture for the industrial Internet of Things—a conceptual model, Sensors (Switzerland) (2020) 20.
[38] C. Vargas-Salgado, J. Aguila-Leon, C. Chiñas-Palacios, E. Hurtado-Perez, Low-cost web-based supervisory control and data acquisition system for a microgrid testbed: a case study in design and implementation for academic and research applications, Heliyon. 5 (2019), https://doi.org/10.1016/j.heliyon.2019.e02474.
[39] N. Hosseinzadeh, A. Al Maashri, N. Tarhuni, A. Elhaffar, A. Al-Hinai, A real-time monitoring platform for distributed energy resources in a microgrid—Pilot study in oman, Electronics (Switzerland) (2021) 10, https://doi.org/10.3390/electronics10151803.
[40] A. Yasin, T.Y. Pang, C.T. Cheng, M. Miletic, A roadmap to integrate digital twins for small and medium-sized enterprises, Appl. Sciences (Switzerland) (2021) 11, https://doi.org/10.3390/app11209479.
[41] I. González, A.J. Calderón, J.M. Portalo, Innovative multi-layered architecture for heterogeneous automation and monitoring systems: application case of a photovoltaic smart microgrid, Sustainability (Switzerland) 13 (2021) 1–24, https://doi.org/10.3390/su13042234.
[42] I. Zyrianoff, A. Heideker, D. Silva, J. Kleinschmidt, J.P. Soininen, T.S. Cinotti, et al., Architecting and deploying IoT smart applications: a performance–oriented approach, Sensors (Switzerland) (2020) 20, https://doi.org/10.3390/s20010084.
[43] S. Latif, M. Driss, W. Boulila, Z.E. Huma, S.S. Jamal, Z. Idrees, et al., Deep learning for the industrial internet of things (Iiot): a comprehensive survey of techniques, implementation frameworks, potential applications, and future directions, Sensors 21 (2021), https://doi.org/10.3390/s21227518.
[44] M. Lombardi, F. Pascale, D. Santaniello, Internet of things: a general overview between architectures, protocols and applications, Information (Switzerland) 12 (2021) 1–21, https://doi.org/10.3390/info12020087.
[45] O. Ali, M.K. Ishak, M.K.L. Bhatti, I. Khan, K. Il Kim, A comprehensive review of internet of things: technology stack, middlewares, and fog/edge computing interface, Sensors 22 (2022) 1–43, https://doi.org/10.3390/s22030995.
[46] M. Burhan, R.A. Rehman, B. Khan, B.S. Kim, IoT elements, layered architectures and security issues: a comprehensive survey, Sensors (Switzerland) 18 (2018) 1–37, https://doi.org/10.3390/s18092796.
[47] S. Latif, Z. Zou, Z. Idrees, J. Ahmad, A novel attack detection scheme for the industrial Internet of Things using a lightweight random neural network, IEEE Access 8 (2020) 89337–89350, https://doi.org/10.1109/ACCESS.2020.2994079.
[48] T.S. Fun, A. Samsudin, Recent technologies, security countermeasure and ongoing challenges of industrial internet of things (Iiot): a survey, Sensors 21 (2021) 1–30, https://doi.org/10.3390/s21196647.
[49] P. Bellini, P. Nesi, G. Pantaleo, IoT-enabled smart cities: a review of concepts, frameworks and key technologies, Appl. Sci. (Switzerland) (2022) 12, https://doi.org/10.3390/app12031607.
[50] RTD PT100 Datasheet (accessed on 14 March 2023). https://docs.rs-online.com/9186/0900766b815bb292.pdf.
[51] S7-1500 6ES7516-3AN00-0AB0 CPU Datasheet (accessed on 14 March 2023). https://mall.industry.siemens.com/mall/en/ww/Catalog/DatasheetDownload?downloadUrl=teddatasheet%2F%3Fformat%3DPDF%26caller%3DMall%26mlfbs%3D6ES7516-3AN00-0AB0%26language%3Den.
[52] P. Sethi, S.R. Sarangi, Internet of Things: architectures, protocols, and applications, J. Electr. Comput. Eng. (2017) 2017, https://doi.org/10.1155/2017/9324035.
[53] Modbus Organization (accessed on 14 March 2023). http://www.modbus.org/docs/Modbus_Application_Protocol_V1_1b.pdf .
[54] S. Jaloudi, Communication protocols of an industrial internet of things environment: a comparative study, Future Internet 11 (2019), https://doi.org/10.3390/fi11030066.
[55] C. Qian, X. Liu, C. Ripley, M. Qian, F. Liang, W. Yu, Digital twin—cyber replica of physical things: architecture, applications and future research directions, Future Internet 14 (2022) 1–25, https://doi.org/10.3390/fi14020064.
[56] CERN: Web History (accessed on 14 March 2023). https://web30.web.cern.ch/web-history.html.
[57] H. da Rocha, R. Abrishambaf, J. Pereira, A.E. Santo, Integrating the IEEE 1451 and IEC 61499 standards with the industrial internet reference architecture, Sensors 22 (2022), https://doi.org/10.3390/s22041495.
[58] A.J. Calderón Godoy, I.G. Pérez, Integration of sensor and actuator networks and the SCADA system to promote the migration of the legacy flexible manufacturing system towards the industry 4.0 concept, J. Sensor Actuator Netw. 7 (2018), https://doi.org/10.3390/jsan7020023.
[59] O. Givehchi, K. Landsdorf, P. Simoens, A.W. Colombo, Interoperability for industrial cyber-physical systems: an approach for legacy systems, IEEE Trans. Ind. Inf. 13 (2017) 3370–3378, https://doi.org/10.1109/TII.2017.2740434.
[60] M. Wollschlaeger, T. Sauter, J. Jasperneite, The future of industrial communication, PCI-Paint Coatings Ind. 29 (2017).
[61] F. Martin-Martínez, A. Sánchez-Miralles, M. Rivier, A literature review of Microgrids: a functional layer based classification, Renew. Sustain. Energy Rev. 62 (2016) 1133–1153, https://doi.org/10.1016/j.rser.2016.05.025.
[62] History and feature of Node-RED (accessed on 14 March 2023). https://www.clarify.io/integrations-browse/node-red.
[63] Node-RED (accessed on 14 March 2023). https://nodered.org/.
[64] F.J. Folgado, I. González, A.J. Calderón, Simulation platform for the assessment of PEM electrolyzer models oriented to implement digital Replicas, Energy Convers. Manage. 267 (2022), https://doi.org/10.1016/j.enconman.2022.115917.
[65] A. Weiß, A. Siebel, M. Bernt, T.-.H. Shen, V. Tileli, H.A. Gasteiger, Impact of intermittent operation on lifetime and performance of a PEM water electrolyzer, J. Electrochem. Soc. 166 (2019) F487–F497, https://doi.org/10.1149/2.0421908jes.
[66] A.A. Mirani, G. Velasco-Hernandez, A. Awasthi, J. Walsh, Key challenges and emerging technologies in industrial IoT architectures: a review, Sensors (Basel) 22 (2022) 1–31, https://doi.org/10.3390/s22155836.
[67] I. González, A.J. Calderón, Integration of open source hardware Arduino platform in automation systems applied to Smart Grids/Micro-Grids, Sustain. Energy Technol. Assess. 36 (2019), https://doi.org/10.1016/j.seta.2019.100557.
[68] J.M. Pearce, Economic savings for scientific free and open source technology: a review, HardwareX 8 (2020), https://doi.org/10.1016/j.ohx.2020.e00139.

Anexo III

Referencia

Folgado F.J., González I., Calderón A.J., PEM Electrolyzer Digital Replica based on internal resistance determination applied to hydrogen energy storage, Journal of Energy Storage, 2024; 75: 109694. DOI: 10.1016/j.est.2023.109694

Derechos de autor

Journal of Energy Storage 75 (2024) 109694

Contents lists available at ScienceDirect

Journal of Energy Storage

journal homepage: www.elsevier.com/locate/est

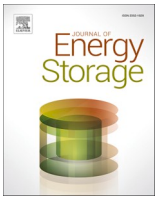

Research Papers

PEM Electrolyzer Digital Replica based on internal resistance determination applied to hydrogen energy storage

Francisco Javier Folgado *, Isaías González, Antonio José Calderón

Department of Electrical Engineering, Electronics and Automation, Universidad de Extremadura, Avenida de Elvas, s/n, Badajoz 06006, Spain

ARTICLE INFO

Keywords:
PEM Electrolyzer
Hydrogen
Microgrid
Digital Replica
Model
Energy storage

ABSTRACT

The rise of hydrogen as an energy storage means and its associated technologies have prompted the implementation of hydrogen generation systems based on electrolyzers. Electrolyzers exhibit complex behaviour and their implementation is not immediate, leading to the use of tools such as Digital Replicas (DR) for their study. This paper presents a DR for a Proton Exchange Membrane Electrolyzer (PEMEL) through the development of an Equivalent Circuit Model (ECM) that describes the static behaviour of the individual cells comprising it. This research is focused on contributing to hydrogen generation with the main objective of using this energy vector for energy storage applications. For this purpose, an installation consisting of a PEMEL and a set of auxiliary equipment required for its proper operation and for measuring key electrolyzer parameters such as current, voltage, hydrogen flow rate, temperature, etc. is implemented. Furthermore, a Data Acquisition System (DAQ) is available to collect process information for later analysis. The PEM cell model is obtained through an experimental process based on the determination of internal resistance to calculate the remaining key parameters. The successful functioning and suitability of the DR and developed model are reported through experimental data obtained from the PEMEL under operating conditions.

1. Introduction

The escalating energy demand and the scarcity of traditional resources like fossil fuels have driven the advancement and exploration of renewable energy technologies. Among these, solar thermal and photovoltaic technologies are extensively investigated and deployed for various industrial and domestic purposes. These technologies are continuously researched to enhance their performance via energy management approaches [1] and novel materials [2,3]. Additionally, modern technologies and processes have been developed to harness emerging renewable energy sources such as hydrogen. The importance of this element has been increasing in recent years, making its presence felt through applications in multiple sectors such as the automotive industry [4], healthcare [5], and energy [6].

Hydrogen generation is carried out through devices called electrolyzers. These devices allow the separation of a compound into its primary parts through the electrochemical process of electrolysis. Electrolyzers fall into four categories: alkaline, Proton Exchange Membrane (PEM), solid oxide, and Anion Exchange Membrane (AEM). The main difference between these types is the nature of the electrolyte that enables electrolysis. Alkaline types employ liquid electrolyte solutions like potassium hydrogen (KOH) or sodium hydroxide (NaOH) [7]. PEM types incorporate solid polymer membranes as electrolytes [7,8]. Solid oxide types utilize solid ceramic electrolytes [9]. Lastly, AEM electrolyzers generate hydrogen from a semi-permeable membrane that allows the passage of hydroxide ions (OH-) [7,10]. The hydrogen produced by such equipment is commonly denoted by colour, which varies based on the input compound and the energy source used. Thus, hydrogen generated from water and renewable energy sources is recognized as green hydrogen [11]. Fuel cells, serving as counterparts to electrolyzers, operate in reverse, producing electricity by consuming hydrogen [12]. Another application for hydrogen is energy storage. Nowadays, various physical and chemical methods are employed, including compression, liquefaction processes, and solid-state techniques such as metal hydrides [13]. The application of these storage methods, tailored to specific characteristics and diverse storage capacities, demonstrates the potential for advancing the future hydrogen-based economy [14,15].

In the energy sector, the availability of hydrogen as an alternative energy source, achieved through the combination of electrolyzers and fuel cells, has induced a transformation in prevailing paradigms within

* Corresponding author.
E-mail addresses: ffolgar@unex.es (F.J. Folgado), igonzp@unex.es (I. González), ajcalde@unex.es (A.J. Calderón).

https://doi.org/10.1016/j.est.2023.109694
Received 23 May 2023; Received in revised form 6 October 2023; Accepted 9 November 2023
Available online 18 November 2023

systems such as microgrids and smart microgrids. Microgrids consist of a cluster of loads, distributed generation units and energy storage systems operated in coordination to reliably supply electricity, connected to the host power system at the distribution level [16,17]. The smart connotation refers to the system's capacity for self-management through dedicated elements, such as Programmable Logic Controllers (PLC) [18]. These adaptable systems facilitate the incorporation of new hydrogen-harnessing devices, resulting in hybrid systems that blend renewable energies with hydrogen technology [6]. In this context, PEM electrolyzers (PEMEL) are employed alongside water for hydrogen generation. The use of hydrogen as an energy storage solution, supplying microgrids during periods of generation shortfall or heightened energy demand, is emphasized [19]. This approach mitigates energy fluctuations within the microgrid over the medium to long term [20]. Notably, PEMEL are favoured in renewable energy applications due to their swift response to fluctuations in input conditions [21]. Moreover, the significance of hydrogen and electrolyzers is highlighted as a strategic approach aligned with the UN Sustainable Development Goals. Specifically, hydrogen is anticipated to contribute to the fulfilment of Goal 7, promoting accessible and clean energy [22].

Concerning their operation, the intricate nature of electrolyzers poses challenges to their direct integration into a process or system. Thus, a thorough analysis of the device is essential to comprehend its behaviour and interaction with other system components. Digital Replicas (DR) play a crucial role in this study. A DR can be described as a virtual version of the physical device, replicating its real-time operation. Nonetheless, there is currently no single generally accepted definition for the concept of DR. Therefore, in the framework of this research, the definition given in [23] has been considered, which defines DR as the interaction between two parts: the model of the physical system and the connection/communication for data exchange between model and real system. This model can take different forms, such as those based on equations or physical laws [24] or black-box models, like neural networks [25]. For PEMEL, the most commonly used models are Equivalent Circuit Models (ECM), whose electrical components are related to the physical effects of the device's operation [26]. This digital tool streamlines device study without requiring physical disposal, isolating it from other components. DR facilitates testing various conditions, including those beyond real system limits due to technical or economic factors [27].

To undertake this research, a brief literature review has been conducted, focusing on works related to: diverse models of PEMEL, applications of these devices in the energy sector, and papers detailing the equipment and methodology employed. In Atlam and Kolhe [20], the behaviour of a PEM cell is described using an ECM model. In this work, the various key parameters of the cell as well as the effect of working temperature and pressure on these parameters are studied. In addition, an expression is introduced for the voltage of a PEMEL as a function of the number and distribution of the cells that compose it. Awasthi et al. [24] develop a model for a PEM cell under elevated temperature and pressure operating conditions using MATLAB-Simulink. This model is used to determine the cell voltage and perform a graphical comparison of the results. In Ismail et al. [28], a photovoltaic system for hydrogen production is modelled and simulated, where the PEMEL model is developed using experimental data to obtain the voltage-current relationship and determine the optimal operating point of the system. Analogously, Albarghot et al. [29] describe a model for a solar panel - PEMEL system at laboratory scale, where the hydrogen flow rate produced is studied employing a MATLAB-Simulink simulation of the model. In Guilbert and Vitale [30], the modelling of a PEMEL using a dynamic behaviour analysis is reported. In this analysis, the key parameters of the PEMEL are studied and the experimental process followed for their determination is explained. In Espinosa-López et al. [31], the modelling and validation of a 46 kW PEMEL operating at high pressure are carried out, where the effect of the working temperature on the behaviour of the electrolyzer is studied. The model is designed in MATLAB-Simulink and the results obtained are validated graphically and employing statistical metrics. The model described in Hernández-Gómez et al. [32] studies the static-dynamic behaviour of the cell voltage for a PEMEL under adaptive parameters.

The literature reviewed reinforces the presence of a wide variety of models, describing the behaviour of the PEMEL under a multitude of operating conditions for applications in the energy sector. Nonetheless, scarce details have been found regarding the description of the physical equipment used for the development of the model, as well as the experimental process executed for its determination. Additionally, there is a noticeable trend to validate models based on voltage-current comparisons, sometimes overlooking important PEMEL parameters such as power consumption and hydrogen flow rate. Graphical comparative curves are frequently used to present these results, occasionally with statistical analysis.

The work presented in this paper is motivated by the research gaps identified in the reviewed literature. As a result, this study covers the three key topics sought in the literature, with a special focus on detailing the equipment employed and outlining the experimental process conducted.

This paper describes the design and validation of the DR of a PEMEL employing an ECM-based model. This model focuses on reproducing the static operation of the individual cells that compose the PEMEL. For this purpose, an installation has been set up with equipment dedicated to the correct operation of the PEMEL and its study for the determination of the model. Furthermore, the experimental process performed to develop the cell model is described, which aims to determine the cell voltage using the calculation of the internal resistance. The DR generated from the PEMEL is studied under nominal operating conditions, analysing the results obtained at the individual cell level and as a stack.

The aforementioned PEMEL and its ancillary equipment comprise the hydrogen generation subsystem, whose operation is framed within a photovoltaic-powered smart microgrid hybridized with green hydrogen. This generation subsystem aims to produce green hydrogen for energy storage purposes, intended for subsequent application through a fuel cell. Previous works describe the set of equipment that constitutes the smart microgrid, as well as its operation [33,34].

The structure of the rest of the manuscript is as follows. Section 2 describes the principle of operation of the electrolyzer, as well as the implemented setup and equipment associated with the operation of the PEMEL. Section 3 details the design of the model and the experimental process conducted to obtain it. Section 4 illustrates the results obtained from the deployment of the DR and a discussion thereof. Finally, the most relevant conclusions of the study are presented.

2. Materials and methods

2.1. Fundamentals of electrolysis in PEMEL

As mentioned above, the electrolyzer is a device that generates hydrogen from a compound through the process of electrolysis. These devices are composed of a set of cells that are responsible for carrying out electrolysis. These cells can be arranged in series, referred to as a stack, or in parallel. In the case of a water-fed PEMEL, the cell structure is illustrated in Fig. 1.

Within the cell, electrolysis is performed as a result of two processes: a reduction at the cathode and an oxidation at the anode. Both processes are defined in Eq. (1) and Eq. (2) respectively.

$$2H^+ + 2e^- \rightarrow H_2 \tag{1}$$

$$H_2O \rightarrow 2H^+ + \frac{1}{2}O_2 + 2e^- \tag{2}$$

The electrolysis process resulting from both half-reactions is indicated in Eq. (3):

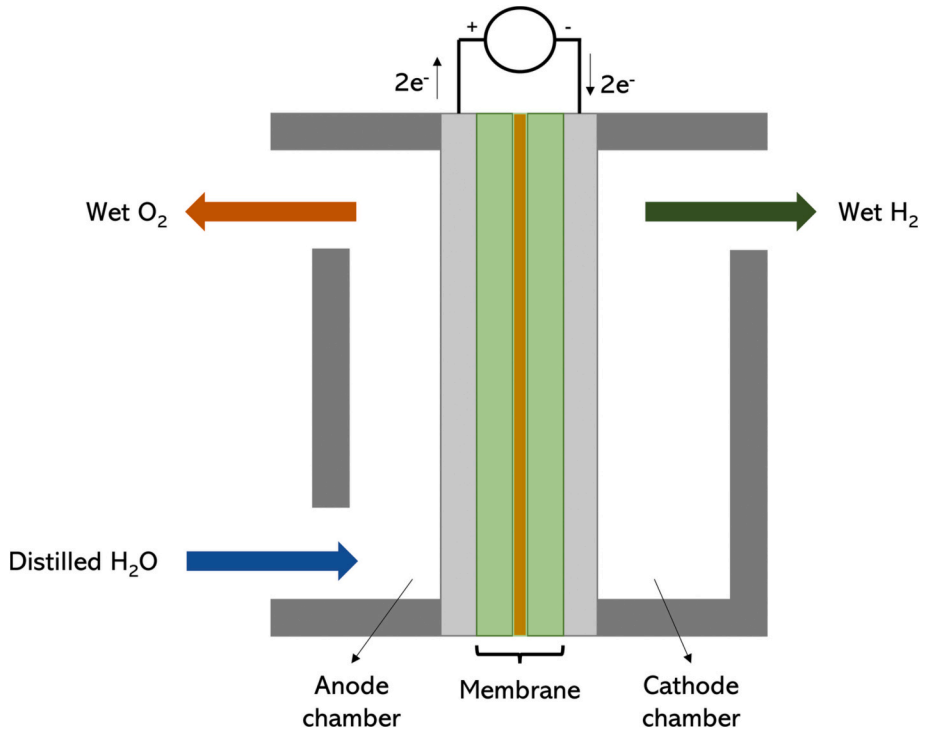

Fig. 1. Structure and operation of a PEM cell.

$$H_2O \rightarrow H_2 + \frac{1}{2}O_2 \quad (3)$$

2.2. PEM Electrolyzer and ancillary equipment

For this research, a 6-cell stack PEMEL has been employed. The geometry and number of cells of the stack are depicted in Fig. 2a. In Fig. 2b, the installed stack is displayed, where several components are coupled to it: a PT-100 temperature sensor [35] is located on the lateral part to monitor the operating temperature of the stack. A fan [36] is installed on the frontal part to control the working temperature within the nominal operating range of the PEMEL. Finally, a connector has been included on the bottom of the stack to collect the voltages of each cell, which is a crucial aspect for the development of the model that is further explained below.

Table 1 lists the main technical specifications for the operation of the electrolyzer.

Table 1
Technical specifications of the electrolyzer.

Number of cells	6 cells in series
Input current (A)	0 to 8 A
Stack voltage (V)	12 to 15 V
Working pressure (bar)	0.1 to 6 bar
Working temperature (°C)	25 to 50 °C
Flow rate generated (ml/min)	250 ml/min; 15 Nl/h
Hydrogen purity	>99.9999 %
Dimensions (mm)	267 × 382 × 470 mm

The electrolysis process described in Section 2.1 results in wet hydrogen, i.e. hydrogen with water content. This is due to the non-ideality of the electrolyzer, which results in the need to employ additional equipment for the removal of this unwanted moisture to obtain high-purity dry hydrogen. To this end, a series of auxiliary equipment complementary to the electrolyzer has been installed to achieve dry

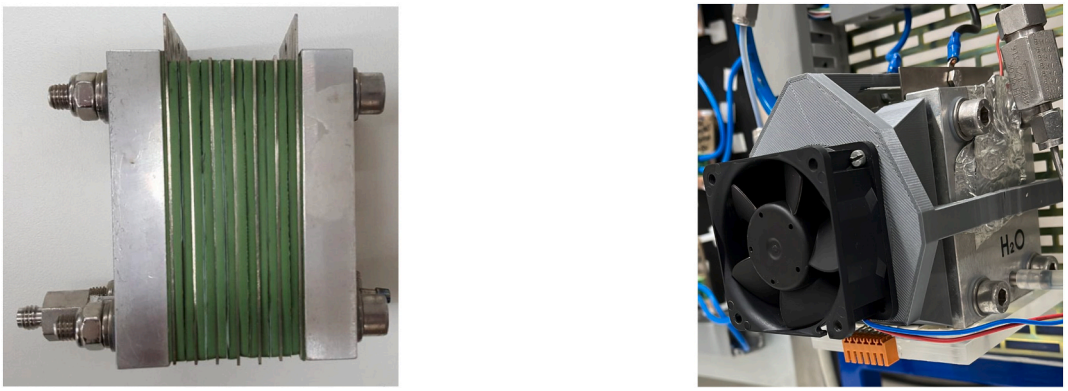

Fig. 2. PEM Electrolyzer. (a) Stack appearance and number of cells. (b) Stack installed alongside coupled elements.

hydrogen. The installation and each of the components are detailed below.

First, the electrical current is supplied to the hydrogen generation subsystem via a low voltage DC bus, materialised by a Lithium-Ion battery (referred to as 'Microgrid power supply' in Fig. 3). This DC bus ensures a reference voltage level as well as a smooth and stable power flow to the PEMEL. This flow from the DC bus is directed to the input of the PEMEL through a programmable DC/DC converter [37]. The programmable feature of the converter enables to adjust its output in order to suit the desired working point of the PEM stack.

The water flow is supplied by gravity from a tank above the stack. After the electrolysis process, the resulting oxygen is returned to the water tank, while the wet hydrogen is transferred to a phase separator. Within the phase separator, the water particles descend by gravity and accumulate at the bottom part, where they are redirected to the water tank for re-utilisation. Meanwhile, the hydrogen flows through a series of silica filters that remove the remaining humidity from the hydrogen to produce a dry, high-purity product. Finally, the dry hydrogen flow rate is measured utilising a flow meter [38] and stored in a metal hydride bottle. Moreover, the pressure of the hydrogen circuit is obtained using a pressure sensor [39]. Fig. 3 depicts the described installation employing a diagram based on synoptics, detailing the location of each device and the flow of products and sub-products resulting from its operation. In addition, Fig. 4 shows the appearance of the installation, where the components involved can be observed. In addition, the PLC employed for data acquisition is displayed in the bottom right-hand margin.

2.3. Data acquisition system

To develop the model discussed in this research, a data acquisition system (DAQ) was employed to capture essential electrolyzer performance parameters during experimentation.

Sensors and actuators controlling the PEMEL process were connected to a Siemens S7–1500 PLC [40]. This facilitated real-time data collection of key PEMEL variables. For process visualisation and data storage, a user-friendly Graphical User Interface (GUI) has been developed in LABVIEW [41]. LABVIEW software is oriented to the design and implementation of a diversity of systems, highlighting GUIs and SCADA systems, through a graphical programming language and a wide variety of tools and synoptics [33].

Regarding the operation of the DAQ, the data acquired by the PLC is read by the GUI through a client-server structure based on the Open Platform Communications (OPC) protocol. OPC is a widely used standardised data exchange technology to deal with heterogeneity and interoperability in automation systems. [42].

The GUI developed acts as the OPC client, simultaneously performing the functions of visualisation and data storage. The visualisation of the process information is achieved using graphs and numerical indicators that display the real-time status of the key variables of the PEMEL. On the other hand, data storage is accomplished by exporting the read data to an Excel spreadsheet. This storage is crucial for the disposal the acquired data in a more manageable format to facilitate subsequent processing. Fig. 5 depicts the DAQ elements, information flow, and communication among them.

3. Model development

3.1. Cell Equivalent Circuit Model

The ECM is a tool that allows representing the operation of a device through an electrical schematic composed of simple components such as power sources, resistances, capacitors, coils, etc. Particularly for PEMEL, and as indicated in Section 1, there is a wide variety of models in the literature reviewed. These models are mainly distinguished by their application context and complexity. Simplified models describe the behaviour of the PEMEL using an electrical diagram with few components, addressing the study of its operation in a more general manner. In contrast, more complex models are highlighted by more detailed electrical diagrams, where a more thorough study is conducted, and specific phenomena/effects are related to certain electrical components.

For this research, a simplified model of the PEMEL cell is proposed to describe its static behaviour, employing two components: a power supply and a resistance. These elements are used in other well-known models such as those of Atlam and Kolhe [20] and Guilbert and Vitale [30] to describe the electrolysis process and the energy losses incurred, respectively. Moreover, these components rely on parameters like

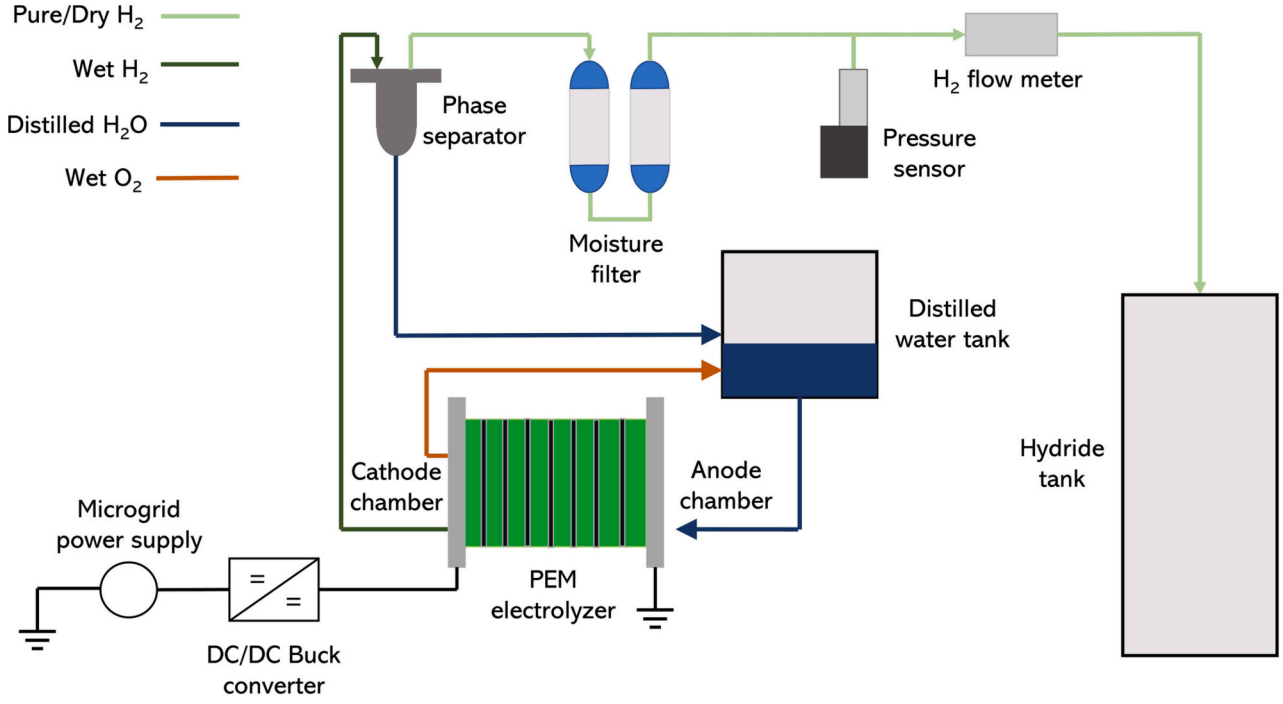

Fig. 3. PEMEL and complementary equipment for high-purity dry hydrogen generation and storage.

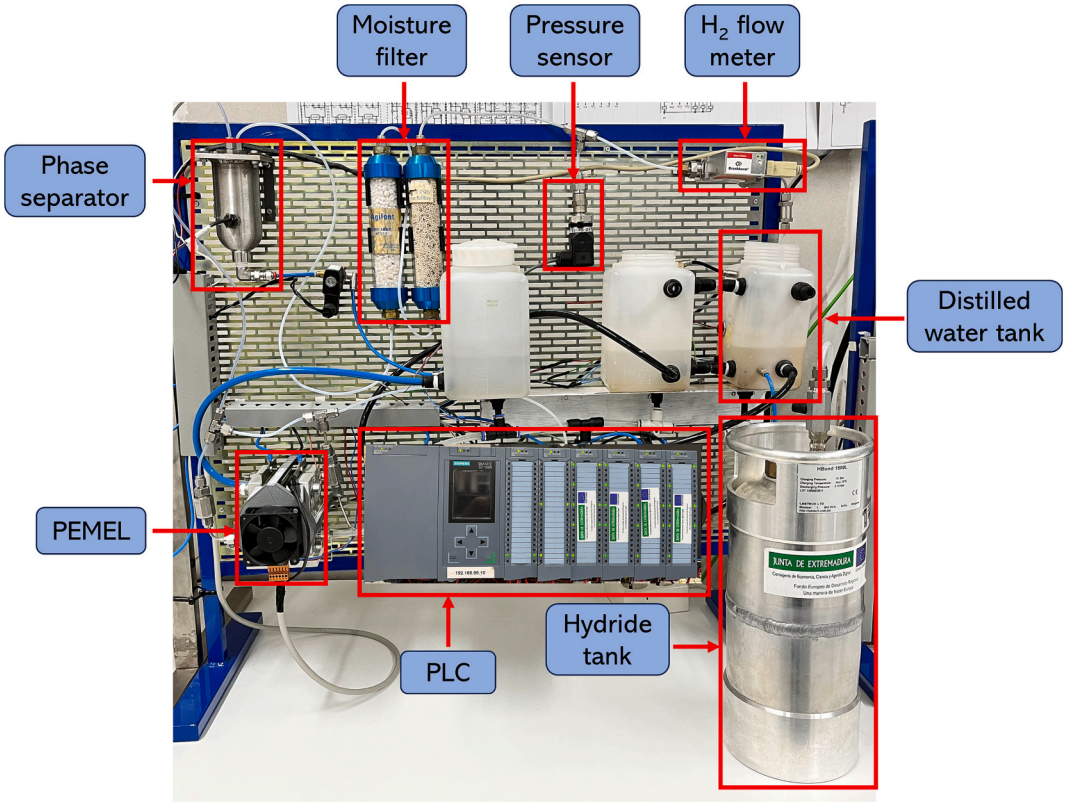

Fig. 4. Installation appearance and equipment employed.

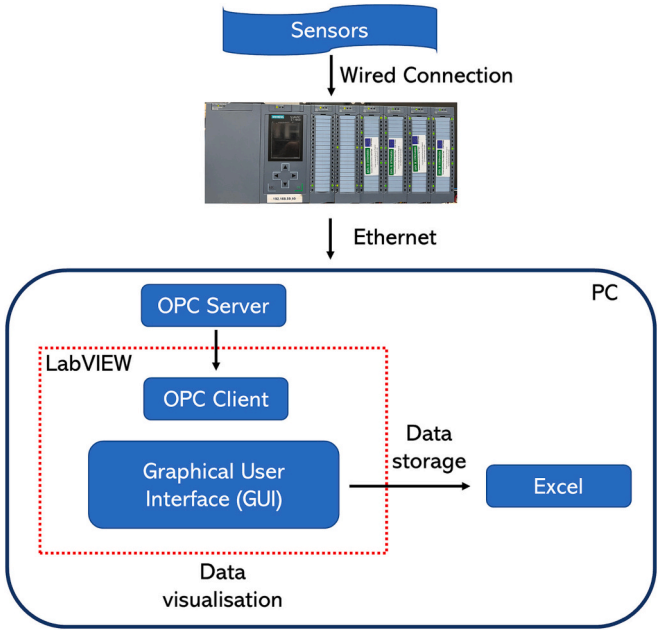

Fig. 5. DAQ for visualisation and storage of process data.

temperature, pressure, and input current. This allows for studying the effects of fluctuation on cell operation. Fig. 6 depicts the ECM utilised in the PEM cell.

Where I (A) refers to the current consumed, R_{int} (Ω) is the internal resistance that simulates the power dissipation due to cell operation, and V_{int} (V) is the ideal (electrochemical) voltage or potential required for the electrolysis process. Thus, the cell voltage V_{cell} (V) is defined in Eq. (4) as:

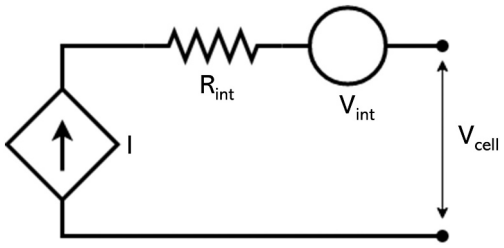

Fig. 6. ECM of the PEM cell.

$$V_{cell} = IR_{int} + V_{int} \tag{4}$$

V_{int} is calculated in Eq. (5) based on the Gibbs free energy ΔG (J mol^{-1}) and Faraday's constant (96,487 C mol^{-1}) [43]:

$$V_{int} = \frac{\Delta G}{2F} \tag{5}$$

For liquid water, ΔG is obtained by Eq. (6) for a given temperature T (°C) [43]:

$$\Delta G = 285840 - 163.2(273 + T) \tag{6}$$

The power consumed in the electrolysis process $P_{e,cell}$ (W) is obtained from the ideal voltage employing Eq. (7):

$$P_{e,cell} = IV_{int} \tag{7}$$

Using Eq. (5) and Eq. (6), Eq. (4) can be rearranged as follows, giving the expression Eq. (8) for V_{cell}:

$$V_{cell} = IR_{int} + \frac{285840 - 163.2(273 + T)}{2F} \tag{8}$$

The total power consumed by the cell $P_{t,cell}$ (W) is expressed in Eq. (9):

$$P_{t,cell} = IV_{cell} \tag{9}$$

The hydrogen flow rate $v_{H,cell}$ (ml/min) is stated in Eq. (10) as a function of the consumed current I and the molar volume v_M (l) [43]:

$$v_{H,cell} = v_M(\mathrm{l})\left(\frac{10^3 \mathrm{ml}}{\mathrm{l}}\right)\left(\frac{60\ \mathrm{s}}{min}\right)\left(\frac{I\left(\frac{\mathrm{C.}}{\mathrm{s}}\right)}{2F\ (\mathrm{C.})}\right) = v_M(10^3)(60)\left(\frac{I}{2F}\right) \tag{10}$$

where v_M is obtained from Eq. (11) as a function of the working temperature T, the working pressure p (atm) and the ideal gas constant R (0.082 l atm K^{-1} mol^{-1}):

$$v_M(\mathrm{l}) = \frac{R(273+T)}{p} \tag{11}$$

Finally, the cell efficiency η_{cell} is given by Eq. (12) and is defined as the parameter that relates $P_{e,cell}$ and $P_{t,cell}$. Since both variables depend on I, the expression is reduced to the ratio between V_{int} and V_{cell}:

$$\eta_{cell} = \frac{P_{e,cell}}{P_{t,cell}} = \frac{IV_{int}}{IV_{cell}} = \frac{V_{int}}{V_{cell}} \tag{12}$$

3.2. Experimental process for the determination of the internal cell resistance

Among the equations presented in Section 3.1, R_{int} is the only cell parameter that cannot be measured or calculated directly. This parameter is crucial to determine the value of V_{cell}, so Eq. (8) has been rearranged to determine R_{int}, resulting in Eq. (13):

$$R_{int}(T,I) = \left[V_{cell}(T,I) - \left(\frac{285840 - 163.2(273+T)}{2F}\right)\right] \Big/ I \tag{13}$$

Eq. (13) expresses R_{int} as a function of T, I and V_{cell}. Thus, to obtain the values of the internal resistance over the complete range of T and I, it is required to know beforehand the value of V_{cell} at each operating point. To this end, an experimental process has been conducted to obtain an expression that defines the value of R_{int} within the operating range of the cell (T (°C) = {25,50} and I (A) = {0,8}).

Initially, the PEMEL has been subjected to various tests of constant current operation with temperature variation. In this way, the value of $V_{cell}(T,I)$ has been obtained for the whole temperature range in each of the operating currents. The data obtained during the test are gathered using the DAQ, visualised by the LABVIEW GUI and stored in an independent Excel spreadsheet for each of the tests. Subsequently, the data has been filtered and processed to calculate $R_{int}(T,I)$. As an example, Fig. 7a and b display the graphs $V_{cell}(T,I)$ and $R_{int}(T,I)$ respectively, obtained as a result of the test carried out at a current of 6 A for each of the cells.

To determine the expression of $R_{int}(T,I)$ from the experimental data obtained, the MATLAB Curve Fitting Toolbox [44] has been employed. This tool facilitates the fitting of curves and surfaces to the data provided by employing regression, interpolation and smoothing techniques. Concerning its operation, the toolbox requires input data to perform the fitting process. For this purpose, it is necessary that said data are previously loaded in the MATLAB Workspace. Therefore, as an initial step, for each cell, the experimental values of T,I and $R_{int}(T,I)$ are read from the Excel file in matrix format. Then, in the toolbox, the values of T, I and $R_{int}(T,I)$ are associated with the variables X,Y, and Z of the fitting expression, respectively. Finally, the desired type of fit is selected, optionally including a weight matrix that modifies the fitting configuration. As a result, the toolbox displays the surface generated from the fitting process, as well as the resulting mathematical expression, the values of the coefficients and a set of indices associated with the goodness of the fit (SEE, R-square, Adjusted R-square and RMSE). Fig. 8 depicts the interface of the Curve Fitting Toolbox for the case of the surface obtained from $R_{int}(T,I)$ of cell C1. This figure highlights the different areas that comprise the toolbox.

For this particular application, the "Custom Equation" fitting option has been employed, enabling the incorporation of a customisable expression. The expression integrated into the toolbox was achieved during the preliminary data filtration and initial analysis process within Excel, facilitated by the employment of the ThreeDify XLGrapher add-on [45]. This supplementary tool streamlines the three-dimensional representation of surfaces within Excel, utilising input data. Additionally, it facilitates a straightforward fitting process through a wide variety of equations. However, this add-on only represents the fitted surface according to the general equation selected, without indicating the mathematical expression that defines the surface or the values of its coefficients. Therefore, ThreeDify XLGrapher has been employed to determine the general equation used in the fitting process, while the MATLAB Curve Fitting toolbox has been used to obtain the complete particularised expression of $R_{int}(T,I)$ for each cell.

Fig. 9 expands the information displayed in the results window of the

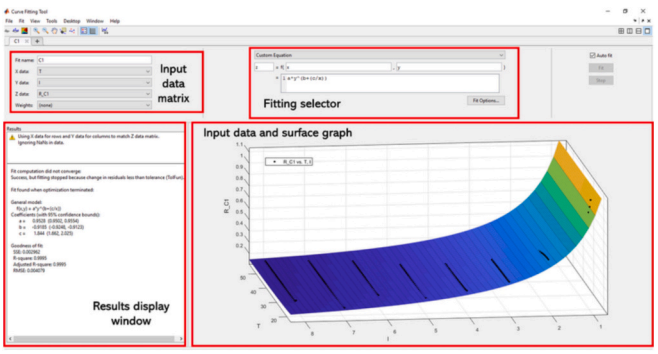

Fig. 8. MATLAB Curve Fitting Toolbox. Resulting surface for $R_{int}(T,I)$ of cell C1.

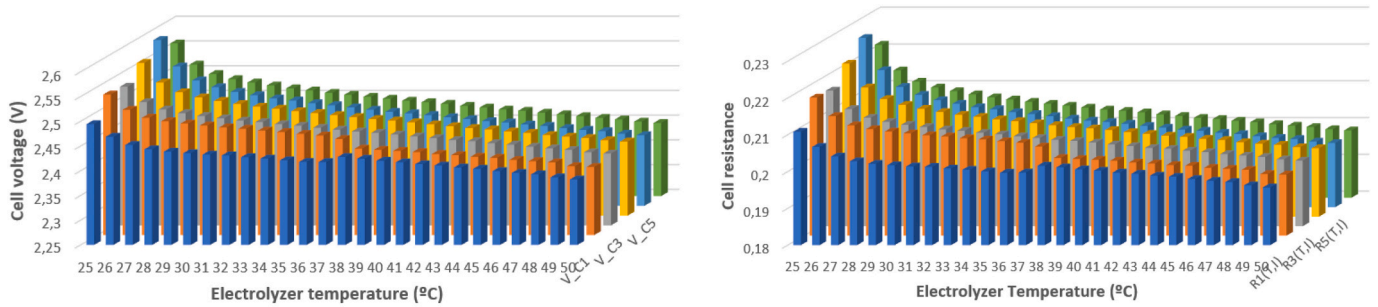

Fig. 7. Results obtained for each cell in the test at 6 A. (a) Values for $V_{cell}(T,I)$. (b) Values for $R_{int}(T,I)$.

General model:
f(x,y) = a*y^(b+(c/x))
Coefficients (with 95% confidence bounds):
a = 0.9528 (0.9502, 0.9554)
b = -0.9185 (-0.9248, -0.9123)
c = 1.844 (1.662, 2.025)

Fig. 9. Generated surface equation and coefficients of $R_{int}(T,I)$ for cell C1.

Curve Fitting toolbox, showing the expression used for the fit, called the "general model", as well as the values of the coefficients a, b and c.

For the remaining PEMEL cells, the process to determine $R_{int}(T,I)$ is homologous. This process is illustrated in Fig. 10, where a flowchart summarises the steps from obtaining experimental data through tests to determining the parameterised expression of internal resistance by means of the toolbox.

Once the process described in Fig. 10 has been completed, an equation is obtained for $R_{int}(T,I)$ of the cell expressed in Eq. (14). Table 2 lists the values of the coefficients particularised for each of the 6 cells that integrate the PEMEL.

$$R_{int}(T,I) = aI^{\left(b+\left(\frac{c}{T}\right)\right)} \tag{14}$$

Combining Eq. (14) and Eq. (8) results in an expression for V_{cell} dependent solely on T and I, as presented in Eq. (15). Based on this expression, the remaining parameters presented in Section 3.1 can be determined.

$$V_{cell}(T,I) = IaI^{\left(b+\left(\frac{c}{T}\right)\right)} + \frac{285840 - 163.2(273+T)}{2F} \tag{15}$$

3.3. PEMEL parameters

After obtaining the key parameters of the PEMEL cells by calculating

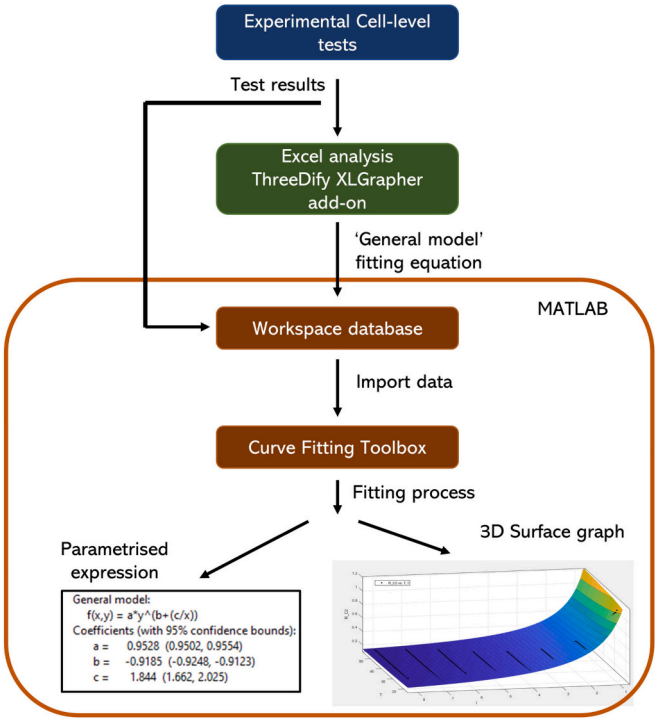

Fig. 10. $R_{int}(T,I)$ determination process for each cell.

Table 2
$R_{int}(T,I)$ coefficient values for each cell.

Cell	Coefficient a	Coefficient b	Coefficient c
C1	0.9528	−0.9185	1.844
C2	1.048	−0.9693	1.922
C3	1.09	−0.9756	1.384
C4	1.105	−0.9847	1.596
C5	1.103	−0.9981	2.035
C6	1.105	−0.9922	1.826

R_{int} and V_{cell}, the expressions that describe the behaviour of the PEMEL as a unit can be determined, under several considerations:

- The PEMEL stack presents a series structure, which implies that the current consumed I by the electrolyzer is the same as the current flowing through each of the cells.
- Due to the technical limitations of the developed installation, the temperature and pressure of the cells are considered to match those measured for the PEMEL as a unit.

Thus, the electrolyzer voltage V_{el} (V) expressed in Eq. (16) is obtained, where the index i refers to the cell number of the PEMEL.

$$V_{el} = \sum_{i=1}^{6} V_{cell}(T,I) = \sum_{i=1}^{6}\left(IaI^{\left(b_i+\left(\frac{c_i}{T}\right)\right)} + \frac{285840 - 163.2(273+T)}{2F}\right) \tag{16}$$

The effective power used by the PEMEL for the electrolysis process $P_{e,el}$ (W) is calculated by Eq. (17), where n_{cell} refers to the total number of cells that comprise the PEMEL:

$$P_{e,el} = In_{cell}V_{int} \tag{17}$$

The total power consumed by the PEMEL $P_{t,el}$ (W) is determined by Eq. (18):

$$P_{t,el} = IV_{el} \tag{18}$$

The total generated hydrogen flow rate $v_{H,el}$ (ml/min) is obtained using Eq. (19):

$$v_{H,el} = n_{cell}v_M(1)\left(\frac{10^3\,\text{ml}}{1}\right)\left(\frac{60\,\text{s}}{min}\right)\left(\frac{I\left(\frac{\text{C}}{\text{s}}\right)}{2F\ (\text{C})}\right) = n_{cell}v_M\left(10^3\right)(60)\left(\frac{I}{2F}\right) \tag{19}$$

Finally, the overall efficiency of the PEMEL η_{el} is expressed in Eq. (20) as the ratio between the useful voltage employed in the electrolysis and the total voltage of the electrolyzer:

$$\eta_{el} = \frac{P_{e,el}}{P_{t,el}} = \frac{In_{cell}V_{int}}{IV_{el}} = \frac{n_{cell}V_{int}}{V_{el}} \tag{20}$$

4. Results and discussion

After describing the expressions defining the individual cell and the PEMEL models, the suitability of DR is assessed by employing experimental data gathered from the PEMEL under its nominal operation.

First, the behaviour of the parametrised cell model for each PEMEL cell is tested. For this purpose, a comparison is made between the experimental (exp) and theoretical (teo) values of the variables V_{cell} and $R_{int}(T,I)$. The experimental values of V_{cell} reflect the directly measured voltage of each cell. The theoretical values of V_{cell} are determined from the model using Eq. (15) parametrised for each cell. Regarding $R_{int}(T,I)$, the experimental values are determined using Eq. (13), leveraging the experimental V_{cell} values. Meanwhile, the theoretical values are calculated from Eq. (14) obtained employing the MATLAB toolbox Curve Fitting and parameterised for each cell.

Fig. 11 presents a graphical comparison of these variables, depicting the set of R_{int}-T and V_{cell}-T curves for each individual cell.

As shown in the graphs presented in Fig. 11, the experimental and theoretical values of R_{int} and V_{cell} are similar, coinciding and overlapping in some cases, as in cells 5 and 6. Furthermore, the behaviour of both parameters is homologous with regard to temperature variations, presenting a downward trend with increases in the working temperature. This trend is reflected in a lower voltage for the same current consumed,

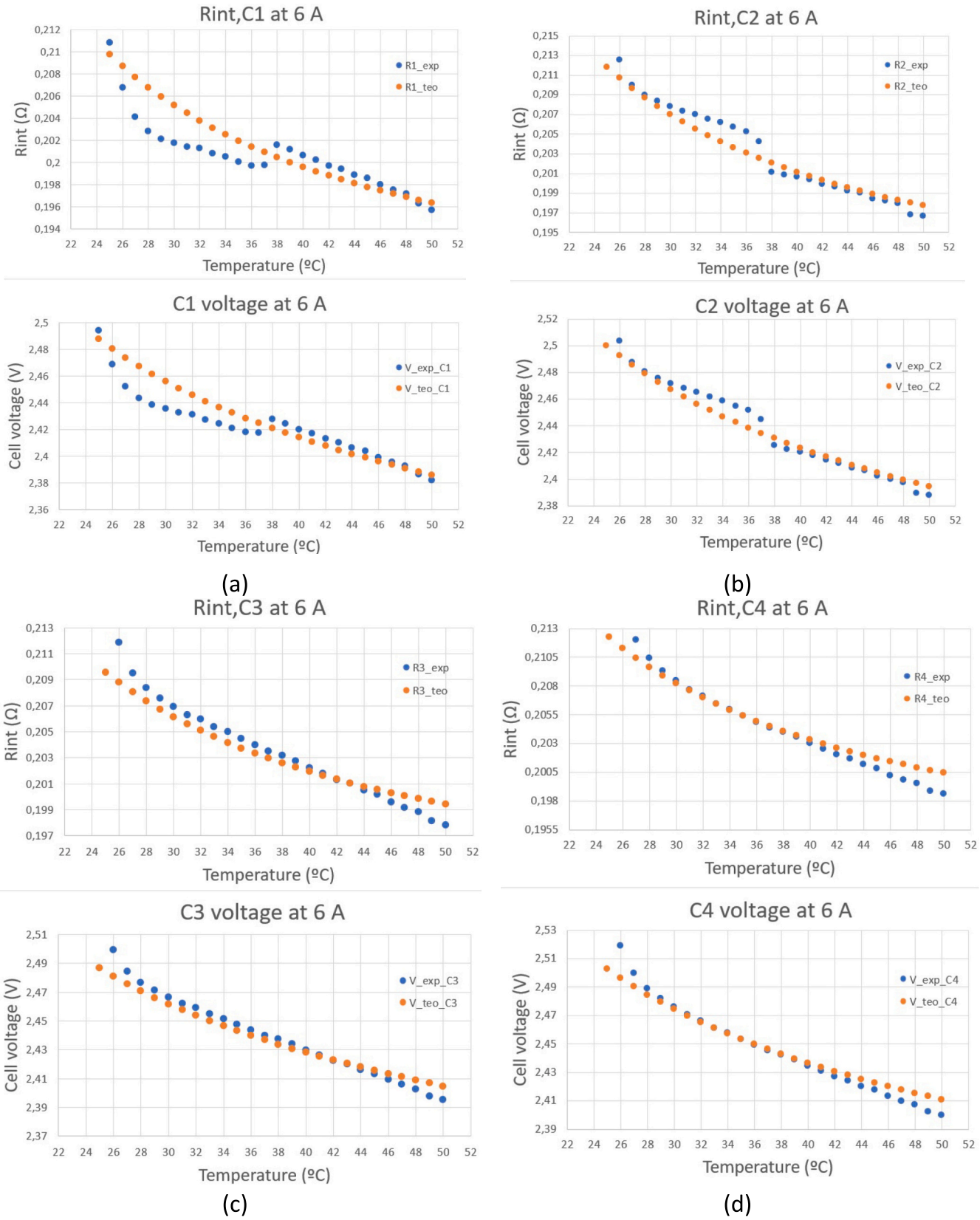

Fig. 11. R_{int}-T and V_{cell}-T curves obtained for each cell with a constant current of 6 A. (a) Cell 1. (b) Cell 2. (c) Cell 3. (d) Cell 4. (e) Cell 5. (f) Cell 6.

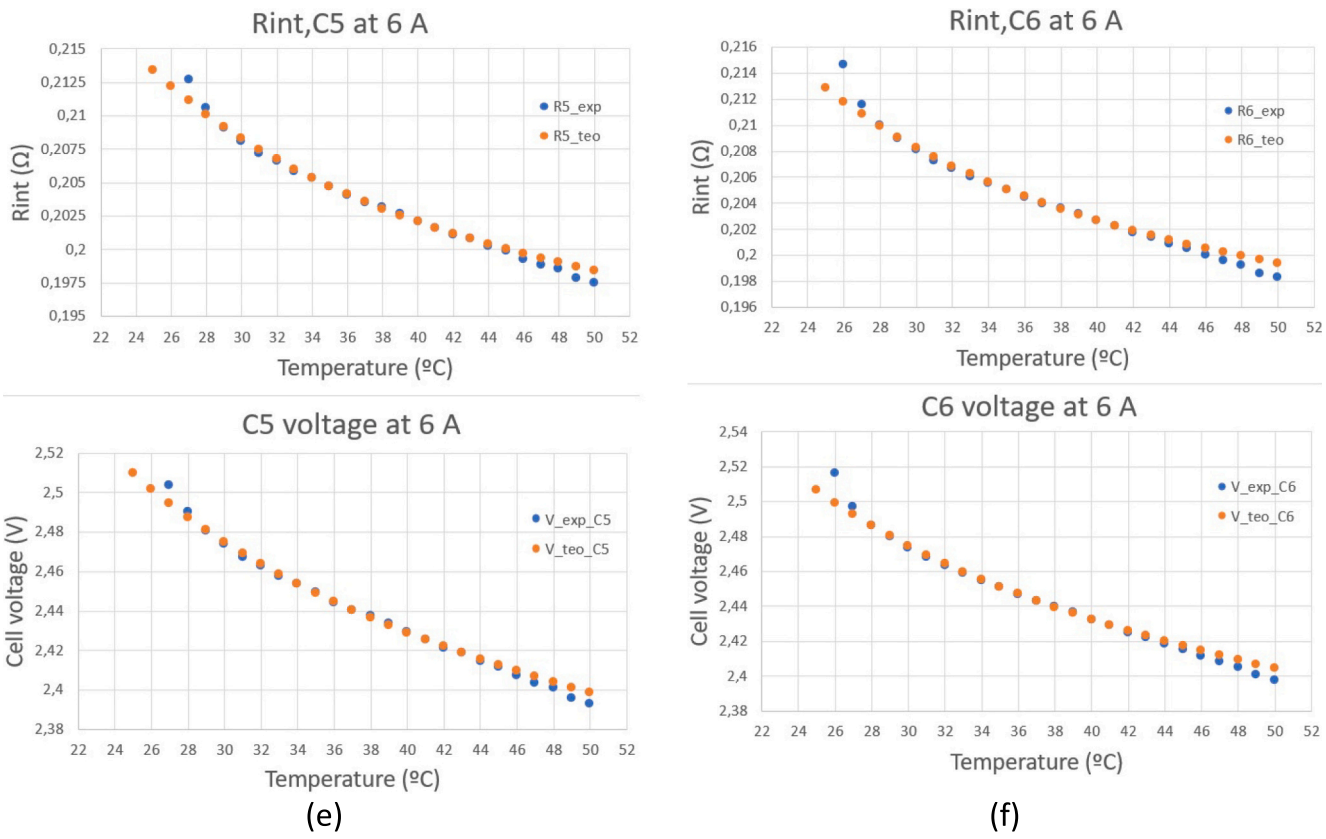

Fig. 11. (*continued*).

which results in a reduction of the total power consumed (Eq. 9) as well as an increase in the efficiency of the cell (Eq. 12).

To corroborate these results, a series of statistical metrics have been applied to the V_{cell} of each of the cells. Specifically, the Root Mean Square Error (RMSE), the Mean Absolute Error (MAE) and the Coefficient of Determination (R^2) have been applied.

The RMSE indicates the standard deviation of the residual values, which are a measure of the distance between the data points and the regression line. This metric allows quantifying the level of dispersion of the residual values and calculating the level of concentration of the data on the regression line. This metric is calculated by Eq. (21), where y_{exp} and y_{teo} refer to the values obtained experimentally and theoretically, respectively. Moreover, the parameter n indicates the sample size.

$$\mathrm{RMSE} = \sqrt{\frac{\sum_{i=1}^{n}\left(y_{exp,i} - y_{teo,i}\right)^2}{n}} \tag{21}$$

The MAE is a measure of the average magnitude of the absolute errors between experimental and theoretical measurements. This value is determined utilising Eq. (22).

$$\mathrm{MAE} = \frac{\sum_{i=1}^{n}\left|y_{exp,i} - y_{teo,i}\right|}{n} \tag{22}$$

R^2 illustrates the level of coincidence between the experimental data and those obtained in the theoretical model. Thus, R^2 presents a measure of the overall accuracy of the model. Such measure is evaluated by Eq. (23), where e refers to the difference between the experimental and theoretical values and $\overline{y_{exp}}$ indicates the average of the experimental values.

$$R^2 = 1 - \left(\frac{\sum e^2}{\sum\left(y_{exp} - \overline{y_{exp}}\right)^2}\right) \tag{23}$$

Table 3 reports the values obtained for these metrics for each cell voltage.

The values presented in Table 3 reflect a successful and accurate performance of the model at cell level. Regarding the RMSE, the calculated values are reduced and close to zero, indicating a high concentration between the experimental and theoretical values concerning the regression line. Furthermore, the MAE values reflect a narrow absolute error for each cell, which corroborates the correct static behaviour of the model. Finally, the R^2 obtained displays values close to the unit, which confirms the accuracy of the model.

After obtaining these results at cell level, the performance of the model was tested to determine the parameters of the PEMEL as a unit. For this purpose, the PEMEL is arranged under rated operating conditions in such a way that it covers the entire input current range in an upward direction. By obtaining the experimental data, the cell-level parameters have been calculated using the proposed model. Hereafter, the key parameters of the PEMEL have been determined theoretically. Once the experimental and theoretical PEMEL data have been obtained, the characteristic curves of the electrolyzer can be plotted and compared.

Table 3
Statistical metrics for each cell voltage derived from 6 A operation.

	RMSE	MAE	R^2
C1	0.01185519	0.00980082	0.75988013
C2	0.00945017	0.00666523	0.93704076
C3	0.01042611	0.00632603	0.89706081
C4	0.0128881	0.0064928	0.88255837
C5	0.01620467	0.00566716	0.86372224
C6	0.01105357	0.00426088	0.91337222

First, the V_{el}-I curve depicted in Fig. 12 illustrates the relationship between the input voltage and current of the PEMEL, representing the main curve that defines the behaviour of the electrolyzer. The values of V_{el_exp} have been obtained by direct measurement of the electrolyzer voltage, while V_{el_teo} has been calculated by means of Eq. (16).

This curve describes the operation of the PEMEL by means of two differentiated zones: a first zone located in the low current range (from 0 A to 0.5 A) and another one in the nominal current range (from 0.5 A to 8 A). In the first zone, an abrupt and sudden behaviour of the voltage is observed, represented by a variation from 0 V to 12–13 V. This phenomenon is due to the PEMEL requirement of a minimum operating current. When this condition is satisfied, the voltage varies spontaneously increasing to a first start voltage. As the input current is increased, the electrolyzer behaviour is described by the second zone. In the last region, the voltage traces a linear curve around 14–15 V, where the nominal value of the operating voltage is reached. The slope of this curve is dependent on the temperature and working pressure of the PEMEL, decreasing with increasing temperature and ascending with increasing pressure.

The $P_{t,el}$-I presented in Fig. 13 represents the relationship between the total power consumed and the input current. As indicated in Eq. (18), this relationship is linear, with a maximum value around 120 W for 8 A. P_{t,el_exp} and P_{t,el_teo} have been determined using Eq. (18), employing in the said equation, for each case, the values of V_{el_exp} and V_{el_teo}, respectively.

Fig. 14 depicts the $v_{H,el}$-I curve, which relates the total hydrogen flow rate generated and the current consumed. Similar to the $P_{t,el}$-I curve, it presents a linear geometry, reaching the nominal hydrogen production value (250 ml/min) for 7 A and a maximum value of around 300 ml/min at 8 A. The values of v_{H,el_exp} are obtained by measuring the hydrogen flow rate through the installed H_2 flow meter. v_{H,el_teo} is calculated by means of Eq. (19).

As a last characteristic curve, Fig. 15 shows the η_{el}-I curve, which illustrates the relationship between the overall efficiency of the PEMEL and the current consumed. This curve has an inverse geometry to the V_{el}-I curve, with the efficiency being higher in the low current range and decreasing as the current increases. This value stabilises for the nominal current range at around 0.5, which represents an overall efficiency of 50 % under nominal operating conditions. η_{el_exp} and η_{el_teo} have both been calculated by means of Eq. (20), employing the values of V_{el_exp} and V_{el_teo}, respectively.

The curves represented in Figs. 12 to 15 confirm a satisfactory performance of the described model, presenting values that are close and accurate to those measured experimentally for all the key parameters of the PEMEL. As in the case of the individual cells, this graphical comparison is supported by statistical metrics in order to numerically corroborate the suitability of the model presented in this research.

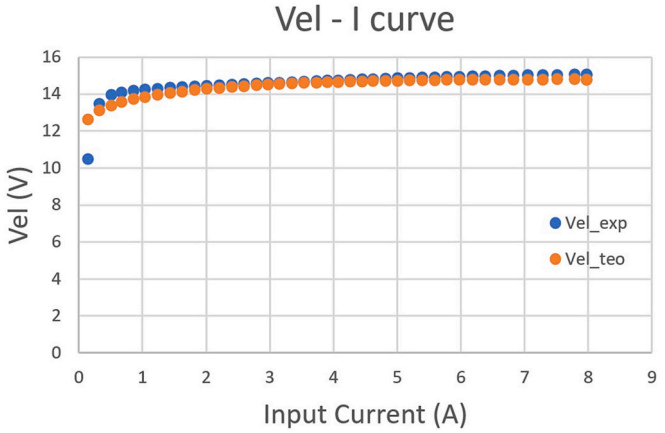

Fig. 12. PEMEL V_{el}-I curve.

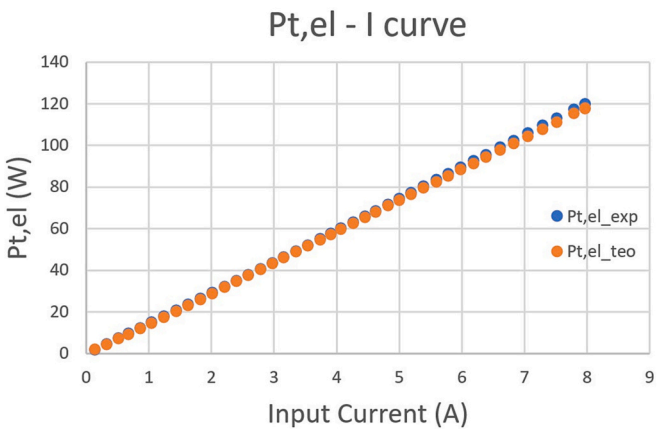

Fig. 13. PEMEL $P_{t,el}$-I curve.

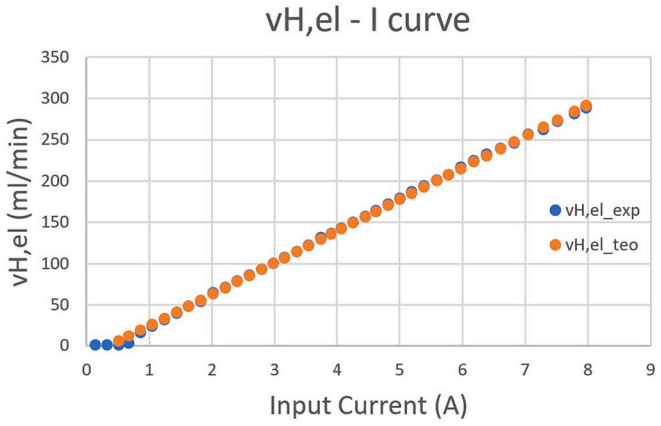

Fig. 14. PEMEL $v_{H,el}$-I curve.

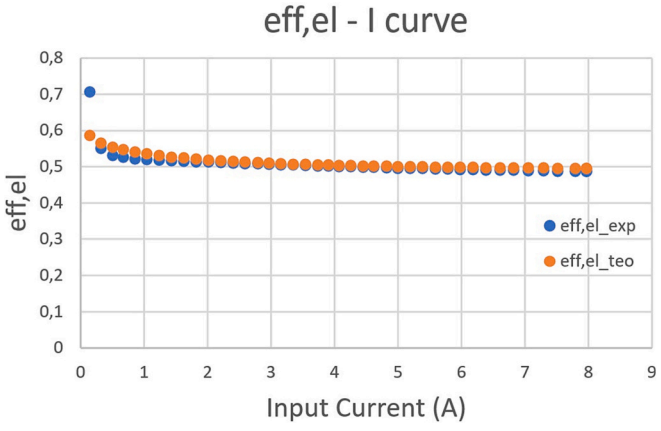

Fig. 15. PEMEL η_{el}-I curve.

Table 4
Statistical metrics for each key parameter of the PEMEL performance.

	RMSE	MAE	R^2
V_{el}	0.405435273	0.250501812	0.88535682
$P_{t,el}$	0.955620569	0.748756913	0.99927021
η_{el}	0.020408517	0.009754147	0.8363784
$V_{H,ell}$	0.977475729	0.768943431	0.99915947

Table 4 reports the values of the RMSE, MAE and R^2 metrics for the key parameters of the PEMEL.

Similar to the values shown in Table 3 for the case of individual cells, the metrics displayed for the PEMEL corroborate an optimal and accurate performance of the DR compared to the experimental data gathered. Regarding the RMSE, values lower than the unit are observed, denoting a high clustering between experimental and theoretical data, confirming a minimum dispersion.

Concerning MAE, the results obtained for the key variables denote a significantly reduced mean absolute error for the entire operating range of the PEMEL, which translates as an optimal and well-fitted operation of the DR. For instance, the MAE of $P_{t,el}$ is 0.75 W for an operating range with a maximum of 120 W. Within the nominal operating range (0.5 to 8 A), the total power consumed by the PEMEL remains considerably higher than the MAE of the DR, representing a negligible and acceptable deviation under the presented test conditions.

The R^2 metric exhibits a range of values between 0.83 and 0.99, close to the unit. These values corroborate the accuracy and suitability of the model applied in the DR for all the key variables of the PEMEL.

5. Conclusions

This paper has presented the design and validation of the DR of a PEMEL framed in a smart microgrid devoted to the generation of green hydrogen from water and photovoltaic energy for subsequent energy storage.

Regarding the equipment employed, the operating principle of the PEM cell and the main technical specification of the 6-cell PEMEL stack are described. Furthermore, the remaining ancillary equipment used in the installation for the proper operation of the PEMEL is outlined. A DAQ system has been implemented in order to gather, visualise and store experimental data by means of a PLC and a GUI designed in LabVIEW and communicated via OPC protocol.

For the design of the DR, an ECM-type model has been employed to describe the static behaviour of the individual cells that comprise the PEMEL. Moreover, this model facilitates the study of key variables such as voltage, total power consumed, hydrogen flow rate, and efficiency. This model is based on the determination of the internal resistance of the cell, which is a novelty in the literature, describing in detail all the stages required to obtain the designed model, and with it, the proposed DR.

The process conducted to obtain the model required several experimental tests and the utilisation of the MATLAB toolbox Curve Fitting to determine the expression of the particular internal resistance for each cell. A model for the PEMEL stack has been defined by obtaining the expressions of the key variables from the cell model.

The operation of the proposed DR has been tested for the cases of individual cells and the complete PEMEL, by means of a graphical and numerical comparison of the experimental and theoretical data. The results obtained verify the suitability and accuracy of the DR, corroborating the validity of the process described in the research.

From a practical standpoint, the experimental setup described in this work is comprised of commercial equipment, such as the PLC and various sensors utilised for measuring key variables. The nature of these devices streamlines the implementation and maintenance of the setup, without requiring equipment specifically manufactured for this application. Consequently, this approach achieves an adaptable and robust system that is easily reproducible and scalable.

In terms of technical requirements, the methodology employed for the development of the model relies mainly on two software environments: Excel and MATLAB. Both environments are widely known and used in the field of scientific research for their mathematical calculation capabilities, coinciding in their proprietary software nature. From a computational point of view, the data collected by the DAQ and the results obtained from the tests performed generate a moderate density of information. The magnitude of this dataset does not represent a processing problem (computational time, computational effort, etc.) for equipment such as current computers with modest technical specifications. Once the parameters have been determined using MATLAB curve fitting, the expressions to be coded for the calculations of the PEMEL variables are simple, facilitating their programming in automation and supervision equipment.

In relation to the context of the paper, the work presented is framed within the smart microgrids and renewable energies due to the equipment employed. Nevertheless, the results presented in this research are not limited to a single application within this framework. These results can be used in various contexts and applications thanks to the detailed description of the methodology developed.

Future work in relation to this line of research consists of comparing the proposed DR with other models in the literature, as well as applying the DR to the management of hydrogen generation systems by means of predictive strategies. In addition, the methodology employed in this paper could be applied to develop a DR of another PEMEL with different characteristics, such as number of cells, voltage and input current range, or flow rate of hydrogen generated. Finally, another line of future work involves the study of the dynamic behaviour of PEM cells and the experimental PEMEL.

CRediT authorship contribution statement

Francisco Javier Folgado: Conceptualization, Software, Investigation, Data curation, Writing- original draft, Review & editing. Isaías González: Methodology, Investigation, Writing- Preparation, Writing-review & editing. Antonio José Calderón: Conceptualization, Methodology, Validation, Investigation, Data curation, Writing – review & editing, Supervision.

Declaration of competing interest

The authors declare that they have no known competing financial interests or personal relationships that could have appeared to influence the work reported in this paper.

Data availability

The authors are unable or have chosen not to specify which data has been used.

Acknowledgements

Project co-financed by European Regional Development Funds FEDER and by the Junta de Extremadura (IB18041).

References

[1] K. Shinde, P.B. Mane, Review on high penetration of rooftop solar energy with secondary distribution networks using smart inverter, Energy Rep. 8 (2022) 5852–5860, https://doi.org/10.1016/j.egyr.2022.03.086.

[2] Y. Cao, E. Kamrani, S. Mirzaei, A. Khandakar, B. Vaferi, Electrical efficiency of the photovoltaic/thermal collectors cooled by nanofluids: machine learning simulation and optimization by evolutionary algorithm, Energy Rep. 8 (2022) 24–36, https://doi.org/10.1016/j.egyr.2021.11.252.

[3] K. Wang, W. Sun, W. Liu, X. Huo, R. Yin, J. Liu, et al., Mitigating interfacial and bulk defects via chlorine modulation for HTL-free all-inorganic $CsPbI_2Br$ carbon-based perovskite solar cells with efficiency over 14%, Chem. Eng. J. 445 (2022) 136781, https://doi.org/10.1016/j.cej.2022.136781.

[4] H. He, X. Wang, J. Chen, Y.-X. Wang, Regenerative fuel cell-battery-supercapacitor hybrid power system modeling and improved rule-based energy management for vehicle application, J. Energy Eng. 146 (2020) 04020060, https://doi.org/10.1061/(asce)ey.1943-7897.0000708.

[5] X. Yuan, J. Liu, C. Han, Y. Li, Y. Feng, Simultaneous nutrient-energy recovery from source-separated urine based on bioelectrically enhanced bipolar membrane-driven in-situ alkali production coupling with gas-permeable membrane system, Chem. Eng. J. 431 (2022) 134161, https://doi.org/10.1016/j.cej.2021.134161.

[6] I. González, A.J. Calderón, J.M. Andújar, Novel remote monitoring platform for RES-hydrogen based smart microgrid, Energ. Conver. Manage. 148 (2017) 489–505, https://doi.org/10.1016/j.enconman.2017.06.031.

[7] C. Li, J.B. Baek, The promise of hydrogen production from alkaline anion exchange membrane electrolyzers, Nano Energy 87 (2021) 106162, https://doi.org/10.1016/j.nanoen.2021.106162.
[8] K.W. Ahmed, M.J. Jang, M.G. Park, Z. Chen, M. Fowler, Effect of components and operating conditions on the performance of PEM electrolyzers: a review, Electrochem 3 (2022) 581–612, https://doi.org/10.3390/electrochem3040040.
[9] M. Ni, M.K.H. Leung, D.Y.C. Leung, Technological development of hydrogen production by solid oxide electrolyzer cell (SOEC), Int. J. Hydrogen Energy 33 (2008) 2337–2354, https://doi.org/10.1016/j.ijhydene.2008.02.048.
[10] A. Khataee, A. Shirole, P. Jannasch, A. Krüger, A. Cornell, Anion exchange membrane water electrolysis using AemionTM membranes and nickel electrodes, J. Mater. Chem. A 10 (2022) 16061–16070, https://doi.org/10.1039/d2ta03291k.
[11] M. Noussan, P.P. Raimondi, R. Scita, M. Hafner, The role of green and blue hydrogen in the energy transition—a technological and geopolitical perspective, Sustainability (Switzerland) 13 (2021) 1–26, https://doi.org/10.3390/su13010298.
[12] Y. Wang, Y. Pang, H. Xu, A. Martinez, K.S. Chen, PEM fuel cell and electrolysis cell technologies and hydrogen infrastructure development — a review, Energy Environ. Sci. 15 (2022) 2288–2328, https://doi.org/10.1039/d2ee00790h.
[13] D. Tang, G.L. Tan, G.W. Li, J.G. Liang, S.M. Ahmad, A. Bahadur, et al., State-of-the-art hydrogen generation techniques and storage methods: a critical review, J. Energy Storage 64 (2023) 107196, https://doi.org/10.1016/j.est.2023.107196.
[14] P.M. Falcone, M. Hiete, A. Sapio, Hydrogen economy and sustainable development goals: review and policy insights, Curr. Opin. Green Sustain. Chem. 31 (2021) 100506, https://doi.org/10.1016/j.cogsc.2021.100506.
[15] J.D. Hunt, A. Nascimento, N. Nascimento, L.W. Vieira, O.J. Romero, Possible pathways for oil and gas companies in a sustainable future: from the perspective of a hydrogen economy, Renew. Sustain. Energy Rev. 160 (2022) 112291, https://doi.org/10.1016/j.rser.2022.112291.
[16] D.E. Olivares, A. Mehrizi-Sani, A.H. Etemadi, C.A. Cañizares, R. Iravani, M. Kazerani, et al., Trends in microgrid control, IEEE Trans. Smart Grid 5 (2014) 1905–1919, https://doi.org/10.1109/TSG.2013.2295514.
[17] A. Hirsch, Y. Parag, J. Guerrero, Microgrids: a review of technologies, key drivers, and outstanding issues, Renew. Sustain. Energy Rev. 90 (2018) 402–411, https://doi.org/10.1016/j.rser.2018.03.040.
[18] T.M. Lawrence, M.C. Boudreau, L. Helsen, G. Henze, J. Mohammadpour, D. Noonan, et al., Ten questions concerning integrating smart buildings into the smart grid, Build. Environ. 108 (2016) 273–283, https://doi.org/10.1016/j.buildenv.2016.08.022.
[19] L.P. Van, K. Do Chi, T.N. Duc, Review of hydrogen technologies based microgrid: energy management systems, challenges and future recommendations, Int. J. Hydrogen Energy 48 (2023) 14127–14148, https://doi.org/10.1016/j.ijhydene.2022.12.345.
[20] O. Atlam, M. Kolhe, Equivalent electrical model for a proton exchange membrane (PEM) electrolyser, Energ. Conver. Manage. 52 (2011) 2952–2957, https://doi.org/10.1016/j.enconman.2011.04.007.
[21] Q. Feng, X.Z. Yuan, G. Liu, B. Wei, Z. Zhang, H. Li, et al., A review of proton exchange membrane water electrolysis on degradation mechanisms and mitigation strategies, J. Power Sources 366 (2017) 33–55, https://doi.org/10.1016/j.jpowsour.2017.09.006.
[22] A. Sánchez, Q. Zhang, M. Martín, P. Vega, Towards a new renewable power system using energy storage: an economic and social analysis, Energ. Conver. Manage. 252 (2022), https://doi.org/10.1016/j.enconman.2021.115056.
[23] A. Pujana, M. Esteras, E. Perea, E. Maqueda, P. Calvez, Hybrid-model-based digital twin of the drivetrain of a wind data generation, Energies 16 (2023), https://doi.org/10.3390/en16020861.
[24] A. Awasthi, K. Scott, S. Basu, Dynamic modeling and simulation of a proton exchange membrane electrolyzer for hydrogen production, Int. J. Hydrogen Energy 36 (2011) 14779–14786, https://doi.org/10.1016/j.ijhydene.2011.03.045.
[25] Á. Bárkányi, T. Chován, S. Németh, J. Abonyi, Modelling for digital twins—potential role of surrogate models, Processes 9 (2021), https://doi.org/10.3390/pr9030476.
[26] F.J. Folgado, I. González, A.J. Calderón, Simulation platform for the assessment of PEM electrolyzer models oriented to implement digital replicas, Energ. Conver. Manage. 267 (2022), https://doi.org/10.1016/j.enconman.2022.115917.
[27] D. Zhao, Q. He, J. Yu, M. Guo, J. Fu, X. Li, et al., A data-driven digital-twin model and control of high temperature proton exchange membrane electrolyzer cells, Int. J. Hydrogen Energy 47 (2022) 8687–8699, https://doi.org/10.1016/j.ijhydene.2021.12.233.
[28] T.M. Ismail, K. Ramzy, B.E. Elnaghi, M.N. Abelwhab, M.A. El-Salam, Using MATLAB to model and simulate a photovoltaic system to produce hydrogen, Energ. Conver. Manage. 185 (2019) 101–129, https://doi.org/10.1016/j.enconman.2019.01.108.
[29] Mohamed Albarghot, Mahmud Sasi, Luc Rolland, MATLAB/Simulink modeling and experimental results of a PEM electrolyzer powered by a solar panel, J. Energy Power Eng. 10 (2016), https://doi.org/10.17265/1934-8975/2016.12.009.
[30] D. Guilbert, G. Vitale, Dynamic emulation of a PEM electrolyzer by time constant based exponential model, Energies 12 (2019), https://doi.org/10.3390/en12040750.
[31] M. Espinosa-López, C. Darras, P. Poggi, R. Glises, P. Baucour, A. Rakotondrainibe, et al., Modelling and experimental validation of a 46 kW PEM high pressure water electrolyzer, Renew. Energy 119 (2018) 160–173, https://doi.org/10.1016/j.renene.2017.11.081.
[32] Á. Hernández-Gómez, V. Ramirez, D. Guilbert, B. Saldivar, Cell voltage static-dynamic modeling of a PEM electrolyzer based on adaptive parameters: development and experimental validation, Renew. Energy 163 (2021) 1508–1522, https://doi.org/10.1016/j.renene.2020.09.106.
[33] A.J. Calderón, I. González, M. Calderón, F. Segura, J.M. Andújar, A new, scalable and low cost multi-channel monitoring system for polymer electrolyte fuel cells, Sensors (Switzerland) 16 (2016), https://doi.org/10.3390/s16030349.
[34] I. González, A.J. Calderón, F.J. Folgado, IoT real time system for monitoring lithium-ion battery long-term operation in microgrids, J. Energy Storage 51 (2022) 104596, https://doi.org/10.1016/j.est.2022.104596.
[35] RTD PT100 datasheet (accessed on 14 March 2023) n.d. https://docs.rs-online.com/9186/0900766b815bb292.pdf.
[36] DC axial fan datasheet (accessed on 14 March 2023) n.d. https://docs.rs-online.com/6d6e/A700000007525942.pdf.
[37] Droking programmable DC/DC converter (accessed on 14 March 2023) n.d. https://www.droking.com/Power-Supply-Module-DC10V-75V-to-0-60V-12A-720W-Buck-Converter-Voltage-regulator-CNC-Control-Module-DC-12V-24V-36V-48V-Adapter.
[38] Bronkhorst mass flow meter datasheet (accessed on 14 May of 2023) n.d. https://www.bronkhorst.com/int/products/gas-flow/el-flow-select/f-111b/?pdf=true.
[39] Pressure transmiter Wika A-10 datasheet (accessed on 14 March 2023) n.d. https://shop.wika.com/media/Data-sheets/Pressure/Pressure-sensors/ds_pe8160_en_co.pdf.
[40] S7-1500 6ES7516-3AN00-0AB0 CPU datasheet (accessed on 14 March 2023) n.d. https://mall.industry.siemens.com/mall/en/ww/Catalog/DatasheetDownload?downloadUrl=teddatasheet%2F%3Fformat%3DPDF%26caller%3DMall%26mlfbs%3D6ES7516-3AN00-0AB0%26language%3Den.
[41] National Instruments (NI) LABVIEW main page (accessed on 14 March 2023) n.d. https://www.ni.com/en-gb/shop/labview.html.
[42] I. González, A.J. Calderón, J. Figueiredo, J.M.C. Sousa, A literature survey on open platform communications (OPC) applied to advanced industrial environments, Electronics (Switzerland) 8 (2019), https://doi.org/10.3390/electronics8050510.
[43] Fuel Cell Handbook, 6th ed., US National Energy Technology Laboratory, 2002. November. DOE/NETL-2002/1179.
[44] MATLAB curve fitting toolbox (accessed on 14 March 2023) n.d. https://uk.mathworks.com/products/curvefitting.html.
[45] ThreeDify XLGrapher (accessed on 12 August 2023) n.d. https://3dexcel.com/xlgrapher-3d-graphing-add-in-for-microsoft-excel/.